Silica

ULLMANN'S ENCYCLOPEDIA OF INDUSTRIAL CHEMISTRY

Otto W. Flörke, Institut für Geologie, Mineralogie und Geophysik, Ruhr-Universität, Bochum, Federal Republic of Germany

Heribert A. Graetsch, Institut für Geologie, Mineralogie und Geophysik, Ruhr-Universität, Bochum, Federal Republic of Germany

Fred Brunk, Dr. C. Otto Feuerfest Gmbh, Bochum, Federal Republic of Germany

Leopold Benda, Niedersächsisches Landesamt für Bodenforschung, Hannover, Federal Republic of Germany

Siegfried Paschen, Kieselgur- und Kalksandsteinindustrie, Henrich Meyer-Werke Breloh GmbH & Co. KG, Munster, Federal Republic of Germany

Horacio E. Bergna, E. I. du Pont de Nemours & Company Inc., Wilmington, Delaware 19 880–0262, United States

William O. Roberts, E. I. du Pont de Nemours & Company Inc., Wilmington, Delaware 19 880–0262, United States

William A. Welsh, Grace Davison, W. R. Grace & Co.-Conn., Columbia, Maryland, United States

Cristian Libanati, Grace Davison, W. R. Grace & Co.-Conn., Columbia, Maryland, United States

Manfred Ettlinger, Degussa-Hüls AG, Standort Wolfgang, Hanau, Federal Republic of Germany

Dieter Kerner, Degussa-Hüls AG, Standort Wolfgang, Hanau, Federal Republic of Germany

Monika Maier, Degussa-Hüls AG, Standort Wolfgang, Hanau, Federal Republic of Germany

Walter Meon, Degussa-Hüls AG, Standort Wolfgang, Hanau, Federal Republic of Germany

Ralf Schmoll, Degussa-Hüls AG, Werk Weeseling, Wesseling, Federal Republic of Germany

Hermann Gies, Ruhr-Universität, Bochum, Federal Republic of Germany

Dietmar Schiffmann, Institut für Toxikologie, Universität Würzburg, Würzburg, Federal Republic of Germany

DOI: 10.1002/14356007.a23_583.pub3

1. Silica Modifications and Products

1.1. Occurrence and Geochemistry

Silica [*7631-86-9*], silicon dioxide, SiO_2, is the major constituent of rock-forming minerals in magmatic and metamorphic rocks. It is also an important component of sediments and soils [1–3]. Bound as silicates it accounts for ca. 75 wt % of the Earth's crust [4]. Free silica predominantly occurs as quartz, which makes up 12–14 wt % of the lithosphere.

Quartz is the thermodynamically stable modification at ambient conditions (Fig. 1) occurring as one of the main products of slowly cooled silica-rich magmas such as granites, granodiorites, and related rocks. It is also a primary mineral of pegmatites and hydrothermal veins formed during late stages of magmatic processes. In metamorphic rocks like schists, migmatites, and quartzites which suffered high temperature and pressure due to deep burial in the Earth's crust, quartz is also a major constituent. Owing to its hardness and low solubility, quartz is able to resist erosion and occurs abundantly in sedimentary rocks such as sand and sandstones. Quartz is also the final product of the diagenesis process of noncrystalline biogenic silica deposited in sea floor sediments. In the form of chalcedony, microcrystalline quartz occurs as secondary filling of veins and cavities in rocks and in petrified wood and other organic matter. Flint nodules, frequently occurring in limestone formations, also consist of chalcedony.

Quartz owes its abundance to the action of water in rock-forming processes. In rocks that were formed at high temperatures under dry conditions – volcanic eruptiva, silicate meteorites, moon rocks and silica slags, for example – quartz is rare. Here the high-temperature silica modifications cristobalite and tridymite crystallize (Fig. 1). Under the influence of high pressure induced by burial in great depth or by meteoritic impact, the high-pressure modifications coesite and stishovite are stable.

Under more ambient conditions waterborne unstable silica varieties such as micro- and noncrystalline opals and chalcedony are formed.

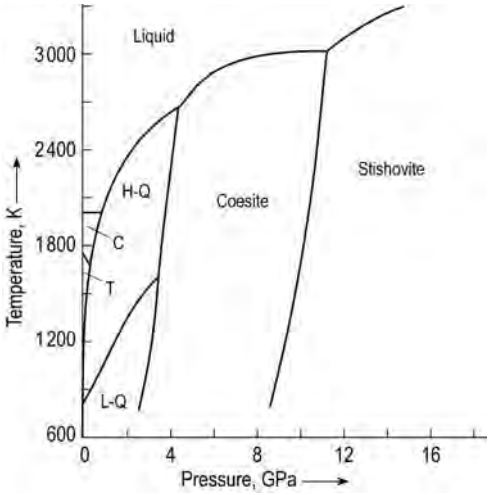

Figure 1. Calculated phase diagram of the SiO_2 system [6] H-Q: high quartz, L-Q: low quartz, C: high cristobalite, T: high tridymite (for the stability field of tridymite, see text).

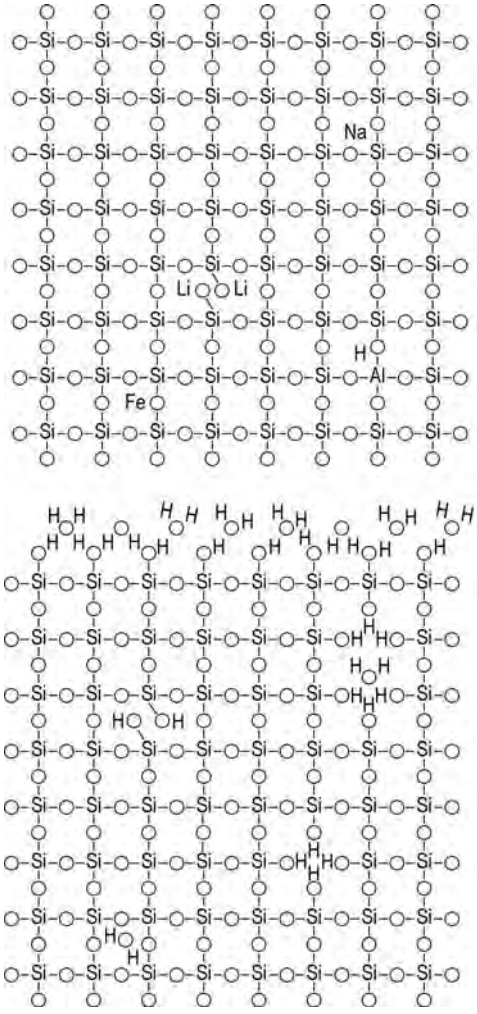

Figure 2. Two-dimensional scheme of incorporation of impurities in silica
Top: chemical point defects introduced by occupation of silicon lattice sites and of interstitial sites by foreign atoms. Bottom: water incorporated in the silica framework by forming hydrolytic nonbridging oxygen (German: *Trennstellen*) and by occupation of silicon vacancies or interstitial sites, and water located at the surface as silanol groups and adsorbed water molecules.

Deep-sea sediments consisting of large masses of biogenic silica, for example, are altered in a diagenetic process with increasing burial depth from noncrystalline opals via microcrystalline opals to chalcedony and chert. Micro- and noncrystalline silica minerals are described in more detail in [5].

Keatite, silica W, and porosils (except for melanophlogite) are artificial crystalline silica products that do not occur in nature. They do not have a stability field of their own and can be synthesized under hydrothermal conditions only in the presence of sodium (keatite) or with the aid of organic template molecules (porosils). The latter are described in more detail in Chapter 8.

Silica crystals are almost pure SiO_2 which do not contain large quantities of impurities. Water, however, can be incorporated in concentrations from hundreds to several thousands of parts per million in quartz (Fig. 2). The transition from structural incorporation to microstructural inclusion is fluent [7]. At elevated temperatures and pressures water migrates rapidly through the structural framework by splitting Si—O—Si bonds and forming silanol groups. This mechanism of hydrolytic weakening activates plastic deformation, solid-state flow [8], reconstructive transformations, and recrystallization. Traces of alkali metal ions act as efficient transformation activators (Fig. 2) [9]. Alkali metal ions as well as Al and Fe are the most common nonvolatile impurities in silica. Quartz usually contains about 100 ppm of trace elements or less [5, 10, 11]. The concentration of impurities can be higher in tridymite and cristobalite than in quartz, ranging up to 5000 ppm Al, 3500 ppm Na and 1500 ppm K [12, 13]. The trace elements can be incorporated in at least two different ways (Fig. 2) [14]. The first is the substitution of Si^{4+} by Al^{3+}, or Fe^{3+} on lattice sites and simultaneous

addition of Li^+, Na^+, K^+, Mg^{2+}, or Ca^{2+} on interstitial sites. The second is the incorporation of additional alkali metal ions to form alkaline nonbridging oxygen sites (German: *Trennstellen*).

1.2. Si—O Bond and Crystal Structures

Despite its chemical simplicity, SiO_2 displays a remarkable diversity of crystal structures. Apart from the ultrahigh-pressure modification stishovite with octahedrally coordinated silicon (Fig. 3) and artificial silica W with chains of edge-sharing tetrahedra, all crystal structures of silica are made up of a three-dimensional framework of corner-sharing tetrahedra (Fig. 3). The noncrystalline silica phases consist of a continuous random network of corner-sharing tetrahedra. All four sp^3 orbitals of silicon overlap with 2p orbitals of the four coordinating oxygen atoms to form strong σ bonds [15]. Additional minor contributions from π bonding may arise from overlap of Si 3d orbitals with other O 2p orbitals, which partly explains the observed shortening of Si—O bond lengths with increasing Si-O-Si bond angles [16]. The mixed bond character of about 50 % ionic and 50 % covalent results in bent intertetrahedral Si-O-Si angles in the range of 120 to 180° with a mean of about 147° [17–19]. Band theory treatment is given in [20]. The effective ionic radius of Si^{4+} is 0.026 nm for tetrahedral coordination by oxygen (O^{2-}: r = 0.135 nm), and 0.040 nm for octahedral coordination [21]. The mean Si—O bond length is 0.162 nm in the tetrahedra [22] and the mean O—O distance is 0.264 nm (Fig. 3). The short Si—O bond length is responsible for the high bond strength.

The strong bonds and the three-dimensional connectivity of the tetrahedra are the reasons for

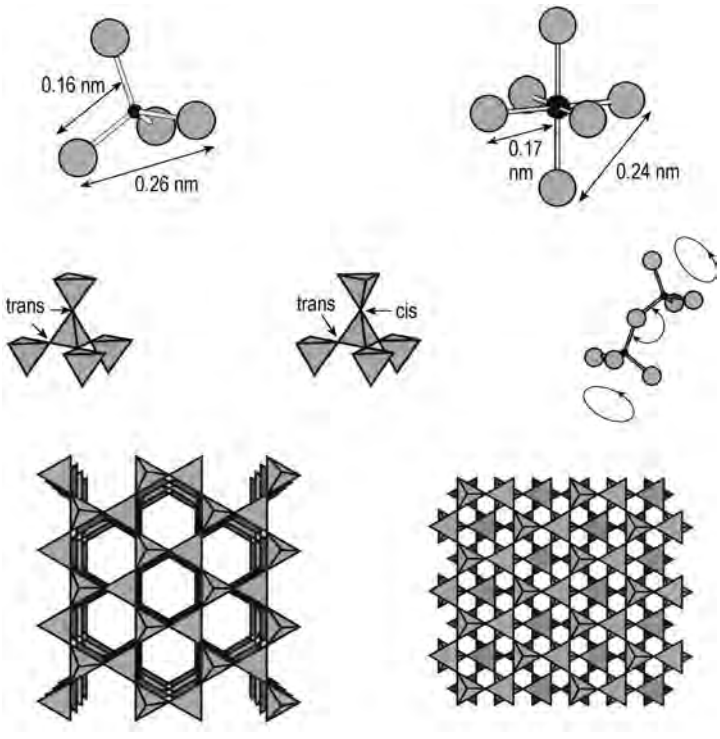

Figure 3. Top: $SiO_{4/2}$ tetrahedron and $SiO_{6/3}$ octahedron.
Middle: tetrahedra configurations in the silica framework structures.
Bottom: stacking principles of idealized six-membered rings of tetrahedra: two-layer sequence in tridymite (left), three-layer sequence in cristobalite (right).

the high hardness (quartz: Mohs hardness 7), the lack of good cleavage, high elasticity, high melting point (cristobalite ca. 2000 K), high activation temperature of the quartz–cristobalite transformation (1300 K) and high transformation temperature of silica glass (1300 K). Contrasting with these properties, the resistivity of silica to electron irradiation damage is relatively low [23].

Silica is an insulator, a property that is utilized in the fabrication of silicon-based microelectronic devices by precipitation of ultrathin insulating films of noncrystalline silica on the semiconductor substrate crystals.

The tetrahedra can be considered as rigid units which remain almost unchanged upon thermal expansion or compression by high pressure. They are rotated or tilted instead. The variability of the intertetrahedral Si-O-Si angles and the unrestricted torsion angle of connected tetrahedra (Fig. 3) also account for the topological diversity of the crystal structures of silica and the tendency for glass formation. At elevated temperatures quartz, cristobalite, tridymite, and melanophlogite displacively transform into dynamically disordered high-temperature phases. Softening of rigid unit modes plays an important role in these thermally induced ferroic transitions [24]. In the variable framework structures, planar defects such as stacking faults in cristobalite and tridymite, and twin planes in quartz and moganite frequently occur. Growth twinning and transformation twinning are also common. Normally, neighboring tetrahedra adopt the electrostatically favorable trans configuration (Fig. 3). Rare exceptions with cis and trans configurations are tridymite [9], melanophlogite, and coesite [26].

1.3. Crystalline Silica Phases

The crystalline silica minerals are listed in Tables 1, 2, and 3 together with their crystallographic data. Table 1 also lists the nonmineral crystalline phases keatite and silica W. The porosils are treated in Chapter 8.

1.3.1. Crystalline Silica Minerals

The *p–T* diagram of silica, with stishovite, coesite, quartz, and cristobalite, is shown in Figure 8 [6]. Tridymite forms only in the presence of impurities which act as mineralizers. The phase transformations between the stable phases are reconstructive, requiring breaking and formation of new Si—O bonds (except for the high quartz–low quartz transition). Apart from high quartz, all high-temperature and high-pressure phases can persist metastably under ambient conditions. Quartz and most of the phases that are metastable under ambient conditions undergo displacive transitions at elevated temperatures without breaking of bonds. Melanophlogite, moganite, and the microcrystalline mineral species have no thermodynamic stability field.

Quartz is the thermodynamically stable form under ambient conditions. The tetrahedra are arranged in the open structure of low or α-quartz as helices along the trigonal *c*-axis. Two types can be distinguished: a small helix formed by three tetrahedra and a larger double helix consisting of six tetrahedra. All threefold screw axes are either left- or right-handed, and this results in the optical activity of quartz with a rotatory power of 27.71°/nm for Na light [10]. The crystals are enantiomorphous with the symmetry of the acentric space groups $P3_121$ or $P3_221$. The right- and left-handed crystals are mirror images of each other (Fig. 4). The twofold symmetry axes perpendicular to the screw axis are polar, and mechanical stress along the axis produces a direct piezoelectric effect. The reverse effect is utilized in oscillatory devices. Standard values of important properties are compiled in [27], and the relationships between crystal structure and properties are given in [28]. The low specific free surface energy of the rhombohedral faces {1011} results in a poor but distinct cleavage.

The thermal expansion of α-quartz is high ($\alpha_{11} = 13.3 \times 10^{-6}\ K^{-1}$, $\alpha_{33} = 7.1 \times 10^{-6}\ K^{-1}$) and drops to even slightly negative values at the displacive phase transition to high or β-quartz at 573 °C (Fig. 5). With increasing temperature the tetrahedra are rotated clockwise or anticlockwise around the dyad axes towards their higher symmetry positions in β-quartz. Additional dyad axes coinciding with the threefold screw axes in the double helices are generated at the transition, turning them into sixfold screw axes. The handedness of the helices is preserved, and the space groups for left- and right-handed

Table 1. Crystalline silica phases: space groups and unit cell parameters

Phase	Space group	Unit cell dimensions in nm					
		a	*b*	*c*	α	β	γ
Mineral phases							
Stishovite	$P4_2/mnm$	0.418	0.418	0.267	90 °	90 °	90 °
Coesite	$C2/c$	0.713	1.240	0.717	90 °	120.3 °	90 °
Low quartz	$P3_221/P3_121$[a]	0.491	0.491	0.540	90 °	90 °	120 °
High-quartz[b]	$P6_222/P6_422$[a]	0.500	0.500	0.546	90 °	90 °	120 °
Moganite	$I12/a1$	0.876	0.488	1.072	90 °	90.1 °	90 °
Low cristobalite	$P4_12_12/P4_32_12$[a]	0.497	0.497	0.693	90 °	90 °	90 °
High cristobalite[c]	$Fd3m$[d]	0.713	0.713	0.713	90 °	90 °	90 °
Low tridymite[e]	Cc[f]	1.849	0.499	2.583	90 °	117.8 °	90 °
L1–T_0 (MC)	Cc[g]	1.852	0.500	2.381	90 °	105.8 °	90 °
Low tridymite[h]	$F1$	0.993	1.722	8.186	90 °	90 °	90 °
L2–T_D ($PO_{5/10}$)							
Low tridymite	Cc[f,i]	0.501	0.860	0.822	90 °	91.5 °	90 °
L3–T_0 (MX-1)							
High tridymite[i]	$P2_12_12_1$	0.499	2.617	0.820	90 °	90 °	90 °
H4–T_0 (OP)							
High tridymite[k]	$C112_1$ $(\alpha\beta0)$[i,l]	0.501	0.875	0.821	90 °	90 °	90.3 °
H3–T_0 (OS)							
High tridymite[m]	$C222_1$	0.502	0.876	0.821	90 °	90 °	90 °
H2–T_0 (OC)							
High tridymite[n]	$P6_3/mmc$[f]	0.505	0.505	0.826	90 °	90 °	120 °
H1–T_0 (HP)							
Melanophlogite	$Pm3n$	1.344	1.344	1.344	90 °	90 °	90 °
Nonmineral phases							
Keatite	$P4_12_12/P4_32_12$[a]	0.746	0.746	0.858	90 °	90 °	90 °
Silica W	$Icma$	0.836	0.472	0.516	90 °	90 °	90 °

[a] Enantiomorphic (right- and left-handed);
[b] At 863 K;
[c] At 573 K;
[d] Average structure;
[e] For the nomenclature of the tridymite phases, see Fig. 8;
[f] Setting according to [53, 62];
[g] Setting according to [54, 63];
[h] Stacking disordered;
[i] Incommensurately modulated;
[j] At 428 K;
[k] At 443 K;
[l] Four-dimensional super space group;
[m] At 493 K;
[n] At 733 K.

β-quartz are $P6_222$ and $P6_422$ with additional twofold rotation axes perpendicular to the hexagonal *c*-axis (Fig. 4). The crystal structure of β-quartz is disordered by intense thermal vibrations of the tetrahedra, and the structure shown in Figure 4 is only an average. An intermediate phase occurs in a narrow temperature range of 1.7 K between α- and β-quartz. It is incommensurately modulated and consists of a regular array of microdomains with the orientation of twins according to the Dauphiné law. The size of the domains rapidly decreases with increasing temperature [29]. Heating untwinned single crystals of quartz to temperatures above the transition point usually results in the formation of Dauphiné twins [30].

Dauphiné twins are intergrowths of two right- or two left-handed quartz individuals which are rotated by 180° with respect to each other around their common *c*-axis. This additional dyad axis is identical with the twofold axis which is lost during the high–low transition. Dauphiné twinning is also referred to as electrical twinning. Twinning according to the Brazil law also occurs abundantly in natural quartz, i.e., in amethyst and chalcedony. In this case right- and left-handed

Table 2. Crystalline silica phases: crystal dimensions, density, and displacive phase transitions

Phase	Crystal dimension[a]	Density g/cm^3	Displacive phase transitions in K
Mineral phases			
Stishovite	2	4.29	–
Coesite	2	2.92	–
Low quartz	1,2,3	2.65	846
High-quartz	4	2.53	846
Moganite	3	2.62	–
Low cristobalite	1,2	2.33	540[b]
High cristobalite	4	2.21	540[b]
Low tridymite	1,2	2.27	398, 423, 493, 723
L1–T_0 (MC)			
Low tridymite	1,2	2.28	398, 423, 493, 723
L2–T_D ($PO_{5/10}$)			
Low tridymite	1,2	2.26	338, 398, 423, 493, 723
L3–T_0 (MX-1)			
High tridymite	4	2.24	398, 423, 493, 723
H4–T_0 (OP)			
High tridymite	4	2.22	398, 423, 493, 723
H3–T_0 (OS)			
High tridymite	4	2.21	398, 423, 493, 723
H2–T_0 (OC)			
High tridymite	4	2.19	398, 423, 493, 723
H1–T_0 (HP)			
Melanophlogite	1,2	ca. 2.0	ca. 333
Nonmineral phases			
Kealtte	2	ca. 2.5	–
Silica W	2 (fibers)	ca. 1.97	–

[a] 1: macroscopic, 2: microscopic, 3: submicroscopic, 4: does not exist at ambient conditions (not quenchable);
[b] Hysteresis of more than 20 K.

individuals are intergrown via the {1011} plane. The new symmetry element introduced by the twinning is a mirror plane parallel to {1120}. Brazil twinning is also called optical twinning. Both kinds of twinning neutralize or reduce the piezoelectric effect of quartz, and crystals suitable for oscillatory and optical purposes must be free from twinning. Twins according to the Japanese law are less abundant. The twin plane is {1122} and the *c*-axes of two twinned crystals form an angle of 84°33′.

Other compounds crystallizing with the quartz structure type are phosphates MPO_4 and arsenates $MAsO_4$ (M = Al, Ga, Fe), BeF_2, the high-temperature form of GeO_2, and the high-pressure modifications of BPO_4, $BAsO_4$, and phosphorus oxynitride (PON) [31–33]. β-Eucryptite $LiAlSiO_4$ and γ-spodumene $LiAlSi_2O_6$-III are stuffed derivatives of β-quartz in which the silicon atoms are partly replaced by Al and Li incorporated on interstitial tetrahedral sites (I_4 position) within the large helices [34].

Cristobalite is the low-pressure, high-temperature modification of silica (Fig. 1). It persists as metastable phase at low temperatures. A displacive phase transition from the tetragonal low-temperature α-form to the cubic high-temperature β-form takes place near 540 K. The transition is of first order with an hysteresis of more than 20 K and a volume discontinuity of ca. 5 %. The crystal structure of β-cristobalite is a derivative of the diamond structure type in which carbon is replaced by silicon and oxygen is located midway between neighboring Si atoms. The framework can be described as a stacking of parallel layers of six-membered rings of tetrahedra. Alternate tetrahedra point upwards and downwards (Fig. 6). The stacking is a three-layer

Table 3. Microcrystalline silica minerals

Mineral or phase	Species[a]		Microstructure	Refractive index	Water content, wt %
Quartz	microquartz		granular grains < 20 μm	1.54–1.55	< 0.3
	chalcedony		length fast fibers, fiber axis <11.0>		
		Ch-w_{LF}	parallel fibrous	1.53–1.54	0.8–2.0
		Ch-h_{LF}	spherulites of radiating fibers	ca. 1.54	0.3–0.8
	quartzine	Ch_{LS}	length slow fibers, fiber axis <00.1>	ca. 1.54	0.5–1.0
Moganite			crystal blades		1.5–3.0
Opal	opal-CT	O-CT_{LS}	length slow fibers (lussatite)	1.45–1.46	
		O-CT_M	lepidospheres of platelets	1.43–1.45	3.0–10.0
	opal-C	O-C_{LF}	parallel platy {101}	ca. 1.46	1.0–3.0
		O-C_M	massy, tangled platy		1.0–8.0

[a] Ch: chalcedony, w: wall lining, h: horizontally banded, LF: length fast (negative optical character of the fiber elongation), LS: length slow (positive optical character of the fiber elongation), C: disordered cristobalite, CT: disordered cristobalite/tridymite, M: massy tangled

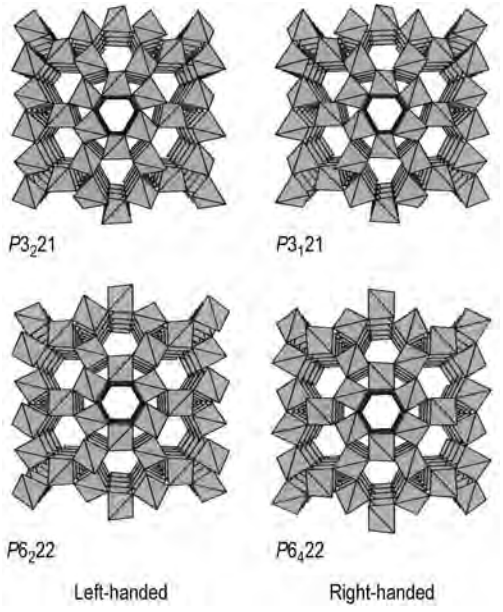

Figure 4. Tetrahedral model of the crystal structures of left- and right-handed quartz. Top: low-temperature quartz; bottom: high-temperature quartz. Perspective view on (001) slices along the *c*-axis; [100] direction vertical.

sequence in cristobalite. In tridymite, similar layers are stacked in a two-layer sequence with antiparallel mutual orientation. Stacking faults occur frequently in cristobalite and tridymite (cf. microcrystalline opals). The space group of the

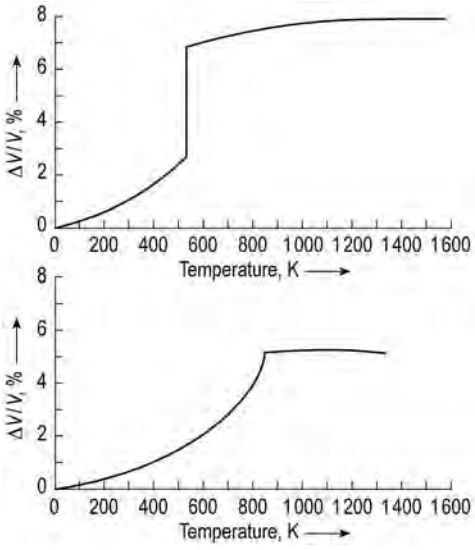

Figure 5. Thermal expansion of the unit cells of cristobalite (top) and quartz (bottom).

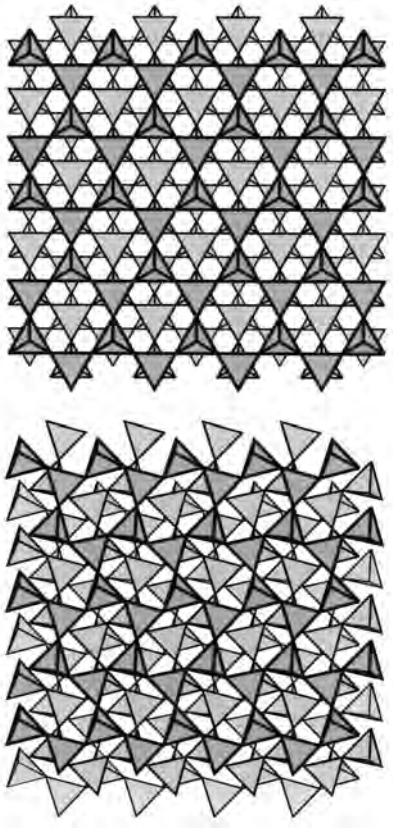

Figure 6. Tetrahedral model of the crystal structure of cristobalite.
Top: (111) slice of the cubic high-temperature form ([110] direction vertical).
Bottom: (101) slice of the tetragonal low-temperature modification ([010] direction vertical).

average structure of β-cristobalite is *Fd*3*m* [35]. The rigid tetrahedra perform rotational vibrations by precessing around the straight Si-O-Si lines [36–39]. At the transition temperature, these motions become unstable, and the structure collapses to form oval rings instead of the hexagonal six-membered rings of tetrahedra in the average high-temperature structure. In α-cristobalite the tetrahedra are arranged in helices containing either left- or right-handed fourfold screw axes parallel to the tetragonal *c*-axis [36]. Two enantiomorphous forms exist with the space groups $P4_12_12$ or $P4_32_12$. Loss of the threefold rotation axis, the inversion center, and the centering of the unit cell during the phase transition result in the formation of 12 twins and antiphase domains [40]. The volume discontinuity at the

transition leads to characteristic fish-scale microcracking. These scales are rectangular if the cristobalite is structurally ordered and are rounded in the presence of stacking disorder [41]. The displacive cubic-to-tetragonal transition cannot be suppressed by quenching, but stacking faults lower the transformation temperature [138]. The structure of β-cristobalite can be stabilized by way of chemical stuffing. In $Ca_{0.02}Al_{0.09}Si_{0.91}O_2$ some of the silicon atoms are replaced by aluminum, and calcium ions are incorporated on interstitial sites in the large cages between the layers of tetrahedra [34].

Other compounds with the α-cristobalite-type of structure are the high-temperature forms of $AlPO_4$, $GaPO_4$, $MnPO_4$, and $AlAsO_4$ [31, 32]. $BAsO_4$, BPO_4, $BeSO_4$ and phosphorus oxynitride (PON) crystallize with the β-cristobalite structure. Stuffed derivatives are carnegieite $NaAlSiO_4$ [42] and a variety of compounds with the formula Na_2MSiO_4 (M = Ca, Be, Zn, Mg) [34].

Tridymite forms between 1200 and 1800 K at ambient pressure, but traces of foreign ions, preferably alkali metals, or hydrothermal conditions [43] are necessary. The growth of tabular crystals always starts with cristobalite nuclei [44].

The crystal structure is a derivative of the hexagonal wurtzite type with Si occupying the Zn and S positions and oxygen placed between the silicon atoms. Layers with six-membered rings of tetrahedra are stacked in antiparallel orientation to give a two-layer sequence. Viewed along the hexagonal *c*-axis the layers are in the totally eclipsed position in high-temperature tridymite, leaving open channels in the structure (Figs. 3 and 7).

With respect to bonding requirements, tridymite is much less balanced than cristobalite. As a consequence tridymite undergoes a cascade of displacive phase transitions [9, 45] (Fig. 8). Similar to β-cristobalite and β-quartz, the hexagonal high-temperature phase of tridymite is dynamically disordered [46]. Upon cooling, different rigid unit modes of the tetrahedra successively freeze in by forming phases with collapsed rings of tetrahedra [47]. In a first step alternate layers of tetrahedra are laterally shifted with respect to each other near 400 °C, reducing the symmetry to orthorhombic [48]. In a second step an incommensurately modulated phase with temperature-dependent lattice parameter $\sqrt{3}a_{hex}$ is formed at 220 °C [49, 50] which discontinuously locks in at ca. 150 °C resulting in a superstructure with a $3\sqrt{3}a_{hex}$ lattice parameter [51, 52]. Finally,

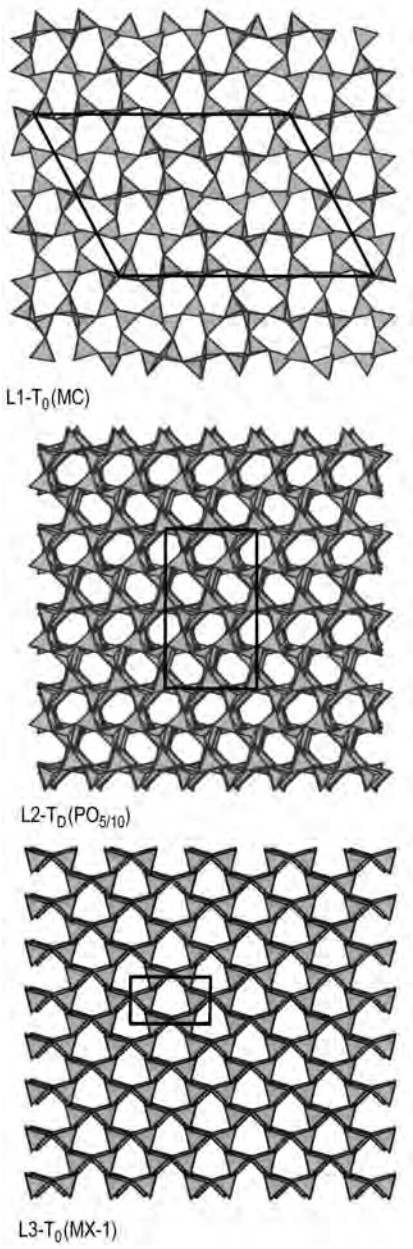

Figure 7. Tetrahedral model of the crystal structures of the three room temperature forms of tridymite.
Top: (010) slice of L1-T_O(MC) with vertical [305] direction. Middle and bottom: (001) slices of L2-T_D($PO_{5/10}$) and L3-T_O(MX-1) with [010] and [100] direction vertical, respectively.

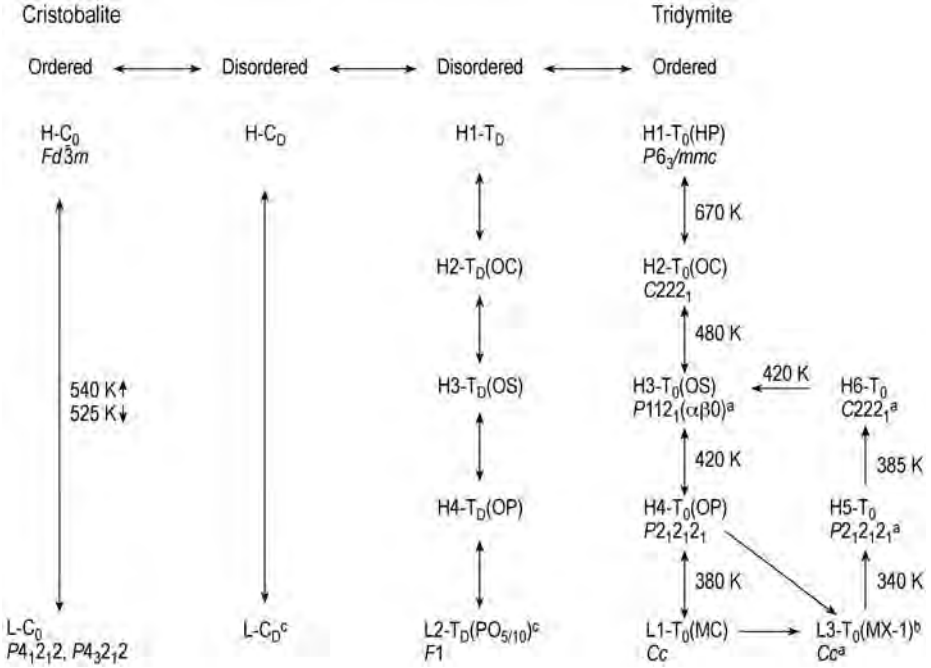

Figure 8. Displacive polymorphism and reconstructive stacking polytypism of cristobalite and tridymite.
[a] phases with incommensurate displacive modulations; [b] phase formed by thermal or mechanical stress (quenching or grinding); [c] transition temperatures depend on the degree of stacking disorder.
Nomenclature of the tridymite phases: L = low-temperature phase, H = high-temperature phase, T_O = ordered tridymite, T_D = stacking-disordered tridymite; in parentheses: M = monoclinic, O = orthorhombic, H = hexagonal, PO = pseudo-orthorhombic, C = C-centered, P = primitive Bravais type, S = superstructure, X = unknown.

a monoclinic phase with a complex superstructure is formed at 116 °C in a first-order transformation [53, 54]. This modification is usually obtained by flux syntheses and has been found in moon rocks and meteorites. The transformation path, however, can be modified by thermal or mechanical stress or by lattice imperfections like stacking faults. Most tridymites occurring in terrestrial rocks contain stacking faults and have a triclinic (pseudo-orthorhombic) $2 \times 2\sqrt{3} \times 10$superlattice [55]. The number of high-temperature phases of pseudo-orthorhombic tridymite and the respective transition temperatures depend on the degree of stacking disorder [45]. A third room-temperature modification can be produced by grinding monoclinic tridymite or by quenching from high temperatures [56]. The phase is monoclinic and displays an incommensurate structural modulation [57–59]. Further modulated high-temperature phases can be obtained by reheating incommensurate low tridymite [60].

All three low tridymite modifications and cristobalite can be intergrown in the same crystal [60, 61]. Impurities can be incorporated by coupled substitution on lattice sites and on interstices in the open structural channels parallel to the *c*-axis [13]. In refractory-grade crystals, trace element concentration is 1 wt % [13].

A compound with isotypic phases is $AlPO_4$ [31]. Nepheline ($Na_3KAl_4Si_4O_{16}$) and kalsilite and kaliophilite (both $KAlSiO_4$) are stuffed derivatives of tridymite. Another stuffed derivative is $CaAl_2O_4$ [34].

Coesite is the high-pressure modification of silica with the densest framework of $SiO_{4/2}$ tetrahedra. It is composed of four membered rings of tetrahedra which are linked in the form of chains of rings. The chains are interconnected by symmetrically different four-membered rings of tetrahedra (Fig. 9). In this group the tetrahedra are in *cis* configuration with an exceptionally

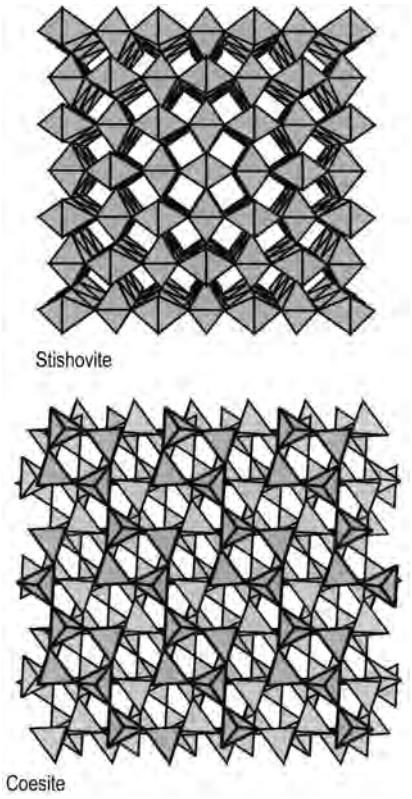

Figure 9. Polyhedral model of the high-pressure modifications coesite and stishovite.
Top: perspective view along the *c*-axis of stishovite ([110] direction vertical).
Bottom: (010) slice of coesite with vertical [101] direction.

large Si-O-Si angle, restricted by symmetry to 180° [25, 26].

Coesite metastably persists up to about 1300 K at ambient pressure. It is much less soluble in hydrofluoric acid than quartz but has a similar solubility to quartz in water under ambient conditions. Coesite and stishovite are rare and were synthesized prior to their detection in nature.

Stishovite crystallizes in the rutile structure type with silicon in sixfold coordination (Fig. 9). The SiO_6 octahedra form chains by sharing two opposite edges. Different chains are connected by linking of octahedra corners [64, 65]. The arrangement results in a very close packing of oxygen, even though the Si—O bonds are longer than in SiO_4 tetrahedra. Stishovite is about 43 % denser than coesite [66]. It is the stable form of silica under the conditions of the Earth's mantle. In the lower mantle stishovite probably transforms from the tetragonal rutile structure to a distorted structure with orthorhombic symmetry (stishovite II). A ferroelastic transformation to the denser $CaCl_2$ structure type is expected at higher pressures which involves tilting of the octahedra [66].

Moganite is closely related to quartz but represents a new structure type with a lower symmetry. The structure can be described as a composition of alternate {1011} layers of right- and left-handed quartz (Fig. 10), that is, a periodic twinning according to the Brazil law on the cell-dimension scale [67]. The only known occurrence of pure moganite is on Gran Canaria, Spain, where it forms microcrystalline fillings of fissures and cooling cracks in the ignimbrite

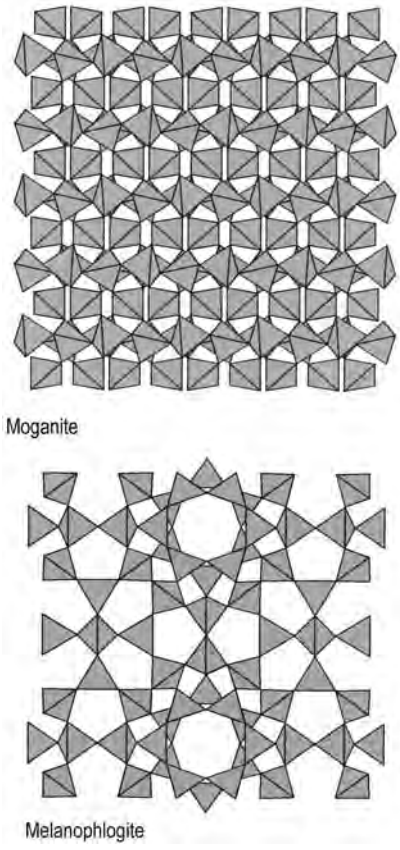

Figure 10. Tetrahedral models of the crystal structures of moganite and melanophlogite. (001) slices with vertical [010] direction.

streams [68, 69]. It has been reported that moganite also occurs as a minor constituent of microcrystalline quartz minerals [70].

The synthesis of a high-pressure, high-temperature modification of phosphorus oxynitride (PON) with moganite-type crystal structure has been reported [33].

Melanophlogite is a very rare mineral with the composition $46\ SiO_2 \cdot 6\ (CO_2,N_2) \cdot 2\ (CH_4,N_2)$. Agrigento and Livorno in Italy and Mt. Hamilton in California are the only known noteworthy occurrences [71, 72]. The guest molecules CH_4, CO_2, and N_2 are incorporated in two types of large cagelike voids of the silica framework (Fig. 10) [73]. A displacive phase transition from tetragonal to cubic symmetry takes place between 40 and 65 °C. Melanophlogite is the only mineral species among the large group of artificial microporous silica phases which are treated in Chapter 8.

Chalcedony and quartzine are microcrystalline quartz minerals (Table 3) [5] consisting of submicroscopic fibers. The fiber elongation occurs perpendicular to the trigonal *c*-axis in chalcedony and parallel to it in quartzine. The microcrystals are highly defective and contain a large number of twin planes (left- and right-handed quartz twinned according to the Brazil law) [74]. Chalcedony is the main constituent of banded agate geodes, flint nodules, and chert. Quartzine sporadically occurs as thin bands in agates. The purity is usually high with less than 1 wt % nonvolatile impurities and less than 2 wt % water. The latter is incorporated at defects of the crystal structure and in the microstructure between the fibers [75].

Microcrystalline opals consist of highly stacking disordered cristobalite and tridymite. A distinction is drawn between opal-CT and opal-C [76, 77]. In opal-CT the stacking is random tridymitic (two-layer sequence) and cristobalitic (three-layer sequence) [78], whereas cristobalite dominates in opal-C [77, 79]. The microstructure consists of fibers (lussatite) or of lepidospheric aggregates of thin crystal blades (Table 3). The water content can reach 10 wt % with a large portion of water molecules dissolved in the defective crystal lattice [80, 81].

1.3.2. Crystalline Nonmineral Silica Phases

Keatite, silica W, zeosils, and most of the clathrasils are synthetic crystalline forms of silica for which no counterpart has been found in nature. The porosils are described in Chapter 8.

Keatite has a tetragonal framework of corner-sharing tetrahedra which contains five-, six-, and seven-membered rings of tetrahedra [82]. Structural channels run parallel to the *a*-axes, and helices with fourfold screw axes parallel to the *c*-axis (Fig. 11) [83]. Under mild hydrothermal conditions microcrystalline fibers of keatite are obtained by using silica glass as starting material and dilute NaOH solutions [84]. It is a metastable intermediate crystallization product. Keatite can also be prepared under dry conditions

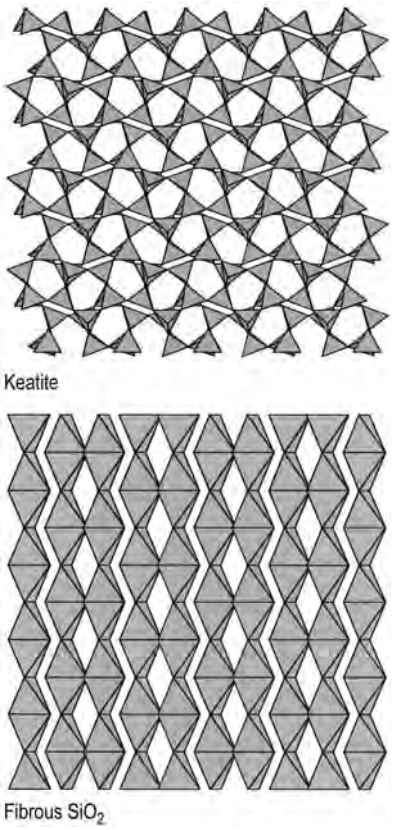

Figure 11. Tetrahedral model of the crystal structures of keatite and silica W.
Top: (100) slice of keatite with vertical [001] direction.
Bottom: (110) slice of silica W with vertical [001] direction.

by heating lithic silica gels with chromium oxide as additive [85].

Stuffed derivatives of keatite are β-spodumene $LiAlSi_2O_6$ and $HAlSi_2O_6$, which show ionic conductivity.

Silica W [86] forms above ca. 1500 K in the vapor transport reaction:

$$H_2(g)+SiO_2(s)\rightarrow SiO(g)+H_2O(g)$$

The crystal structure is isotypic with that of SiS_2. Infinite chains of edge-sharing tetrahedra run parallel to one another and are held together by weak interatomic forces (Fig. 11). At ambient temperature, this very unstable configuration collapses immediately on coming into contact with traces of water. Tempering under the formation conditions produces cristobalite [86].

SiO_2-X is an alkali metal silicate hydrate with the approximate formula $MSi_{11}O_{20.5} \cdot 3\ H_2O$ (M = K, Rb, Cs) [87].

1.4. Noncrystalline Silica Minerals

Noncrystalline (antiquated: amorphous) silica has a short-range order of corner-sharing SiO_4 tetrahedra like crystalline silica but no long-range order and consists of a continuous random network instead of an ordered framework structure. The intertetrahedral Si—O—Si angles cover the full range from 120° to 180° with a maximum near 144° in silica glass [88]. The density of the network and other properties are variable. In nature, noncrystalline silica minerals are formed by melting and subsequent quenching (lechâtelierites), by pressure densification (diaplectic glasses), by rapid quenching of silica from hydrothermal solutions or by precipitation from a solution, sol, or gel near ambient conditions (opals). The range of Si—O—Si angles is narrower in opals than in silica glass [89]. The mean Si—O—Si angle is reduced in densified glass [90]. The mineral species are listed in Table 4.

Due to the lack of structural order and stoichiometry, the boundary between silica glass and silicate glass is fuzzy. For natural silica glass it can be arbitrarily drawn at about 3 mol % of nonsilica components. Opals, however, can contain considerable amounts of water and different varieties (opal-A_G and -A_N) can be distinguished by their microstructure and water content.

Lechâtelierites originate from molten silica formed by lightning strikes (fulgurites) or by meteoritic impact (meteoritic glass) on quartz sand or silica rocks [5, 10]. The glass body is featureless like synthetic fused silica but may contain some pores, inhomogeneities, and relicts of quartz grains. The water content is usually less than 0.1 wt %.

Opal-A_G consists of a close packing of noncrystalline silica spheres with diameters ranging from ca. 100 to 500 nm. Water fills the interstices of the packing and is incorporated within the spheres [80]. Homodisperse spheres form a regular cubic, hexagonal or mixed closest packing [91], which gives rise to Bragg diffraction of visible light and produces the characteristic play of color of precious opals

Table 4. Noncrystalline silica minerals

Mineral or phase[a]	Species[a]	Microstructure	Refractive index	Water content, wt %
Opal-A (water containing noncrystalline silica particles)	opal-A_G precious opal	close packing of homometric $SiO_2 \cdot nH_2O$ spheres	1.45–1.46	4–6
	potch opal	irregular packing of heterometric $SiO_2 \cdot nH_2O$ spheres	1.45–1.46	4–6
(water containing natural silica glass)	opal-A_N or hyalite	botryoidal with striations and bubbles from degassing	1.45–1.46	2–4
Lechâtelierite (almost water free natural silica glass)	silica fulgurite	relics of quartz grains and pores		
	meteoritic silica glass[b]	schlieren, meteoritic detritus and reaction products	ca. 1.458	< 0.1

[a] A: noncrystalline; G: gel structure; N: network structure;
[b] e.g., Libyan desert glass.

[92]. Heterodisperse spheres form irregular packings that result in diffuse scattering rather than in diffraction of light (potch opal).

Geyserite is precipitated in hot springs as sinter from silica-rich aqueous solutions. *Biogenic opal-AG* stems from plants (grass can contain up to 5 wt % silica, rice husks even up 19 wt %) or from skeletal remains of silica plankton. Silica deposits on the sea floor locally formed massive sediment layers with a total thickness of several hundreds of meters (e.g., Monterey, California). The water content usually ranges from 5 to 8 wt % (mostly molecular water) [5, 80] but can reach up to 16 wt % in biogenic opals [93].

Opal-A_N or hyalite is a water-containing silica glass that was formed in volcanically active areas by quenching of a silica-rich fluid or steam. It can be found as botryoidal crusts and fillings of vesicles in lava rocks [94]. The microstructure is characterized by striations parallel to the surface. Opal-A_N contains up to ca. 3.5 wt % water, almost 40 % of which is bound as silanol groups within the glass network [80, 95].

1.5. Colored Silica Minerals

Pure silica (e.g., rock crystal) is colorless. Except for precious opal, the color of silica originates from selective absorption by incorporated impurities forming so-called color centers. In several cases X-ray or γ radiation is necessary for the activation of the color centers. Heat treatment has an influence on the color, too. Several colored varieties of silica are traded as gem stones. Review articles on the origin of the color are given in [10, 96, 99].

Amethyst has a violet color due to the incorporation of Fe^{3+} on lattice sites and at I_4 interstitial sites in the helices of the quartz structure. Irradiation removes an electron from iron on lattice sites, turning it into Fe^{4+}. The electron is trapped by interstitial iron, which is reduced to Fe^{2+}. The color is not stable above ca. 300 °C but can be restored by renewed irradiation [97, 98].

Citrine is yellow to yellow brown with a smoky cast. It contains iron only at I_4 interstitial sites. If amethyst is heated in air at 300–560°C, iron oxide particles of submicroscopic size are exsolved, producing a yellow to yellow-brown color with reddish tints.

Rose quartz occurs as massy aggregates of quartz rather than as single crystals. The pale pink to deep rose color originates from Fe – Ti intervalence charge transfer in fibrous nanoinclusions of dumontierite or a closely related phase [100].

Smoky quartz or *morion* contains substitutional Al^{3+} on Si^{4+} lattice sites [101]. The black or grayish brown color is caused by irradiation, which produces an electron hole at oxygen bonded to aluminum. The color center is destroyed by heating above 200 °C but can be renewed by irradiation.

Other colored single-crystal quartz varieties such as pink or blue quartz have been found in nature or produced artificially but have gained only minor commercial importance as gemstones [102]. The color centers are often nonuniformly distributed, but for example in amethyst they are concentrated at Brazil twin boundaries parallel to the {1011} faces [103].

Microcrystalline quartz minerals can be colored by inclusion of foreign pigment particles in the microstructure rather than by color centers in the crystal lattice. *Chrysoprase* is green due to submicroscopic nickel compounds, and the red or brown color of *jasper* is caused by Fe_2O_3 or $Fe(OH)_3$. *Agate* mainly consists of layers of translucent gray or white chalcedony which can be naturally or artificially colored by infiltration of iron or other compounds between the fibers. *Fire opal* is probably also colored red by Fe^{3+} pigmentation.

The colors of *precious opals*, however, are caused by Bragg diffraction of light and not by absorption. Therefore, the color is of higher spectral purity than in other gems. The diffraction originates from the ordered arrangement of homometric silica spheres and water with a lower refractive index in the interstices of the sphere packing. The maximum wavelength of the color depends on the size of the spheres. Opals containing large spheres produce all colors up to red whereas opals with smaller spheres show only a blue or violet color. Different orientations of grains with coherent sphere packing yield different colors. The play of color observed on turning

a stone is enhanced by abundant stacking faults in the packing sequence of the silica spheres, producing diffraction streaks rather than sharp diffraction spots [91, 92].

1.6. Silica Rocks

Many special, trade, and trivial names exist for silica rocks, often with various meanings and imprecise definitions. A classification based on constituent silica phases and microstructure is given in Table 5 [2, 104, 105]. Silica rocks contain more than 90 wt % SiO_2. An ordinary sandstone, for instance, contains only about 65 wt % silica mainly as quartz grains. The rest is matrix and cement (feldspar, $CaCO_3$, mica, clay minerals, etc.). Transitions occur between silica rocks with increasing burial depth in the earth crust which not only result in a reduction of porosity and water content. Quartz sand is solidified to quartz sandstone (arenite or ganister) by cementation of the grains and grades by recrystallization into quartzite under pressure at elevated temperatures. Similarly, noncrystalline biogenetic silica remains of diatoms, radiolaria, etc. are transformed under compression into porcellanite and finally to chert. When the origin is known these rocks are designated as diatomite, radiolarite, or spiculite. Lydite and novaculite are radiolarites of paleozoic age. Tripoli is a friable porous porcellanite but the term is often used in a broader sense for abrasives and polishing media (Section 2.1). Ganister is a quartz sandstone cemented by chalcedony or opal-CT. Sandstone with less than 10 % matrix and cement is called arenite and with more than 10 % matrix wacke (quartz arenite and quartz wacke, respectively, when the total SiO_2 content is higher than 90 wt %). Chert nodules concentrated in layers of cretaceous chalk or limestone are called flint, silex (French), or Feuerstein (German). Agate geodes are fillings of vesicles in volcanic rocks, consisting mainly of chalcedony bands, interstratified by granular microquartz, quartzine, opal-C, opal-CT and coarse quartz crystals [107]. Further silica rocks and stones such as pegmatite quartz, vein quartz, sand, and gravel that are used as raw materials are treated in Chapter 2. A survey of industrial silica rocks is given in [108–110].

1.7. Crystalline Silica Products

Here only silica products made by crystallization from mobile mother phases or by transformation in the solid state are discussed. In contrast to the many noncrystalline silica products, crystalline products are limited to hydrothermally man-made quartz crystals and thermochemically produced polycrystalline silica.

Man-made or cultured quartz is of major economic importance and its use is growing. In contrast, the production of silica refractories for use in high-temperature processes is stagnating.

1.7.1. Cultured Quartz Single Crystals

Manufacture. The growth of quartz single crystals is carried out hydrothermally in sealed steel autoclaves with constant temperature difference and density-driven convection [111] (Fig. 12). Hydrothermal syntheses are defined as reactions or crystal growth at high pressures

Table 5. Silica rocks (> 90 wt % SiO_2)

Classification	Name	Main constituent silica minerals, microstructure	Special, trade, and trivial names (selection)
Sedimentary, nondetrital	diatomite (Chap. 3	opal-A_G; porous coherent diatom accumulation	kieselguhr [3]
	porcellanite	opal-CT; microporous rather strong rock	tripoli [106], opoka
	chert	chalcedony, granular microquartz; nonporous tough rock with conchoidal fracture	hornstein, novaculite, lydite, radiolarite, chert
Sedimentary, detrital	quartz sandstone	quartz grains cemented by direct contact, authigenic outgrowth, chalcedony or opal-CT	quartz arenite, quartz wacke, ganister, zementquartzite
Metamorphic	quartzite	recrystallized quartz grains and cement	crystalline quartzite, felsquartzite
Volcanic	geyserite	opal-A_G, opal-CT; friable, porous	silica sinter

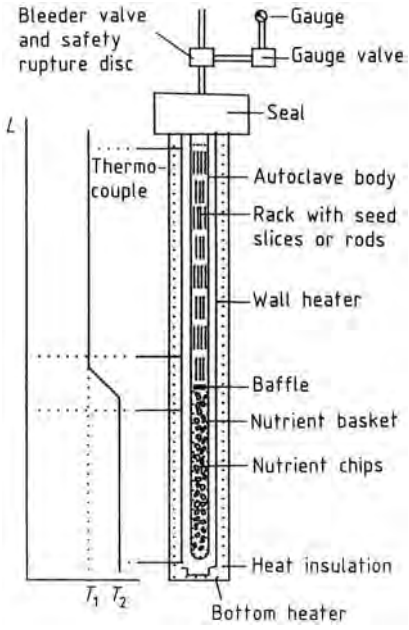

Figure 12. Autoclave for quartz single crystal bar growth

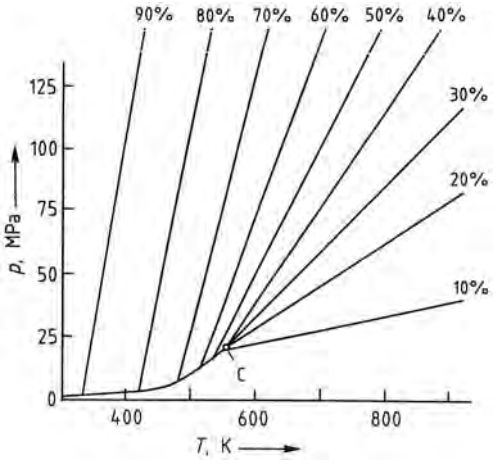

Figure 13. p–T diagram of H_2O, isochores for various percentages of autoclave filling [115, 116]
C: critical point at 22.04 MPa, 547.4 K

and temperatures in aqueous solutions, whether in the sub- or supercritical state [112].

Natural quartz [113] is fractionated into chips (lascas) of controlled size distribution (2.5–4cm) and surface area. They serve as nutrient and are filled into an iron wire basket which is placed in the lower part of the autoclave. The lower part is separated from the upper part by a baffle of defined opening. Seed slices or rods, cut with defined crystallographic orientation from natural or man-made untwinned quartz crystals with a low content of structural defects, are hung in a rack and placed in the upper part of the autoclave. Preferred seeds are Z plates, cut parallel to {0001}, and Y rods, cut parallel to {1120} and {0001} and perpendicular to one of the a-axes.

Aqueous growth solutions with different mineralizers (mainly 0.5–2.0 M NaOH or Na_2CO_3 and additives such as Li_2O) fill ca. 70–80% of the inner autoclave volume. Special syntheses, e.g., the growth of amethyst, which needs structural incorporation of traces of iron, require K_2CO_3 or NH_4F solutions [97, 114]. After sealing, the autoclave is electrically heated to a working temperature of ca. 675 K at the outer wall of the nutrient part (T_2) and ca. 20–40 K less at the seed part (T_1) (Fig. 12). The actual temperature difference ΔT in the reactor is much smaller (5–10 K). With increasing temperature, the pressure increases according to the percentage filling (Fig. 13). Under working conditions, it is ca. 100–150 MPa. A rupture disk in the pressure tubing at the seal prevents hazardous pressure increase.

During heating and cooling of the autoclave, at pressures below ca. 80 MPa, the hydrothermal system passes through a region of retrograde SiO_2 solubility. Above 80 MPa the solubility increases with temperature and pressure (Fig. 14). The mineralizers increase the solubility strongly, for example, at 673 K and 100 MPa from ca. 0.15 wt % SiO_2 for pure water to about

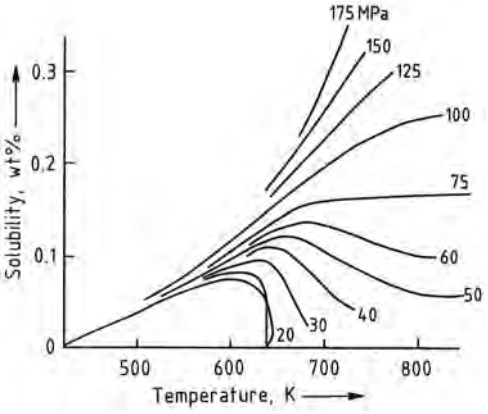

Figure 14. Solubility of SiO_2 in H_2O [117]

2–3 wt %. The solubility is approximately proportional to the mineralizer concentration [117]. Concentrations of NaOH or Na_2CO_3 above 2 mol/L, however, can lead to deposition of sodium silicate glass at the bottom of the autoclave, which obstructs the growth process.

In the nutrient section SiO_2 goes into solution. The solution at the bottom part of the autoclave has a higher temperature than the solution in the seed section and rises in the gravitational field due to its lower density. Above the baffle, it becomes cooler and supersaturated with SiO_2, and growth starts at the seeds. The cooled solution has a higher density and sinks into the nutrient section where it is warmed and becomes subsaturated. It dissolves silica from the nutrient and ascends, and so on in a permanent circulation driven by density difference until the desired quantity of nutrient has been transported to the growing quartz crystals.

The effective nonequilibrium distribution coefficient is defined as

$$k_{\text{eff}} \approx C_{\text{sact}}/C_{\text{lact}}$$

where $C_{\text{s act}}$ is the actual trace element concentration in the solid, and $C_{\text{l act}}$ the actual trace element concentration in the liquid. The trace impurities accumulate in the solution [118] and the grown quartz crystals are of higher purity than the nutrient quartz. Doping with traces of special components changes the physical properties. For example, doping with LiF improves the electrical quality.

Raising p, T, and ΔT increases the rate of SiO_2 transport and of quartz growth. However, the high-temperature strength of the autoclave alloy sets limits on p and T. A low-pressure and a high-pressure process are usually applied. A pressure of 70–100 MPa, a temperature of 620 K, a temperature difference of 10 K, and a 0.6 to 0.8 M sodium carbonate solution are typical of the former and yield a growth rate of about 0.4 mm/d. The high-pressure process (100–150 MPa, 650 K, $\Delta T = 25$ K, 1.0 M sodium hydroxide solution) yields a growth rate of up to 1.0 mm/d, but at the expense of higher costs for equipment [100]. The transition of convection from laminar to turbulent or even cellular flow with increasing ΔT limits these factors as well. Increasing face instability [118] and defect concentrations with increasing rates of transport set further restrictions.

The corrosion of the autoclave steel alloy is inhibited by formation of a dense coating of microcrystalline acmite $NaFe^{III}[Si_2O_6]$ and traces of emeleusite $LiNa_2Fe^{III}[Si_6O_{15}]$ by reaction with the growth solution.

The duration of growth runs varies between one and four months. The grown quartz crystals are formed by grinding to ca. 15–20 cm long bars. The orientation of the bars is determined by X-ray diffraction before cutting them into wafers. An autoclave with 250 mm inner diameter and an inner length-to-diameter ratio of 12 gives a yield of ca. 100 kg of quartz bars per month. The loss by removal of seeds from the bars is ca. 20 wt %. Part of the cutting waste is used in the jewelry industry. The growth parameters which determine yield and quality of man-made quartz, are complexly coupled [120]. Dimensions and yield capacities of autoclaves are given in Table 6.

The largest production capacities exist in Japan, the United States, Russia, and China; smaller capacities are found in Europe, South Korea and South Africa. The total production of cultured quartz was estimated at about 200 t/a in the USA at an average value of ca. $ 186 per kilogram in 2005.

Small amounts of colored quartz [96] for jewelry are grown in Russia. While blue (Co-containing) and light green and yellow (Fe) quartz are already colored in the growth process, the Al and Fe color centers for smoky quartz and for amethyst must be activated after growth by γ radiation. Seeds for the first-mentioned color variations are Z plates, whereas for smoky quartz and amethyst X plates cut parallel to {1011} are used because of face-specific incorporation requirements of the coloring elements.

Filter and oscillator quartz must be free of twinning and need low defect concentrations [121]. Structurally incorporated impurities are determined by chemical trace element analysis. Impurities which produce paramagnetic defects (e.g., Fe) can be detected by electron spin

Table 6. Dimensions and yield capacities of autoclaves for man-made quartz

	Inner diameter, cm	Inner length, m	Inner volume, L	Yield per run, kg
Japan	65	13	4500	2000
United States	40	4.5	560	250

resonance spectroscopy [122]. Traces of water are determined by IR spectroscopy [123, 124]. Inclusions of foreign elements, depending on type, size, and position in the microstructure of the crystal are recognizable by X-ray diffraction, under the polarizing light microscope (PLM), or with the scanning electron microscope (SEM) and can be chemically analyzed by energy dispersive X-ray spectroscopy (EDS) in the SEM or with the electron microprobe [125]. Dislocations produce diffraction contrast in X-ray topography [126, 127]. Brazil twinning can be detected with PLM, but Dauphiné twinning can only be made visible by etching. Both types of twinning can be differentiated by X-ray topography [128, 129].

The quality of resonators is described by the electromechanical Q value. This dimensionless quality factor is defined as:

$$\frac{Q = 2\pi f L}{R}$$

where f is resonance frequency, L inductance, and R resistance.

The Q value increases with decreasing energy loss due to relaxation and internal friction. The slower the decay of the oscillation amplitude after cutting off the excitation, the higher is Q. The quality of the quartz crystals contributes to the resonator Q value. The latter is not measured directly but a material Q is determined instead. A correlation between the IR absorption of structural OH groups (hydrolytic nonbridging oxygen, Fig. 2) at 3580 and 3410 cm^{-1} and the material Q value is usually utilized for quality control [130]. An empirical infrared a value is defined:

$$a = 1/t \log (T_{3800}/T_{3500})$$

where a is the extinction coefficient at 3500 cm^{-1}, t the thickness of the sample in centimeters, and T_n the transmittance at wave number n.

The material Q can be evaluated from

$$10^6/Q = 0.144 + 7.74a + 0.44a^2$$

The three highest grades have a material Q of 1.8, 2.2, or 3.0×10^6

Radiation in space, from uranium or thorium impurities, or from other sources affects the oscillator frequencies by acting on alkali metal impurities. Therefore the quartz must be grown to extreme purity Alkali metal ions on interstitial sites can be removed (swept) electrolytically after growth. This is done at elevated temperature (below the transition temperature of 573 °C in order to avoid electrical twinning) by applying a field of 1 kV/cm [119].

For further specification, the quartz bars are examined for inclusions which might contain acmite impurities that stem from reaction of the hydrothermal solution with the steel walls of the autoclaves. The density of dislocations is determined microscopically after etching with ammonium bifluoride by counting the etch pits or channels. The best grades have dislocation densities of 10, 30, or 100 per cm^2.

Most of the cultured quartz is optically right-handed, as right-handed seed crystals are normally used. Electronic applications are treated in [131, 132]. Natural single-crystal quartz is now used only for a few special applications.

Despite the increasing demand, growth capacities are not markedly increasing because of improved cutting technologies, photolithographic etching, and miniaturization.

The Piezoelectric Effect of Quartz. If stress is applied along one of the three polar twofold rotation axes of quartz an electric polarization is produced (direct piezoelectric effect). The direction of the polarization vector is reversed upon changing from compressive to tensile stress and vice versa. Stress perpendicular to a polar axis and perpendicular to the trigonal c-axis (along the y-axis) also yields an electric polarization along the polar axis.

$$P_i = d_{ijk}\sigma_{jk}$$

$i, j, k = 1, 2, 3$
$P_i =$ electric polarization
$d_{ijk} =$ piezoelectric moduli
$\sigma_{jk} =$ stress tensor

The anisotropy of the piezoelectric effect is described by a third-rank tensor with 27 components. Due to the symmetry of the stress tensor and the point-group symmetry of quartz (32) the number of independent components is reduced to two for quartz

$$d_{111} = -2.31 \times 10^{-12}\ \mathrm{C/N}$$

$$d_{123} = -0.727 \times 10^{-12}\ \mathrm{C/N}$$

for right-handed quartz (the signs of d_{ijk} are reversed for left-handed quartz [133]).

If an electric field is applied in appropriate direction the shape of a quartz crystal changes (<0.1 %). This is called the converse piezoelectric effect. An alternating electric field causes the crystal to vibrate.

$$\varepsilon_{jk} = d_{ijk} E_i$$

$i, j, k = 1, 2, 3$
E_i = electric field
d_{ijk} = piezoelectric moduli
ε_{jk} = strain tensor

Uses The piezoelectric effect was detected by Pierre and Jacques Curie in 1880/1881 using quartz crystals. In 1917, the first sonar was constructed by Langevin to detect submarines. Since the 1920s quartz oscillators have been used for frequency control in radio broadcasting and communication electronics. The first oscillator for frequency stabilization, cut from natural quartz, was described 1921 by Cady [131]. A quartz crystal is stimulated to vibrate mechanically at its resonance frequency. The piezoelectric response in turn is then utilized for stabilization of the frequency of the circuit. The use of quartz resonators increased as a consequence of the mass production of color TVs since the 1960s, quartz clocks and watches since the 1970s, and the developments in digital microelectronics. Today, virtually no appliance or device is working in communication electronics or computer technology without a quartz oscillator.

The resonance frequency depends on the cut and the shape of the quartz crystal. Initially, only cuts perpendicular to the *x*-axis were used for sonar transducers. Today, quartz tuning forks for wristwatches are produced from *x*-cuts. For other purposes, different cuts are preferred. So-called AT cuts are most commonly used. An AT-slice cuts the *y*-axis and forms an angle of 35.3° with the trigonal *c*-axis. As the d_{111} piezoelectric constant has a negative and the d_{123} constant a positive dependence on temperature, an AT cut provides independence of the resonance frequency from temperature [133].

In the megahertz range bulk waves are utilized. For the gigahertz range surface acoustic-wave devices are now produced by photolithographic techniques similar to those used in the semiconductor industry [119].

Due to its good elastic properties and very high stability, quartz is still the most important piezoelectric material. However, in the fields of ultrasonics and piezoelectric sensors and actuators, quartz is widely replaced by materials like lead zirconate titanate (PZT) ceramic which show a much stronger piezoelectric effect [134].

Other uses of quartz single crystals utilize optical properties like optical activity, birefringence, and dispersion.

1.7.2. Polycrystalline Silica Products

Refractory Silica. Dense shaped silica products consist per definitionem of greater than 93 wt % SiO_2 [135]. Usually, the silica content varies between 95 and 97 wt %. Refractory silica is available in three grades: superduty, regular duty, and coke-oven quality [136, 137]. Silica bricks are used up to 1925 K. The major applications of dense silica bricks are coke ovens, superstructures of glass-melting tanks, and hot-blast furnaces (checker bricks). Unshaped silica mixes are used for monolithic structures and repairs.

Silica Bricks. Raw materials for industrial silica brick production are high-grade quartzites or silica cemented quartz sandstones with >97 wt % SiO_2. The raw material is crushed, washed, and sieved. The sieve fractions are mixed to the desired grain size distribution. Small amounts of quartz sand are also used, and 1–4 wt % $Ca(OH)_2$ is added as mineralizer (transformation activator) and bonding agent. Sulfite lye acts as plastifier of the batch and provides sufficient strength for manual or mechanical shaping and drying. The bricks are fired at about 1700–1760 K in tunnel or shuttle kilns for one to three weeks (depending on their shape). The quartz raw material transforms into stacking-disordered cristobalite and tridymite under these conditions. The volume of the bricks increases by 4–5 % due to the higher specific volume of the high-temperature silica modifications. The amounts of cristobalite and tridymite depend on the raw material blend as well as on production parameters, mainly temperature and time of firing [138–140]. Tridymite forms only in the presence of suitable impurities and mineralizers; the longer the duration of firing the more is formed (see Section 1.3.1) [141–144]. The rate of the quartz

transformation varies for the different types of raw materials. It depends mainly on the crystallite size distribution and on the amount and distribution of impurities (Al_2O_3, TiO_2, alkali metal oxides, Fe_2O_3). Quartzite transforms more sluggishly than quartz sandstone with a high content of microcrystalline quartz in the cement.

The burnt silica bricks contain small amounts of residual quartz (<6 wt %) and wollastonite $CaSiO_3$. The latter is a crystallization product of an intergranular glass phase ($SiO_2/CaO/Al_2O_3$). An excess of residual quartz must be avoided because of an irreversible after-expansion (Fig. 15) in service above ca. 1500 K, which is due to the transformation of the residual quartz into cristobalite/tridymite.

The content of residual quartz is easily determined by X-ray powder diffraction [145]. The quantitative determination of cristobalite and tridymite, however, is difficult due to their structural defects [138, 139], and large errors can result if these are not taken into account [146].

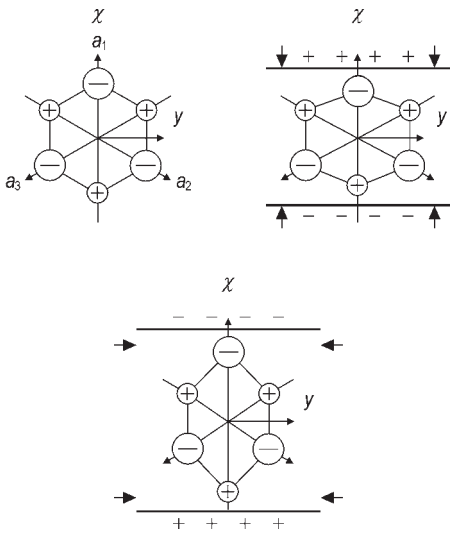

Figure 15. Illustration of the piezoelectric effect in quartz. Left: Simplified structural model of quartz viewed along the trigonal *c*-axis; small circles represent silicon and large circles two oxygen atoms. The trigonal a_i-axes and the orthogonal *x*- and *y*-axes are shown. Middle: Deformation of the structure due to stress applied along the *x*-axis (one of the three polar twofold rotation axes) produces charges on surfaces perpendicular to the *x*-axis (longitudinal direct piezoelectric effect). Right side: Stress applied along the *y*-axis also produces charges on the faces perpendicular to the *x*-axis (transverse direct piezoelectric effect). Change from compression to tension reverses the signs of the electric charges.

Silica bricks expand on heating and reach a maximum between 1075 and 1275 K of ca. 1.3–1.5 vol % and have a small negative expansion at higher temperatures (normally 0.1–0.2 vol %) which is attributed to a structural contraction of the tridymite and cristobalite components [147, 148]. Due to the comparatively low thermal expansion, refractory silica has a very good thermal shock resistance above 875 K. Below this temperature, however, extreme care must be taken on heating and cooling to avoid cracking. A further valuable feature is the extraordinarily good creep behavior of refractory silica under compression at high temperatures. This is attributed to the very small content of liquid phase which is due to the low content of impurities (in particular, < 1.5 wt % Al_2O_3 and < 0.4 wt % alkali). Silica bricks are used up to 1925 K. The corrosion resistance against acid slags is good. However, alkali-containing vapor may cause corrosion by melt formation below 1750 K.

Table 7 gives a survey of the properties of silica bricks. For the production of very dense silica bricks with high thermal conductivity, Si_3N_4 or SiC is mixed into the raw batch. During firing these compounds are oxidized, and the resulting crystalline silica fills the intergranular pores [150, 151].

During operation in a temperature gradient, silica bricks develop zones with different microstructures and silica phases without significant change of shape. Above ca. 1730 K cristobalite predominates, and between 1580 and 1680 K tridymite [147, 152, 153].

The major applications of dense silica bricks are coke ovens, superstructures of glass-melting tanks, and hot-blast furnaces (checker bricks). Unshaped silica mixes are used for monolithic structures and repairs.

Cristobalite sand, powder, and flour are produced from quartz sand by calcination in rotary furnaces at 1800 K or from flint in shaft furnaces with subsequent grinding in ball mills. Another route works with processed sand and addition of mineralizers at 1500 to 1700 K, leading to products with > 99 wt % SiO_2. The former products are used as refractory mortars and ramming mixes in ceramic kilns and for blending with quartz or other mineral sands for various uses (e.g., in foundries) preferably as a modifier of thermal expansion. Heat-insulating

Table 7. Material properties of dense silica bricks [149]

Application	Bulk density, g/cm^3	Apparent porosity, vol %	Cold crushing strength, MPa	Refractoriness under load (differential) T_{05}, °C	Thermal expansion 1000 °C, %	Thermal conductivity 1000 °C, W m^{-1} K^{-1}
Coke oven	1.78–1.90	18–23	30–60	1610–1650	1.3	1.8–2.2
Glass furnace	1.81–1.85	19.5–21.5	30–40	1630–1670	1.4–1.5	1.8–1.9

lightweight (up to 60 % porosity) silica refractories are produced by addition of material that burns off during firing (e.g., sawdust, cork). Diatomaceous earth (see Chap. 3) can also be used as raw material. Burned diatomite consists of about 80 wt % crystalline silica, mainly cristobalite with some quartz. It serves as heat-insulating material for use up to 1200 K.

High-purity cristobalite from processed sand serves as weathering- and exhaust-resistant white filler which has no yellow shade for thermoplastic road marking (flour as pigment, sand as antiskid), for production of plastics, adhesives, wall paint, and texture coatings. Surface treated (preferably with siloxanes) flour is incorporated into silicone rubber and cable coverings and into EVA or PE foils as IR absorber. It is used for glaze frits, engobes, and other ceramics inter alia as modifier of thermal expansion. In silicate chemistry it serves as raw material.

Rice husk ash is prepared by burning the husks at about 800–900 K for ca. 2 h. The husks contain ca. 9–19 wt % noncrystalline silica, the ashes ca. 85 wt %. They are used as additives to Portland cement for reduction of the alkali–silica reaction and the detrimental cracking that is caused by this reaction [154].

Refractory silica cloth is replacing asbestos. It consists of 8–10 mm thick glass fibers with a silica content of more than 96 %.

1.8. Noncrystalline Silica Products

Most of the noncrystalline silica products are treated in Chapters 3–7. Only silica glass and silica fume are briefly described here.

Silica glass is pure vitreous silica with diverse industrial applications. It is produced either by melting natural quartz crystals above 2050 K (fused quartz) or by vapor-phase hydrolysis of $SiCl_4$ in a methane oxygen flame (fused silica). The use of vitreous silica produced by sol–gel processes is restricted to thin-film technologies. The main benefits of silica glass are broad transparency to ultraviolet to near infrared, high resistance to thermal shock due to the low thermal expansion of 5.5×10^{-7} K^{-1} and high chemical corrosion resistance [155]. These properties led to uses as optical material, optical waveguides and chemical apparatus. Silicate glass is treated in detail in → Glass, 1. Fundamentals.

Silica fume is a very fine powder consisting of noncrystalline silica spheres with an average diameter of ca. 0.1 μm. It forms at temperatures of about 2050 K as a byproduct of the reduction of quartz in electric arc furnaces for the production of silicon and ferrosilicon. The silica vapor is condensed and collected to prevent its emission. Silica fume is mainly used as an admixture in cement, concrete, and mortars to improve strength and durability. Due to the small particle size and the large surface area (up to 30 m^2/g), it acts both as a microfiller that reduces the porosity and as a pozzolan which reacts with the calcium hydroxide from the cement [156].

2. Quartz Raw Materials

2.1. Physical Forms and Occurrence

The range of quartz in nature is vast. Table 8 describes the physical forms and Table 9 lists the geological occurrences of raw materials [157–166].

The main characteristics of quartz raw materials are grain size and shape, their distribution functions, surface area and roughness, sorption capacity [163], chemistry, physical properties, and cost. Increasing demand for extremely pure

Table 8. Physical forms of quartz raw materials

Name	Formation and properties	Remarks, synonyms, and trivial names
Idiomorphic quartz	freely grown, euhedral faced, monocrystalline, possibly twinned, transparent colorless or smoky to dark brown or black	rock crystal, smoky quartz
Lump quartz	fragmented, anhedral, monocrystalline, may be twinned, transparent, colorless, smoky, milky, or white	chunk quartz, lascas, brazil pebbles, lump silica
Quartz pebbles	weathering product from quartz veins, worn by action of water, smoothly rounded, mono- or polycrystalline, transparent to white or yellowish white or gray	if transparent: rhinestone or rheinkiesel, grain size 2–60 mm
Granular quartz	xenomorphic product of natural (weathering) or industrial processing from granitic–pegmatitic rocks, monocrystalline, may be twinned, transparent to translucent, yellowish, gray, or smoky	grain size 0.5–1 mm [159]
Quartz sand	unconsolidated, wind- or water-eroded and transported weathering product of fragmented rocks, grumbled into mono- or polycrystalline grains, rounded or angular anhedral, the majority of grains are discernible with the naked eye, white to yellowish in bulk, in the individual grain transparent to translucent	silica sand, grain size 0.06–2.0 mm
Quartz powder	unconsolidated product of grinding or milling of coarser quartz, individual grains not discernible with the naked eye, white opaque in bulk	quartz flour, silica powder, silica flour, grain size 0.002–0.06 mm
Quartz rock	intergrowth of quartz grains or consolidated by cementation of grains	quartzite, quartz sandstones, see text and Table 5

quartz for silica glass production and in the quartz oscillator industry, and the growing use of refined grades of sand makes consistency and long-term availability important [161].

Impurities and their accessibility to refining processes are of major importance. In most cases, trace element analysis gives bulk composition and no information about the location of impurities in the microstructure. This, however, is essential for choice of quartz processing methods. Figure 16 shows the principles of impurity distribution in a crystal.

Quartz gravel and sand are the most important raw materials on a volume basis; the construction industry consumes about 95 % of production (ca. 65 % structural and ca. 30 % civil engineering). In 1995 Germany produced

Table 9. Geological occurrence of quartz raw materials

Name	Occurrence	Remarks
Idiomorphic quartz	grown in veins, vugs, vesicles, and shear fissures of igneous, metamorphic, or sedimentary rocks	chemical purity and transparency increases from base to top of crystal
Vein quartz	xenomorphic and dense quartz filling of veins, cracks, faults, dikes, bedding planes, fractures, or joints in zones of structural weakness of igneous, metamorphic, or sedimentary rocks	
Pegmatite quartz	polymineralic veins, most frequently of granitic composition (quartz, feldspar, mica), however, it may be of any other composition, or coarse crystalline areas in granites or other igneous plutonic rocks but also in metamorphic rocks with all transitions to the rock itself	
Quartz from disseminated hydrothermal deposits	polymineralic fillings of dispersed vein systems in large volumes of rocks, dissemination along cracks and fractures or in zones of high permeability for hydrothermal solutions	quartz frequently contains fluid and solid inclusions [174, 205] (Fig. 16)
Quartz gravel and sand	occurrences are widespread and diverse, mainly in cretaceous, tertiary, and alluvial beddings; detrital product obtained from rocks by various weathering, transport, selection, and bedding conditions [204–207]	

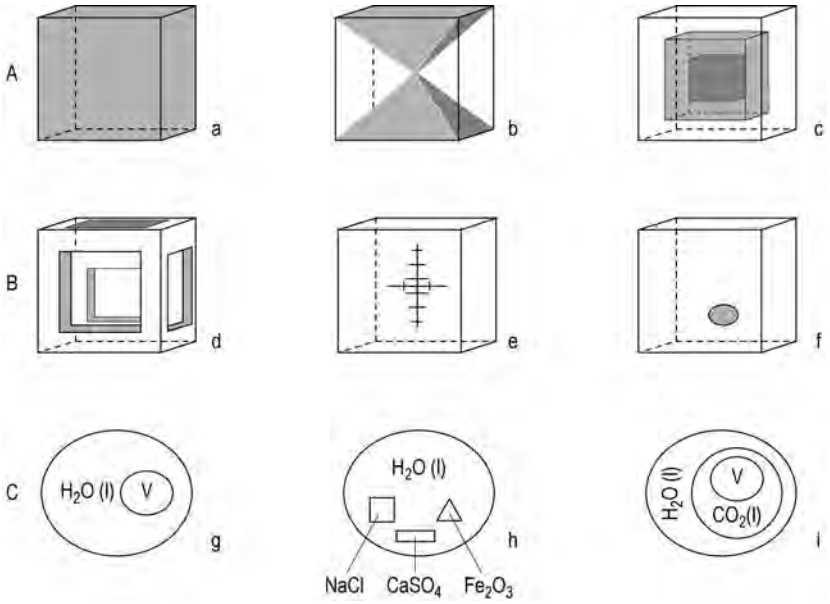

Figure 16. Principles of impurity distribution in a single crystal. A) Structural incorporation a) Random; b) Growth sector specific; c) Zonal B) Microstructural inclusion d) Skeletal growth and face specific adsorption, possibly with subsequent overgrowth; e) Dendritic growth or precipitation; f) Accumulated and accidentally ingrown, e.g., in fissures or dendritic cavities. C) Types of fluid inclusions in quartz [174–176].
v = vapor, l = liquid; squares, rectangles, and triangles represent crystallites.

18×10^6 t of sand (56 % river sand, 44 % high-purity sand with > 98 wt % SiO_2). The overwhelming part of the sand supply for Europe comes from Belgium, Germany, and the Netherlands. In 1995 the EU produced ca 16×10^6 t of high-purity sand. The main consumers were the float- and container-glass industry with rising customer specifications [167]. Recycling of glass reduced the demand for sand in container glassworks.

Tripoli contains ca. 98–99 wt % SiO_2. It occurs in sedimentary strata as a leaching product of calcareous cherts or siliceous limestones. White tripoli is low in iron impurities (< 0.1 wt % Fe_2O_3); rose or cream tripoli contains up to 1 wt % Fe_2O_3. It consists of submicroscopic quartz crystallites. Particles with sizes 5 to 100 μm are crystallite aggregates. White Southern Illinois Tripoli has the composition SiO_2 99.5, Al_2O_3 0.009, Fe_2O_3 0.025, CaO 0.15, TiO_2 0.005 wt %.

Kieselerde is a natural mixture of quartz and kaolinite [168]. The mineralogical and chemical composition of Kieselerde from Neuburg (Donau) follows [168]: 62–84 wt % quartz, 10–30 wt % kaolinite (content increases with decreasing grain size), 6–8 wt % accessorial minerals; 78–87 wt % SiO_2, 8–14 wt % Al_2O_3, < 1 wt % Fe_2O_3, 60 ppm P, and 35 ppm S (both relative to Si).

Chalcedonies (Section 1.3.1) are classified according to their deposition as wall-banded Ch-w or horizontally-banded Ch-h (Table 3). According to the optical character of their fiber elongation, two varieties can be distinguished: chalcedony with length-fast elongation: Ch-w_{LF} and Ch-h_{LF} and quartzine Ch_{LS} with length-slow elongation. Chalcedonies occur in various geological environments, filling veins, vugs, and vesicles in volcanic rocks, sediments, ore deposits, or covering and impregnating plants in regions with volcanic activity [169, 170].

Ch-w is bluish gray in reflected and brownish in transmitted light due to Rayleigh scattering. It has a brown color if it was impregnated with ferrous humic acid waters (then called sarder). It possesses an open submicroporosity which makes it artificially impregnable with coloring solutions and allows penetration of liquid

impurities. The microstructure is monomineralic, of high toughness, and high purity, which makes it a good material for milling devices, mortars, and bearing stones.

Chalcedony is slightly weaker than quartzine. If quartzine is interstratified into chalcedony layers, it forms a raised abrasion relief [171]. Since the resistance to HF etching is reverse, etch leveling is possible. Ch-h has almost no open porosity.

2.2. Processing

Impurities may be fixed on the surfaces of the individual quartz crystals or grains. Then they are rather easily accessible for removal. If they are included as minerals or fluids in the microstructure (Fig. 16) [163, 172, 173], the crystals must be crushed for removal. If the impurities are incorporated into the crystal structure, dissolution of the crystal is required for removal. Detrimental accessory minerals in quartz sands are mainly rutile, zircon, tourmalines, magnetite, hematite, ilmenite, chromite, Mn oxides, feldspars, and clay minerals.

Purity grades of processed natural quartz raw materials are [159]:

Grade	Impurity content (ppm Si)
Low	> 500
Medium high	300–500
High	2–50
Ultrahigh	1–8

Processing of coarse monocrystalline quartz to lumps or lascas [159]:

- Size reduction (weight specification for lascas ca. 15–50 g)
- Under water: sorting out of pieces with visible inclusions; under UV light: fluorescent pieces
- Under visible light: sorting of different grades of transparency.

Product: various grades of lascas.

A special process is γ-irradiation-aided selection of lascas [159]:

- Irradiation with doses $\leq$ 1 Mrad
- Color sorting [177]; the depth of color is mainly a function of the Li/Al trace element concentration ratio (Fig. 17)

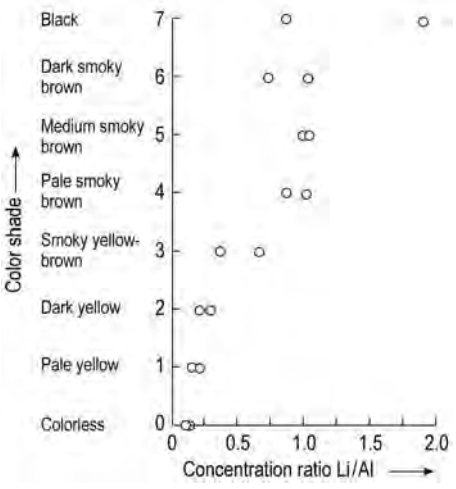

Figure 17. Irradiation color (γ radiation, 1 Mrad) and Li/Al concentration relationship for initially colorless first-grade lascas (Minas Gerais, Brazil) [159].

Processing of quartz rocks, vein quartz, and quartz from disseminated hydrothermal deposits:

- Breaking and sieving.

Product: quartz of low chemical purity for production of high purity silicon compounds.

Processing of granular quartz from deeply weathered feldspathic rocks [159]:

- Crushing and grinding
- Multistage flotation
- High-field magnetic separation
- Chemical treatment with dilute sulfuric or oxalic acid or chlorination at ca. 600 K
- Sieving

Product: medium- to high-purity granular quartz (type QUINTUS, Unimin Corp. New Canaan, Connecticut, USA).

- Acid (HF) leaching
- Elutriation with deionized water to pH $\geq$ 6
- Vacuum drying
- High-field magnetic separation
- Chlorination at ca. 1400 K

Product: high-purity granular quartz (type IOTA, Unimin Corp., New Canaan, Connecticut,

Table 10. Trace element analyses (ppm/Si) of UNIMIN-JOTA-quartz grades [208]

	Li		Na		K		Ca		B		Al		Fe	
Grade	min.	max.	min.	max.	min.	max.	min.	max.	min.	max.	min.	max.	min.	max.
Standard ST	0.7	1.5	0.9	1.5	0.7	1.5	0.4	1.5	0.08	0.10	15.2	22.0	0.3	1.5
JOTA-4	0.2	1.0	1.0	1.3	0.4	1.0	0.6	1.0	0.04	0.05	7.9	10.0	0.6	1.0
JOTA-6	0.2	0.3	0.1	0.2	0.1	0.2	0.5	0.7	0.03	0.04	7.9	9.5	0.2	0.3

USA; Table 10) preferably for production of silica glass implements: halogen and high-intensity discharge lamp tubings and semiconductor applications such as Czochralski crucibles and diffusion tubes.

Processing of quartz gravel:

- Separation of sand
- Washing
- Sizing and drying

Product: filter pebbles, beach pebbles for milling stones, gravel for concrete.

Processing of quartz sand [178, 179] varies depending on the required grade. Process steps are:

- Washing in water to remove loose impurities
- Friction washing (attrition)
- Crushing of agglomerated grains in water
- Rubbing off strongly adhering impurities (iron oxides and oxide hydrates, clay minerals)
- Screening
- Multistage flotation to remove accessory minerals
- Chemical treatment with aqueous acids (sulfuric, oxalic, fluoric)
- Chlorination at ca. 600 K
- Physical treatment by magnetic and electrostatic separation of iron oxide and feldspar contaminants
- Surface treatment with amino-, epoxy-, methyl-, methacryl-, or vinylsilanes [180, 181].

Sand for use in cement-based products should be free of chlorides and clay minerals. Sand for special mortars must be freed from organic residues by calcination [182].

Quartz powders are produced by dry grinding in encapsulated mills with chert or corundum lining and balls. Refining of powder from high-purity vein quartz gives grades with 8–50 ppm Fe/Si.

Processing of quartz rocks includes breaking, milling, sieving, washing, and sizing [178, 179].

Biological removal of iron impurities with cultures of acid-producing bacteria or fungi (e.g., *Aspergillus niger*) on a nutrient of molasses is discussed in [183].

2.3. Uses

Important uses of quartz raw materials or semifinished materials are listed below [161]:

Use	Raw or semifinished material
Abrasives and grinding media	sand, powder, tripoli, novaculite
Ceramics	quartzite, quartz-cemented sandstone, sand, powder
Chemicals	sand, powder
Construction of buildings and roads	gravel, sand, powder, quartzite, sandstone
Fillers, extenders	powder, tripoli
Filters	gravel, sand
Foundry	sand
Gems	monocrystalline quartz, chalcedony, agate, chert
Glasses, enamels, glazes	sand, powder
Hydrothermal growth of quartz single crystals	lump quartz, granular quartz
Metallurgy	quartzite, sandstone, sand, powder
Milling	silex, chalcedony, flint, quartzite
Optical and oscillator devices	monocrystalline man-made and natural quartz
Silicon metallurgical grade, silicon alloys	lump quartz, quartzite, quartz-cemented sandstone
Vitreous silica	lump quartz, granular quartz, sand
Well fracturing	sand

Abrasives and Grinding Quartz Quartz sand and powder are used for grinding, scouring, and polishing. The conchoidal fracture, hardness,

and brittleness provide and maintain particles with sharp cutting edges during use. The use of quartz in sandblasting is decreasing due to health hazards (Chap. 9). Quartz sand is also of declining importance for sandpaper. Quartz powder is utilized in abrasive soaps and in scouring powders. Sandstones are used for grinding. Tripoli is friable and its grains have no sharp edges. Tripoli grades with 98–99 wt % SiO_2 are used for polishing [184]. Novaculite (Table 5) from Arkansas and Missouri, USA, has a microstructure of minute angular quartz grains with open porosity. It is used as oil-soaking whet- and honing stone. Whetstone grades range in porosity from 0.1 to 15 % [184].

Ceramics and Refractories. Batches for stoneware, porcelain, fireclays, and aluminum silicate refractories contain quartz as a nonplastic filler and glass former. White-burning, low-iron quartz powders produced from sand, flint, or quartz rocks are used. Flint is calcined before grinding. In pottery and earthenware, quartz sand and powder act as nonplastic fillers [185]. For silica refractories, see Section 1.7.2.

Chemicals. A wide range of chemicals is produced from quartz. Here, only one important product that is representative of different reaction processes and reaction temperatures, is briefly described.

Sodium or potassium silicate (waterglass; → Silicates) are melted from quartz sand and the alkali metal carbonates. Usually, the sand is of container-glass grade with < 0.1 wt % each of Al_2O_3 and CaO and a very low iron content (< 0.02 wt % Fe_2O_3). Very high purity products require sand with < 0.02 wt % Al_2O_3 and CaO each. Melting is performed in tank furnaces at ca. 1700 K (furnace route) [186].

Waterglass from the hydrothermal route is produced in autoclaves by reaction of quartz sand with aqueous NaOH solution at ca. 430–500 K.

Construction of Buildings and Roads. Quartz sand and gravel are an integral part of asphalt, mortars, and concrete. For good rheological behavior sand or gravel should consist of well-rounded grains or pebbles. Optimized grain size distribution minimizes water demand and shrinkage in the setting reaction and contributes to the development of high binder strength. Quartz sandstones with various cementing material and quartzites have long be used as building stones [187]. Bricks and tiles are fired from mixtures of quartz sand and clay.

Since 1894 when the first calcium silicate (CS) units were industrially produced [188], their use for masonry in central Europe has rapidly developed [189].

Quartz sand (fluviatile) from a broad coastal strip of the Netherlands and North Germany (about 18×10^6 t/a) is processed according to the following (simplified) process scheme:

- Mixing and pretreatment of sand, lime, and water
- Densification and shaping by pressing
- Hardening in the autoclave with steam or water at about 16 bar and 475 K for ca. 6–8 h

In the hardening reaction, the calcium silicate hydrate (CSH) phases, preferably tobermorite and xonotlite, form a cement between the quartz grains. This gives the units a high compression strength. Essential process parameters for the quartz sand are: grain size distribution (sieve line) and the shape and surface of the grains. The accessory minerals [mostly (in wt %) ≤ 5 feldspars and micas, ≤ 3 clay minerals, ≤ 3 calcium carbonates, ≤ 1 iron manganese oxides and oxide hydrates] [190] take part in the hardening reaction. Fe and Mn enter the crystal structures of the CSH phases as doubly charged ions and produce almost no hue. Humic matter spoils the process. About 1.5 t of sand is needed for the production of 1 m^3 CS units. In central Europe CS masonry is appreciated mainly due to its high raw density and sound absorption, its heat capacity and resistance against fire, and the good compression strength which allows the construction of space-saving walls.

Oil Well Cementing. Heat in the depth of oil wells converts the calcium silicate hydrate (CSH) gel of tobermorite character in the settling portland cement with its good cementing properties into α-dicalcium silicate hydrate (α-C_2SH). This causes the development of a porous and weak microstructure with open pathways for corrosive fluids. Addition of quartz sand and powder prevents this deteriorating transformation. Portland cements for use at very

high temperatures contain 35–50 wt % of SiO_2 additives [191].

Fillers and Extenders [192–194]. Quartz and cristobalite fillers are hard and strong with high resistance against chemicals and weathering. They give the final product a characteristic dependence on thermal expansion. In paints, quartz increases the acid resistance and improves flowability, durability, and wear resistance. Silane-treated fillers [195] are used for corrosion prevention in primers instead of heavy metal pigments [196]. In engineering plastics and resins, compressive and flexural strength and thermal shock resistance are improved. The insulator character of quartz and its resistivity to surface leakage currents make it a valuable filler for epoxy resin encapsulations, high-voltage insulation, bushings, switch cases, cast resin transformers, and for filling and fixing of coils. For example, reaction hardening resins may contain up to 80 wt % SiO_2. Silane-treated quartz powder in epoxy castings reduces shrinkage and electrical loss, increases E moduli, compression strength, and thermal conductivity [197, 198]. Quartz is used as a filler in rubbers instead of carbon black when colors other than black are required. In tire linings, it gives improved heat aging, adhesion, and tear strength.

Filters. Quartz pebbles, preferably monocrystalline, and sand are the main filter materials for drinking water purification and softening.

Foundry Technology [160, 178, 179, 199]. Quartz sand is used in molds and cores. Refractoriness (i.e., the temperature at which sintering begins; ca. 1500–1700 K, depending on the content of feldspar), thermal shock resistance, cohesiveness in the moist state, and high-temperature strength are the most important properties. For cast iron, the mold must contain $>$ 85 wt % SiO_2 and for steel castings 95 wt %. Granulometric factors such as particle size distribution, grain shape, state of grain surfaces, and surface area are also important. Coarse sand with low surface area requires less binding agent (usually montmorillonitic clay). Monocrystalline well-rounded grains ensure good permeability to gases evolved during casting. Mold surfaces made of fine sand give smooth molding surfaces that do not require machine finishing. The sands may naturally contain enough clay minerals for good mold strength, or require additional binders, which increases costs.

Specifications for foundry sand grades of different refractoriness:

Beginning of sintering, K	$>$ 1775	1575–1775	$<$ 1575
Quartz, wt % (rest: feldspar and clay minerals)	>99	95–99	$<$ 95

Glasses, Enamels, and Glazes [161, 167, 186, 200–204]. Different types of glasses and enamels require various grades of quartz raw materials. The silica content of glazes is mainly supplied by the silicate ingredients (feldspar, clay). If additional SiO_2 is required, quartz or flint powder is added.

Hydrothermal Growth of Quartz [159] (Section 1.7.1). Brazilian lascas were used worldwide as nutrient chips until the Brazilian quartz embargo in 1974. Since then, many other sources for high-purity low-cost lump quartz and granular nutrient were made accessible.

Metallurgical-Grade Silicon, Silicon Alloys and Silicon Carbide (→ Silicon; → Silicon Carbide, section 4.2.5). For chemical- or metallurgical-grade silicon, quartz lumps or pebbles (25–150 mm) are reduced with coke in electric-arc furnaces. The lumps and pebbles must not decrepitate during heating and therefore should preferably be monocrystalline and free of fluid inclusions. The grade of quartz raw material depends on the required grade of the products. Metallurgical-grade silicon with 99.0 wt % Si requires (in wt %): $\geq$ 99.0 SiO_2, $\leq$ 0.2 Al_2O_3, $\leq$ 0.1 Fe_2O_3, $\leq$ 0.1 MgO and CaO each, $\leq$ 0.02 TiO_2.

Low-grade silicon (98 wt % Si) for steel and aluminum production needs quartz with (in wt %): 98 SiO_2, $\leq$ 0.4 Al_2O_3, 0.2 Fe_2O_3, $\leq$ 0.2 MgO and CaO each, $\leq$ 0.1 P_2O_5, $\leq$ 0.002 TiO_2.

Production of 1 t metallurgical-grade silicon requires ca. 2.5 t of quartz. The worldwide silicon production is ca. 650 000 t/a.

Metallurgy. Quartz in the form of lumps or granules of vein quartz, quartzite, or sandstone is used as a flux in melting metal ores, for slagging iron oxides and basic oxides, and for balancing the silica/lime ratio of blast furnace burdens. In

both cases, the SiO_2 content must be >90 wt % with lumps and granules in the size range of 0.8–2.5 cm.

For welding fluxes, quartz powder is used with a controlled grain size distribution of < 0.25 mm with an average of 0.06 mm for coated standard electrodes. The size of quartz particles in agglomerated fluxes must be < 0.06 mm.

Milling. Nodular chert (flint, silex) and very finely crystalline quartzite with > 96 wt % SiO_2 and homogeneous microstructure serve as linings for mills. Rounded flint nodules are preferably used as grinding pebbles.

Belgian silex consists of chalcedonic silica with evenly distributed calcite as secondary mineral phase and represents a material with high overall toughness. Yugoslavian silex has a coarser microstructure and sometimes contains coarse quartzite but is nevertheless of very good durability. Quartzite can only be used if it is free of accessory minerals. Translucent iron-free chalcedony from agates is used in ball mills and mortars for size reduction of high-purity quartz and silica glass.

Quartz for Optical and Oscillator Devices. Natural monocrystalline idiomorphic quartz is preferably used for optical devices as wafer plates, Brewster windows and prisms, birefringent filters, and tuning elements for laser optics. Only small amounts of man-made quartz are used in these applications. Oscillator quartz devices, however, are almost exclusively made from man-made quartz, for reasons of quality (low damping) and cost advantages.

Vitreous Silica. Transparent silica glass is melted from lascas or granular quartz with an impurity content < 30 ppm, the latter being by far the most important feed. Translucent to white opaque fused silica is produced from quartz sand with an impurity content of < 300 ppm. In both cases low contents of aluminum and iron impurities are essential.

A titanium content indicates the presence of submicroscopic rutile crystallites, which cause bubble problems in transparent silica glass during tube drawing. Silica glass for semiconductor uses, if not produced from high-purity silicon, must be very low in heavy metal impurities.

Well Fracturing. For hydraulic fracturing of oil, gas, or geothermal wells, a fluid with suspended quartz sand is pumped at high pressure into the well. Existing openings are enlarged and new voids are created. When the fluid is withdrawn, the remaining sand holds the fractures open. Frac sand must have >98 wt % SiO_2 and well-rounded grains to make placement easier and to provide good permeability. It must consist of single-crystalline grains which are clean and, in particular, free of adhering feldspar, clay, or carbonate minerals. The solubility in hydrochloric acid (a measure of the carbonate content) must be < 0.3 wt %. The content of soft particles must be < 1 wt %.

3. Diatomites

3.1. Introduction

The term diatomite (kieselguhr) refers to sedimentary rocks that are mainly composed of the skeletons of single- celled diatoms.

The low density, high porosity — and thus high absorption capacity for liquids — low thermal conductivity, and outstanding filtration properties make diatomite a versatile raw material [209–211].

Deposits with similar petrographic character or analogous physical properties, named according to their origin or area of application, include siliceous earth, "Bergmehl", "Saugschiefer", "Polierschiefer", and tripolite, not all of which are true diatomites.

The designation "tripolite" is derived from the ancient name *terra tripolitana* (after the city of Tripolis). The name referred mainly to minerals used as grinding and polishing agents, but also as lightweight building blocks. Today, the term tripolite refers to extremely fine-grained quartz pelites of inorganic origin [212].

3.2. Formation, Composition, and Quality Criteria [229–231]

Diatoms can be described as being almost "ubiquitous", occurring in marine, brackish, and freshwater environments.

The plant organisms possess a silicified membrane and vary in size between several micrometers and ca. 2 mm (generally 10–150 μm).

The skeletons are composed of opal-like, amorphous silica ($SiO_2 \cdot x\ H_2O$) and exhibit a wide range of porous fine structures and shapes. Including fossil forms, at least 15 000–20 000 different forms have been distinguished.

Rock-forming processes involving diatoms occurred worldwide from the Upper Cretaceous period onwards. Commercially exploitable deposits have been formed since the tertiary period.

The deposits are associated with sedimentation areas in which nutrients were abundant and the supply of silicates or dissolved silica was sufficient that a rich diatom flora developed and the frustules of the dead organisms accumulated to an appreciable thickness on the bed of the water body.

Such conditions are found worldwide, mainly in areas with volcanic activity, but also to a lesser extent in lakes with a largely decalcified environment and intensive chemical weathering of quartz sands or silicates (e.g., the German diatomite deposits) [212, 213].

Formation of diatomites of considerable thickness also occurred in marine coastal areas with continual subsidence, a periodical barrier to the open sea, and a regular supply of nutrients [214]. In addition, diatomites of brackish origin were formed in former saltwater lakes.

Important quality criteria for crude diatomite include the particle-size distribution, shape, and fine structure of the diatoms (Fig. 18). However, these can be altered with regard to their structural framework (and porosity) by calcination (see Section 3.4) [215, 216], which is important for the various applications as filtration agents. Furthermore, the chemical and mineralogical composition plays an important role, since higher contents of certain components can limit economically viable processing and refinement of the crude product.

Apart from water and organic substances the most frequent additional components of diatomites are quartz, calcium carbonate, and clay minerals.

The content of water and organic substances is only of minor significance for quality assessment, since they can be removed by drying or calcination.

Quartz sands or other rock fragments of similar particle size can be removed by air classification. In this respect, the conventional specification of the SiO_2 content of a crude diatomite is not very informative. For the assessment of a diatomite it is not the total SiO_2 content which is decisive, but the content of opal (diatom skeletons).

In contrast, the presence of fine-grained carbonates [$CaCO_3$, $CaMg(CO_3)_2$] in amounts greater than 5–10 mol % is problematic because they form complexes during processing which adversely affect the filtration properties and lower the chemical inertness.

Clay minerals restrict the range of applications, but are advantageous for the production of insulating or refractory bricks or for use as powders.

Higher iron contents, particularly as pyrite or markasite, require refinement by calcination (see Section 3.4). The color of the diatomites becomes reddish-gray or pink due to conversion into Fe_2O_3. The filtration properties are hardly influenced, whereas the use as fillers can be affected considerably by this coloration. In the latter case, a Fe_2O_3 content of > 5–$6\,\%$ can already be a limiting factor.

3.3. Occurrence and Mining

Diatomite deposits are distributed worldwide. Their economic exploitability and market potential depend on numerous factors such as mining conditions, and processing and transport costs. The size and quality of the deposit, exploitation costs, transport conditions as well as the question whether the diatomite is for a domestic market or whether it is to be exported play a significant role. In 1995, the world demand for diatomite was ca. 1.2×10^6 t/a [217].

The largest diatomite deposits in the world are found in the United States in the district of Lompoc, California. These are upper Tertiary (Miocene) marine deposits with an economically exploitable diatomite thickness of ca. 300 m. In addition, large quantities of marine and freshwater diatomites are mined in Georgia, Mississippi, Nevada, Oregon, and Washington. In 1986, the United States accounted for about one-third of world production (575 000 t), followed by Rumania, the CIS, and France, with outputs of $(246\text{–}272) \times 10^3$ t (1986). The production in Rumania and the CIS is almost entirely used in the building construction industry. Further, noteworthy deposits and production sites are located in

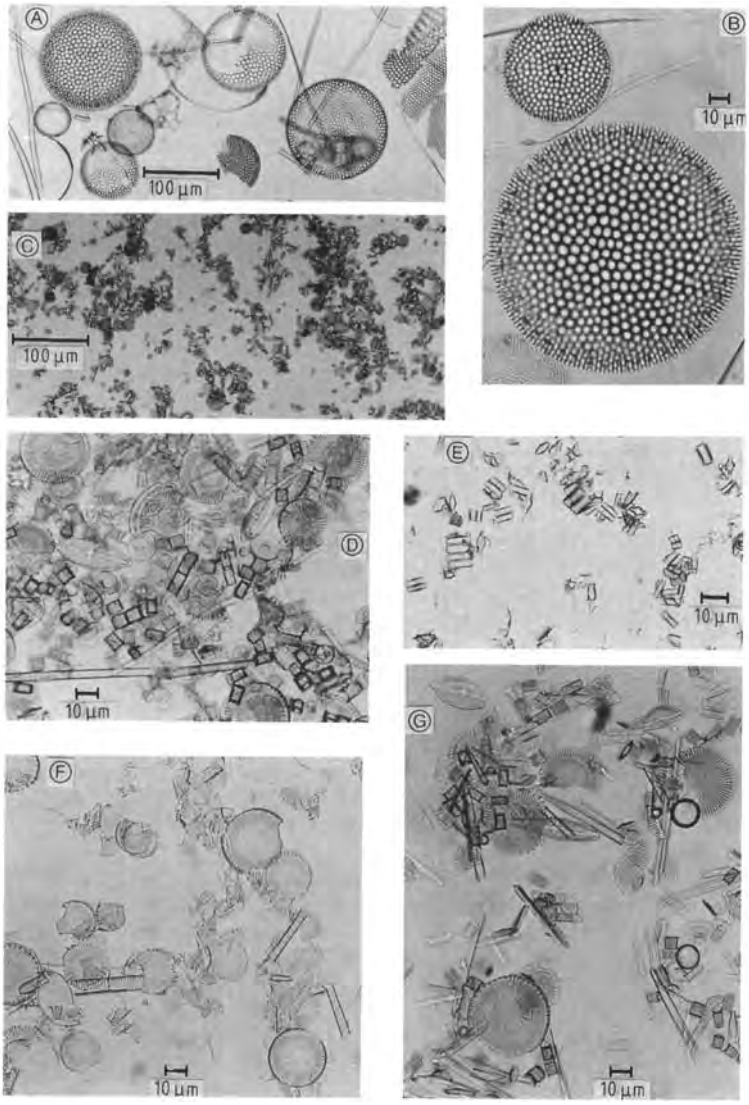

Figure 18. Light micrographs of various diatomites (diatom fraction)
A), B) Lompoc, California, United States; C) Myvatn, Iceland; D), E) Munster-Breloh, Germany; F) Hetendorf/Hermannsburg, Germany; G) Neuohe/Unterlüß, Germany

Algeria, Argentina, Australia, Brazil, Germany, Iceland, Italy, Kenya, Korea, Mexico, Peru, and Spain, whereby in several of these countries the export of diatomite is of no significance [218]. Danish "Moler" is a clay-rich diatomite (diatomaceous earth), which is produced and exported in considerable quantities (63 500–72 600 t/a). It is used predominantly for the production of insulation materials (e.g., fire-resistant insulating bricks).

The only large, economically workable diatomite deposits in Germany are freshwater formations of Pleistocene age. They are situated on the edge of the Lüneburger Heide in the area of Hetendorf/Hermannsburg, Neuohe/Unterlüß, and Munster-Breloh as well as in the Luhetal (Bispingen/Hützel/Schwindebeck). Here industrial usage began with the establishment of the first open-cast mine in 1863. Thus, German diatomite mining represents the earliest modern

exploitation of this raw material. Up to World War I almost the total world requirement could be met, with an export quota of $> 30\,\%$.

Diatomite is generally mined in open-cast mines, occasionally also by subsurface or underwater mining (Myvatn, Iceland). Mining by hand is now rare (Third World countries). Almost everywhere, modern, cost-effective mining methods are used, with excavators and wheel/front loaders, and trucks or conveyor belts for transport.

3.4. Processing

Worldwide, the processing methods for crude diatomite differ only slightly from one another. The most important principle is minimization of mechanical damage to the structure of the diatom skeletons. Hollow forms should not be destroyed and pores not blocked (e.g., by sintering during calcination). The high porosity, the most important property of diatomite, must be retained. The processing steps are shown in Figure 19.

Preliminary size reduction of crude material is carried out with spiked rollers, charging boxes, or sieve kneaders to give a uniform grain size that ensures even heat transfer during further treatment. This is particularly important because of the low thermal conductivity of diatomite.

The following types of processed diatomite are produced.

Dried Diatomite [*61790-53-2*]. Depending on the climatic conditions at the production site, the crude diatomite from the deposits is either stored in the open for predrying or transported immediately to storage hoppers. Crude diatomite contains 30–65 % water, which is removed in countercurrent driers. Simultaneous grinding and drying is also practiced, whereby preheated air is blown into the grinders. However, this is only possible for crude products with a low moisture content. Drying is followed by gentle grinding and screening. Granulation gives products that are used as absorbents (e.g., for oil) or as pet litter.

If the starting material is of high purity and has a low content of organic substances, the dried diatomite can also be used as a filtration agent or catalyst support. These diatomites vary in color

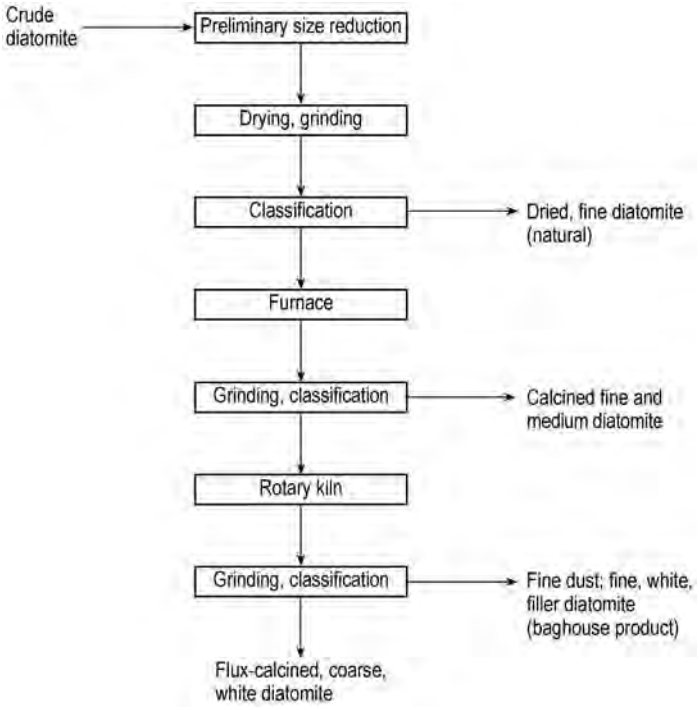

Figure 19. Diatomite processing

from white to yellowish or gray-brown, depending on their origin, and consist predominantly of amorphous silica with a low crystalline content (generally $< 3\,\%$).

Calcined Diatomite [*91053-39-3*]. To remove organic substances and alter the particle size, dried diatomite is calcined in gas- or oil-fired rotary kilns at 800–1000 °C. During calcination, the diatom frustules and their fragments are hardened and partially agglomerated by sintering. The degree of sintering can be controlled by altering the temperature and duration of the process. The diatomite is then ground and classified by cyclones and sorters into grades with different particle-size distributions (fine and medium calcined diatomites). Iron impurities, present as Fe_2O_3 after calcination, color the products pink or yellowish to dark brown.

The old-fashioned furnaces with several decks, similar to pyrite-roasting kilns, are still used to a limited extent. They have the advantage of a slow calcination process at relatively low temperature which causes little damage to the structure. The kilns are loaded with moist crude diatomite, which is dried on the upper decks, calcined in the middle, and cooled on the lower decks.

Fluidized-bed drying and calcination processes were tested as early as the 1920s, but were unsuccessful due to technical problems. Nowadays modern fluidized-bed technology is also used for the processing of diatomite. Advantages include energy savings, short production times, mild treatment of the diatomite, and more compact design of the plants.

Flux-Calcined Diatomite [*68855-54-9*]. In this process, dried or calcined diatomite powder is calcined with the addition of alkaline fluxes. Sodium carbonate is generally used as flux in amounts of 1–6 %, either mixed with the diatomite before calcination or continuously added during calcination. The calcination temperature is 1000–1200 °C. The addition of sodium carbonate leads to the formation of a sodium silicate glass melt which binds the diatom frustules and their fragments into agglomerates. Since the iron contained in the diatomite is also bound, a white product is formed. The degree of agglomeration can be controlled by varying the temperature, the type and amount of flux, and the reaction time. This process is also known as activation. The high calcination temperatures in the presence of alkali lead to a partial transformation (up to 65 %) of the amorphous silica into cristobalite, a crystalline silica modification. The porosity and the specific surface area are strongly decreased. The annealing and cooling processes are followed by grinding and classification, to give white filter diatomite (the main product) and a dust-like fine fraction which is used as white filler and auxiliary.

Commercially Available Forms, Products, and Producers. Powder diatomite is sold in paper sacks containing 15–25 kg as well as loose in big-bags and silo trucks. Granulated material is available in paper or plastic sacks containing 30 kg, sometimes also in big-bags or silo trucks.

Examples of commercial products are:

Celatom (Eagle-Picher Minerals Inc., Reno, United States)
Celite (Celite Corp., Newark, United States)
Clarcel (Ceca SA, Paris, France)
Dicalite (Grefco Inc., Torrance, United States)
Fina/Optima (Meyer-Breloh, Munster, Germany)
Skamol (Skarrehage Molervaerk a/S Nykøbing, Mors, Denmark)

Table 11 lists the chemical and physical properties of several commercially available diatomites.

3.5. Analysis

Chemical and physical testing begins with the crude diatomite in the mine, continues during the individual production stages, and finishes with the test certificate of the end product. The results of the crude diatomite tests determine the working plan for the different regions of an open- cast mine.

The following analyses and tests are undertaken:

Chemical Analysis. The contents of silica, iron, aluminum, calcium, magnesium, manganese, titanium, sodium, potassium, and, depending on requirements, also other elements are determined after alkaline dissolution or acidic

Table 11. Chemical and physical properties of commercially available diatomites[a]

Property	1	2	3	4	5	6	7	8	9
Color	white-gray	yellow-brown	pink	yellow-brown	brown	white	white	white	yellow-brown
SiO_2, %	89.0	72.5	90.7	87.5	86.0	89.5	90.7	91.5	90.2
Al_2O_3, %	3.5	7.1	3.9	4.3	2.8	4.1	3.9	1.6	2.8
Fe_2O_3, %	0.9	5.0	1.4	2.9	4.7	1.6	2.1	0.7	2.5
CaO, %	1.1	1.2	0.5	1.9	0.6	0.5	1.0	4.4	0.7
Na_2O, K_2O, %	0.8	1.4	0.9	0.8	0.7	3.6	3.5	1.9	0.9
Ignition loss, %	2.0	4.7	0.5	0.7	0.3	0.2	0.1	0.1	0.4
Bulk density, g/L	107	290	120	140	125	229	200	195	209
pH value	7.0	5.2	7.5	6.9	7.0	10.0	9.7	9.5	6.7
Water uptake, %	255	200	250	205	201	156	160	200	196
Specific surface area, m^2/g	19.2	25.4	15.2	13.0	16.1	1.9	1.6	3.0	10.6
Average particle size, μm	14.2	19.3	15.9	14.1	13.9	22.5	30.1	6.5	14.7
Wet density, g/L	228	280	271	255	209	297	290	350	357
Permeability, Darcy	0.06	0.09	0.28	0.09	0.08	1.20	1.60		0.08
Crystalline content, %	2.0	2.2	7.6	9.2	9.8	58.1	59.7	62.7	10.3

[a] 1) American filter diatomite, dried; 2) Danish filler diatomite, calcined; 3) American filter diatomite, calcined; 4) French filter diatomite, calcined; 5) German filter diatomite, calcined; 6) American filter diatomite, flux calcined; 7) French filter diatomite, flux calcined; 8) Spanish filler diatomite, flux calcined, very fine; 9) German regeneration filter diatomite, calcined.

extraction. Filter diatomites for breweries are also tested for beer-soluble iron, calcium, and sometimes other elements [219].

Physical Tests. Water content, loss on ignition (at 1050 °C), bulk density, tapped density, pH value (10 % in water), water absorption capacity, and specific surface area are determined by conventional methods [219]. The particle-size distribution is determined by laser scattering or air-jet screening. For the fine fraction, the sedimentation method is used. The wet density is the density in g/L of a filter cake flushed with water. Since the majority of diatomite is used for filtration, the determination of the permeability is of major importance since it determines the performance and the retaining power of a filter diatomite. In general, the methods developed by the individual producers in which the rate of permeation of water is measured, are sufficient. The company CECA (France) possesses a patent for a permeameter which allows fully automatic measurement. The EBC filter is of simpler construction and allows Darcy values to be precisely measured [220]. Apart from the relative units used by the diverse producers, the Darcy has become generally accepted as the unit for the permeability of a filter agent. For filter materials with the permeability of 1 Darcy the flow rate of a liquid of viscosity of 1 mPa · s is 1 mL · s^{-1} · cm^{-2} filter area for a filter-cake thickness of 1 cm and a pressure difference of 0.1 MPa. Since the permeability can be determined rapidly, this is a suitable method for differentiating between fine, medium, and coarse diatomites [219, 221–223].

The amorphous silica content of a diatomite is determined by the alkali solubility. This property is of significance for catalyst diatomites, or for diatomites which serve as a silica source in cement, or as chemical reagents in other silica-containing products. The specific surface area is used to assess the porosity of a diatomite. It is generally determined by nitrogen adsorption (BET method). The degree of whiteness is measured with a leucometer.

3.6. Storage and Transport

Processed diatomite is stored in steel or stainless steel silos, mostly with a circular cross section and equipped with various discharge aids, since diatomite tends to form bridges. Material packed in sacks is stored and transported on wooden palettes in amounts of 600–1000 kg enveloped by a shrink film, and also in big-bags made from plastic-coated webbing with a capacity of

600–1500 kg. Loose material is transported in silo road vehicles or rail containers with a capacity of 30–75 m^3. The diatomite is conveyed pneumatically or with screw and vibrational conveyors.

3.7. Environmental and Health Protection

Diatomite rarely contains toxic compounds. Since, however, it can contain crystalline modifications of SiO_2 in addition to amorphous silica, dust safety measures are of special significance. This is especially true of white activated diatomites, which can contain up to 65 % crystalline cristobalite. The MAK value for uncalcined diatomite is 4 mg/m^3 and for calcined diatomite, 0.3 mg/m^3. The TLV for uncalcined diatomite is 10 mg/m^3. The International Agency for Research on Cancer (IARC) published a monograph concerning crystalline silica in 1987 [224]. This summarizes the research results concerning the influence of crystalline silica on humans and concluded that apart from causing silicosis it may also cause cancer (see also Chap. 8). Hence, crystalline silica is classified in group 2 A. As a result of this, the diatomite producers founded the International Diatomite Producers Association (IDPA), whose aims include informing personnel working in the diatomite industry and the consumer about these hazards, and to ensure adherence to the work protection regulations by increasing the information available [225, 226]. The regulations of individual countries concerning the handling of dusts containing crystalline silica differ widely:

United States: 29th Federal Statute book 1910.1000 from 19. 01. 1989, which classifies crystalline silica as a hazardous substance and specifies tolerance levels.

EC: Directive 67/548/EEC from 18. 09. 1979 concerning the classification, packaging, and labeling of hazardous substances.

United Kingdom: Control of substances which damage health No. 1857 from 1988.

Germany: UBG 119–4.86 Quartz: protection against dust dangerous to health; UBG 100–4.85, rule G.1.1.: concerning the health precautions; GefStoffV 8.86: labeling regulations.

France: No. 50.1289 from 16. 10. 1950 changed into No. 63 576 from 11. 06. 1963 concerning medical precautions against occupational silicosis. No. 11 453 from 19. 07. 1982 determines the dust concentration in the air of the work place. No. 87–200 from 25. 03. 1987 regulates the content of safety data sheets for dangerous substances. L 231–6 from 10. 10. 1983 lists dangerous substances and determines the packaging and labeling regulations.

Spain: from 27. 11. 1985 classification and labeling of dangerous substances.

Italy: No. 256 from 29. 05. 1974, No. 927 from 24. 11. 1981, No. 141 from 20. 02. 1988 concerning the classification, packaging, and information for hazardous materials.

3.8. Uses

The main uses of diatomite are the following: 60 % of world production is used as a filtration agent; ca. 25 % as filler diatomites, including carrier materials; and ca. 15 % for other uses.

Filtration Agents. Diatomite is used in both pressure and vacuum filters of various designs. Fine, medium, and coarse diatomites, as well as mixtures thereof, are employed, depending on the desired clarity and flow rate [227]. Coarse diatomites are used for precoat filtration in pressure filters in amounts of ca. 1 kg/m^2 of filter area. Fine and medium diatomites are added to the slurry to be filtered, usually in amounts of 100–200 g/m^2 filter area (→ Filtration, 2. Equipment, Chap. 16.). For use as filter aids diatomites must fulfil the following requirements:

1. Good preservation of the diatom structure
2. Optimal particle-size distribution
3. Low content of soluble components
4. High volume and therefore high capacity for materials causing turbidity
5. Formation of filter cakes with high permeability, low compressibility, and low tendency to form cracks

The most important uses of diatomite are for the filtration of beer, wine, fruit juice, sugar cane juice, swimming pool water, solvents for chemical cleaning, wastewater, varnishes, and paints etc. Large quantities of diatomite are used for the production of cellulose-based filter beds, filter candles, and special filter papers.

Fillers. Diatomite is used as filler and auxiliary, for example, to modify the rheological properties of polymers. It increases the thermal stability of bitumen, the Shore A hardness of silicone rubber, and is a reinforcing filler in plastics, rubber, and adhesives. Dust-like, white, activated diatomite is used as a delustering agent, for adjusting the viscosity of paints, and as an antiblocking agent for plastic films.

Insulators. Loose diatomite has long been used for insulating double-walled kilns made from fireclay bricks, as well as for producing insulating sheets and bricks. Danish Moler is especially well suited for producing insulating bricks, since its clay content functions as a ceramic binder. In the VSI process (vacuum super insulation), a special form of diatomite acts as a supporting and insulating layer in double-walled elements that contain a high vacuum. Thus, extremely high insulation values are achieved. The VSI process is being tested for long-distance heat transport.

Absorption Agents. Due to their high capacity for liquids, diatomites are used to produce gas purification agents as well as absorption agents such as cat litter and drying agents. Diatomite is also used to ensure the flowability and to prevent clotting of foodstuffs, fire extinguisher powders, and seeds.

Other Uses. Diatomite serves as a fine scourer in polishes and cleaners such as car polishes, toothpastes, and silver polishes. Diatomite is employed as a catalyst support, for the production of pyrotechnics and matches, as a packing material for the transportation of hazardous liquids, and for the filling of acetylene bottles. In some countries it is used as the silica source for the production of cement and calcium silicate.

3.9. Recycling

Attempts to regenerate diatomite have been undertaken for many years [228]. This is only economically viable for diatomites loaded with organic residues, which can be purified by leaching or calcination. In Germany, the company Tremonis operates a thermal process for recycling filter residues from breweries. The flow diagram of the plant is shown in Figure 20. The regenerated diatomite is classified as fine diatomite. It is added to the fresh diatomite for beer filtration in quantities of up to 50 %.

4. Colloidal Silica

4.1. Introduction

Silica sols are stable disperse systems in which the dispersion medium (or continuous phase) is a liquid and the disperse or discontinuous phase is silicon dioxide in the colloidal state of subdivision. This state comprises particles with a size sufficiently small (< 1 μm) not to appear affected by gravitational forces but sufficiently large (> 1 nm) to show marked deviations from the properties of typical solutions (see → Colloids, Chap. 4.).

The limits given for the colloidal size range are not rigid since they depend to some extent on the properties under consideration [232].

Silica sols are commonly known as *colloidal silica.* Although the ultimate particles that constitute silica gels, xerogels, cryogels, aerosols, and pyrogenic (fumed), precipitated, and coacervated silica have lost their mobility by aggregation. They are also in the colloidal range of particle size and are therefore known as colloidal silicas. However, in this chapter the terms silica sol and colloidal silica are used as synonyms. Figure 21 illustrates the relationship between silica sols, gels, and powders [233].

In commercial silica sols the disperse silica is amorphous and the dispersion medium in most cases is water (aquasols or hydrosols). Dispersions in organic solvents are also commercially available (organosols). Silica sols are fluid and stable toward gelation and settling. Most commercial sols are close to monodisperse and consist of dense discrete spheres with a diameter range between ca. 4 or 5 nm and 100 nm. Also

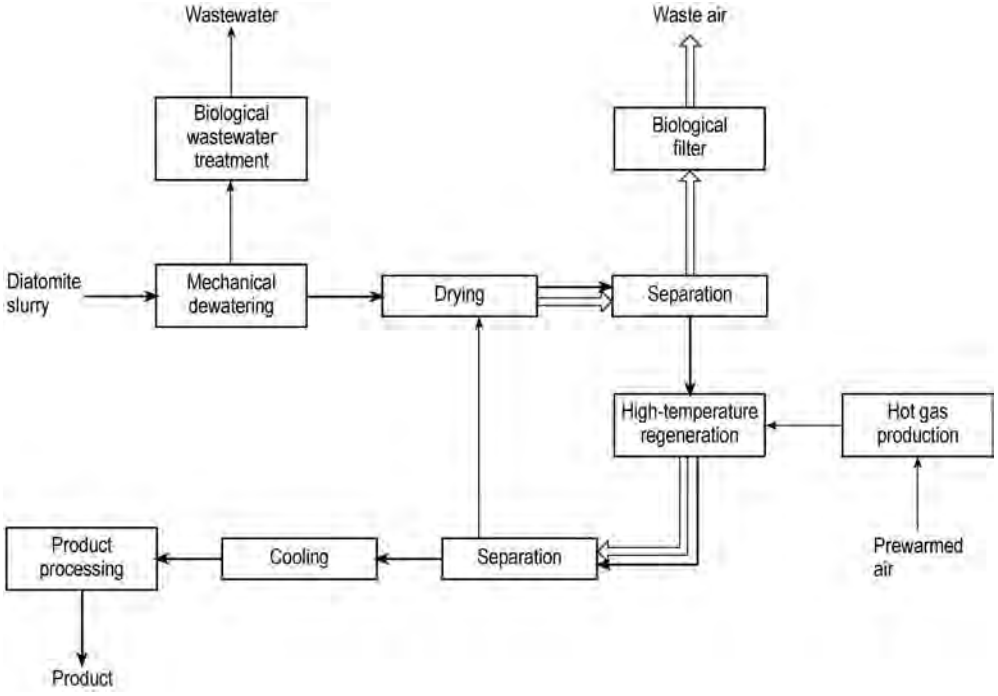

Figure 20. Flow sheet of thermal diatomite regeneration (Tremonis GmbH, Dortmund, Germany)

commercially available in the form of sols or powders are grades with particles between 0.1 and ca. 1.5 μm. Particle size, particle-size distribution, and concentration of solids determine the appearance of sols. Silica sols look milky if the particle size is large and the concentration is high, opalescent if the size is intermediate, or clear and almost colorless if the particles are of the smallest size range.

Although there are earlier references to what are now known as silica sols, it was Graham [234] who coined the term *colloidal* in 1862 to refer to products such as the one he obtained by reacting acid with silicate and removing the electrolytes by dialysis. Stable and relatively concentrated silica sols were not available until the 1930s when I. G. Farbenindustrie first made 10 wt % ammonia-stabilized silica sols [235]. However, the real breakthrough in colloidal silica technology came in 1941 when Bird [236] patented a process for removing the alkali from a dilute solution of sodium silicate by ion exchange. The next landmark in the development of concentrated silica sols was the first process for making colloidal silica particles of uniform and controlled size reported in 1951 by Bechtold and Snyder [237].

By 1990 colloidal silica constituted a growing market valued at an estimated \$ 50×10^6 in North America [238] and € 15×10^6 in Europe [239]. Applications of silica sols are based on characteristics such as particle size, high specific surface area that gives them good binding ability, stability towards gelation and settling, and surface properties. These characteristics enable colloidal silica to be used in a wide variety of applications. Major uses are in investment casting, silicon-wafer polishing, and fibrous ceramics.

4.2. Structure of Colloidal Silica Particles

The building block of silica is the SiO_4 tetrahedron, four oxygen atoms at the corners of a regular tetrahedron with a silicon ion at the central cavity or centroid [240] (see Chap. 1). The oxygen ion is so much larger than the Si^{4+} ion that the four oxygens of a SiO_4 unit are in

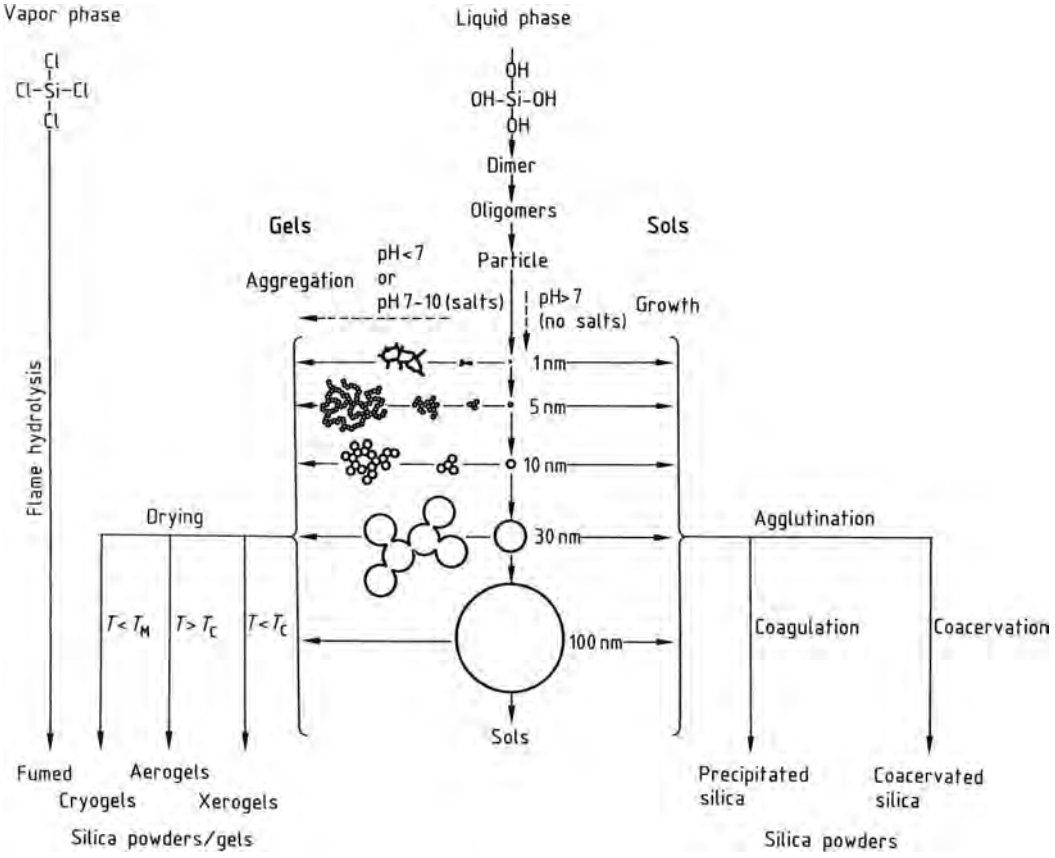

Figure 21. Formation of silica sols, gels, and powders by silica monomer condensation–polymerization followed by aggregation or agglutination and drying [233]
Growth of nascent colloidal particles with decrease in numbers occurs in basic solutions in the absence of salts. In acid solutions or in the presence of flocculating sols the colloidal silica particles form gels by aggregation into three-dimensional networks. Aerogels are made by drying wet gels under supercritical conditions, that is, above the critical temperature T_C and critical pressure of the liquid. Cryogels are made by drying wet gels below the melting temperature T_M of the liquid. Fumed or pyrogenic silicas are formed at high temperature by flame oxidation–hydrolysis of silicon halides

mutual contact and the silicon ion is said to occupy a tetrahedral hole [240]. In amorphous silica the bulk structure is determined, as opposed to the crystalline silicas, by a random packing of $[SiO_4]^{4-}$ units, which results in a nonperiodic structure (see Fig. 22). As a result of this structural difference amorphous silica has a lower density than the crystalline silicas: 2.2 g/cm^3 versus 3.01, 2.65, 2.26, and 2.21 g/cm^3 for coesite, α-quartz, β-tridymite and β-cristobalite, respectively.

Figure 23 represents a two-dimensional random network of a dehydrated but fully hydroxylated amorphous silica particle.

Impurities such as Na, K, or Al, picked up during synthesis of silica aquasols in alkaline media, may be occluded inside the colloidal particles, replacing internal silanol protons (Na, K) or forming isomorphic tetrahedra (Al) with an additional negative charge on the surface or inside the particles (see Fig. 24). Sols obtained by hydrolysis of alkoxysilanes or by dispersion of pyrogenic silica in water or an organic solvent are pure and substantially free of alkali metals or aluminum.

Many of the adsorption, adhesion, chemical, and catalytic properties of colloidal silica depend on the chemistry and geometry of its surface. In 1934 Hofman [243] postulated the existence of silanol (Si–OH) groups on the silica surface. It is now generally accepted that surface silicon atoms tend to have a complete tetrahedral

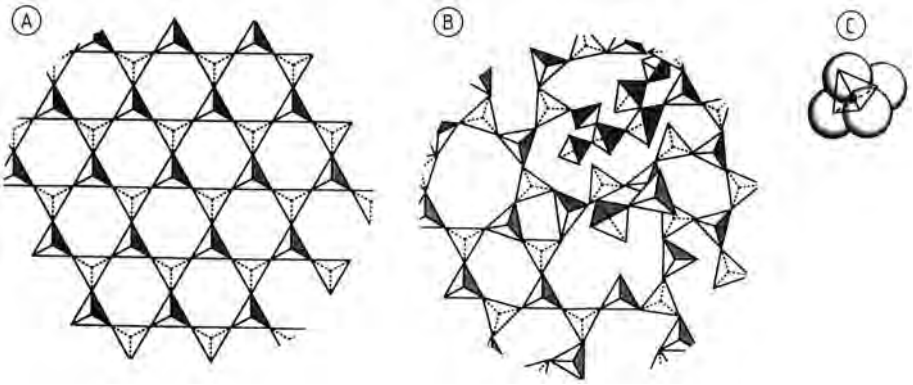

Figure 22. Tetrahedral configuration of crystalline (A) and amorphous (B) silica; (C) represents a silicon atom (filled circle) coordinated by four oxygen atoms (large atom spheres) [241]

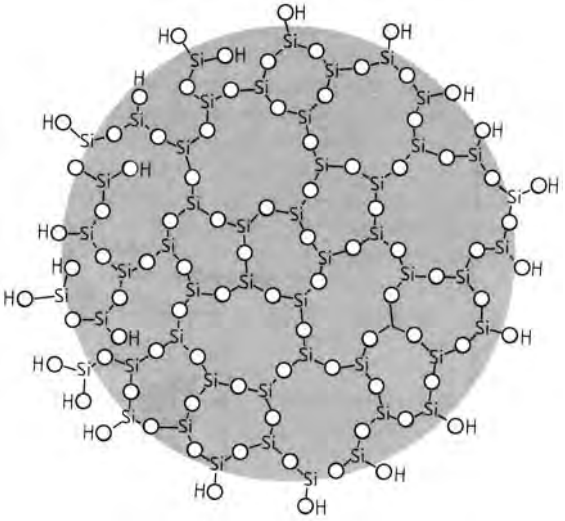

Figure 23. Two-dimensional random network of a dehydrated but hydroxylated colloidal silica particle
Four rules apply [242]: each oxygen ion is linked to no more than two silicon ions. The coordination number of oxygen ions about the central Si cation is 4 (the fourth oxygen not represented in the figure is directly above or below the Si cation). Oxygen tetrahedra share corners, not edges or faces. At least two corners of each tetrahedron are shared. Since the particle is fully hydroxylated each surface Si ion is bonded to one or two hydroxyl ions: the silanol number is 4.6 OH/nm^2. Depending on the method of formation some internal Si ions may be linked to hydroxyl ions. Surface of occluded alkali-metal ion impurities may replace surface or internal protons. Aluminum ion impurities or added modifiers may replace internal or surface tetrehedral Si. The particle surface may be esterified, silanized (silylated), or ion exchanged. The concentration of OH groups on the surface decreases monotonically with increasing temperature when silica is calcined

configuration and in an aqueous medium their free valence becomes saturated with hydroxyl groups forming silanol groups. Under appropriate conditions, silanol groups in turn may condense to form siloxane bridges: ≡Si−O−Si≡.

In the meantime most of the following postulated groups have been identified on the surface or in the internal structure of amorphous silica (see Fig. 25).

1. Single silanol groups, also called isolated or free silanol groups
2. Silanediol groups, also called geminal silanols
3. Silanetriols, postulated but existence not yet generally accepted [244]
4. Hydrogen-bonded vicinal silanols (single or geminal), including terminal groups

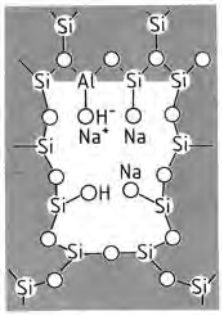

Figure 24. Internal structure of an amorphous silica particle showing an internal silanol group and occluded Na and Al ions

5. Internal silanol groups involving OH groups, sometimes classified as structurally bound water (see Fig. 25 B)
6. Strained and stable siloxane bridges
7. Physically adsorbed H_2O, hydrogen-bonded to all types of surface silanol groups (see Fig. 25 B)

Silanol groups are formed on the silica surface in the course of its synthesis during the condensation polymerization of $Si(OH)_4$ or by rehydroxylation of thermally dehydroxylated silica with water or aqueous solutions.

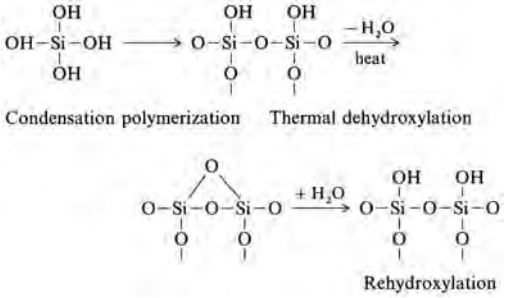

The silanol groups on the silica surface may be classified according to their nature, multiplicity of sites, and type of association [245].

An isolated silanol has an OH group sufficiently remote from neighboring hydroxyl groups that hydrogen bonding cannot occur ($\geq$ 0.33 nm). A silicon site of this kind is designated as Q^3 in NMR Q^n terminology, where n is the number of bridging oxygens bonded to the central silicon. The isolated silanol shows a sharp band at around 3750 cm^{-1} in the IR spectrum [246, 247].

Geminal silanols are silanediol groups located on Q^2 silicon sites. Their existence was postulated by Peri [246–248] but only confirmed experimentally with the advent of solid-state ^{29}Si cross-polarization magic angle spinning nuclear magnetic resonance (CP MAS NMR) [249].

Vicinal or hydrogen-bonded or associated silanols are SiOH groups located on neighboring Si atoms such that the OH - - - O distance is sufficiently short for hydrogen bonding to occur. Hydrogen bonding causes a reduction in the O—H stretching frequency, the magnitude of which depends on the strength of the hydrogen bond and thus on the O—H—O distance [250]. The characteristic IR band of vicinal groups occurs at about 3660 cm^{-1} [251].

Geminal Q^2 silanol sites bonded to a neighboring Q^3 silicon through a single siloxane bridge also result in a hydrogen-bonded pair. The remaining OH group experiences very weak hydrogen bonding.

Silanol groups are also found within the structure of the colloidal particles. These groups are designated as internal silanols and in some cases are erroneously referred to as structurally bound water. The concentration of internal silanol groups depends on the synthesis temperature and other variables.

Surface and internal silanol groups may condense to form siloxane bridges. Strained siloxane bridges are formed on the hydroxylated silica surface by thermally induced condensation of hydroxyl groups up to about 500 °C. At higher temperature, the strained siloxane bridges are converted into stable siloxane bridges [250].

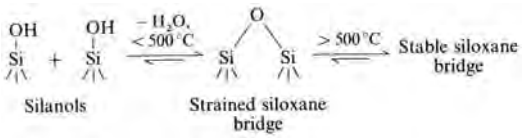

Strained siloxane groups undergo complete rehydroxylation on exposure to water in a matter of hours or a few days, depending on type of silica powder and conditions of exposure [251]. Stable siloxane groups are rehydroxylated at a slower rate. For example, a wide-pore sample of 340 m^2/g calcined in air at 900 °C required five years of contact with water at room temperature for complete rehydroxylation [252].

Surface silanol groups are the main centers of adsorption of water molecules [252]. Water can associate by hydrogen bonding with all types of surface silanols, and in some cases with internal silanol groups.

Surface silanol groups of silica aquasols stabilized in an alkaline medium exchange protons for ions such as Na^+, K^+, or NH_4^+ (Fig. 26). The surface silanol groups can be esterified, as in the case of silica organosols, or silanized (silylated)

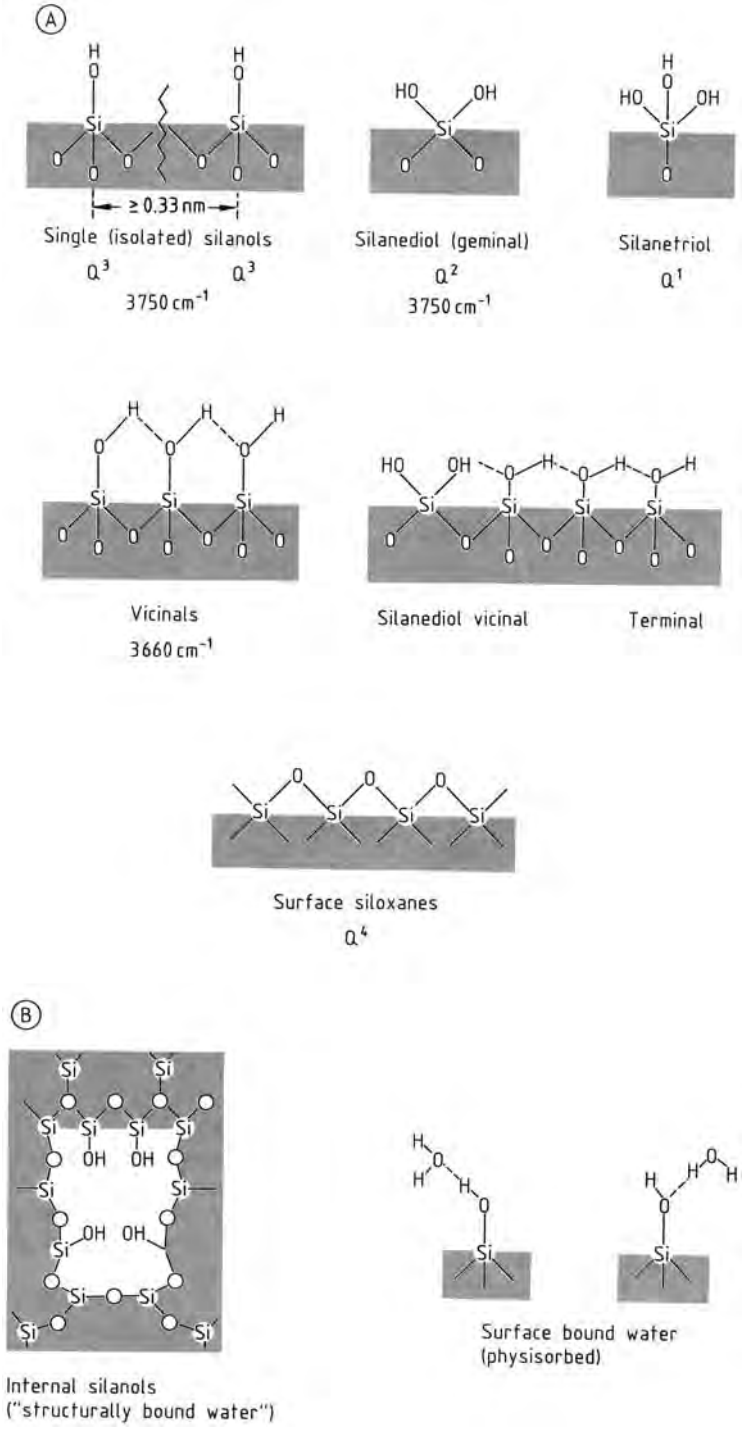

Figure 25. A) Possible types of silanol groups and siloxane bridges occurring on the surface of colloidal silica particles Characteristic bands in the infrared spectrum and Q^n site designation is included (*n* is the number of bridging oxygens bonded to the central silicon atom); B) Surface bound water and internal silanols

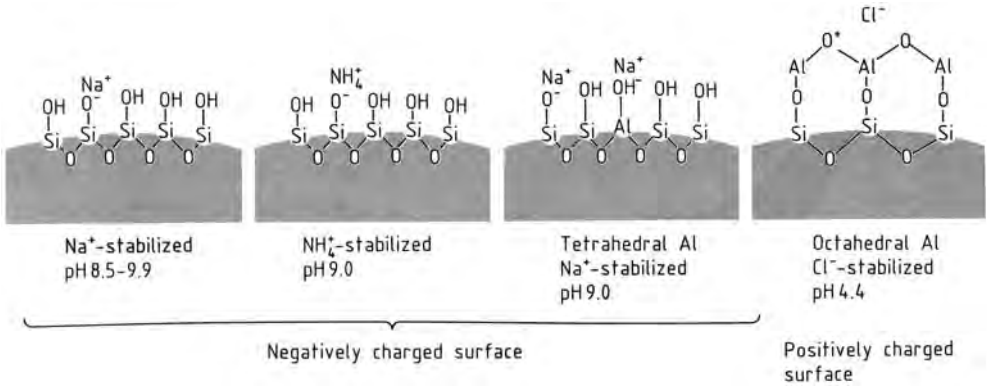

Figure 26. Modified colloidal silica surface

(Fig. 27). Derivatization, that is modification of the silica surface, is the basis for the use of silica in analytical and process chromatography.

The surface charge of pure silica aquasols is negative at a pH higher than ca. 3. The isoelectric point (IEP) is ca. 2. The IEP can be shifted by partial substitution of surface silicon groups by tetrahedral aluminum (see Fig. 26). In this way the pH range of stability of aquasols may be varied. The surface charge can be reversed by adsorption of octahedral aluminum ions such as those present in basic aluminum chloride [253] (Fig. 26). Aquasols obtained in this manner are commercially available in various particle sizes and concentrations as *positive sols.*

The concentration of silanol groups on the silica surface α_{OH} expressed as the number of OH groups per square nanometer is the silanol number [252]. For a dehydrated but fully hydroxylated amorphous colloidal silica powder α_{OH} is 4.6 [252].

The threshold temperature corresponding to the completion of dehydration, that is removal of physisorbed water from the silica surface, and the beginning of dehydroxylation by condensation of surface OH groups, is estimated to be 190 ± 10 °C [252].

The concentration of OH groups on the surface decreases monotonically with increasing temperature when silicas are heated under vacuum (Fig. 28). Most of the physisorbed water is removed at about 150 °C. At 200 °C all the water from the surface is gone so that the surface consists of single, geminal, vicinal, and terminal silanol groups and siloxane bridges. At ca. 450–500 °C all the vicinal groups condense yielding water vapor and only single, geminal, and terminal silanol groups and strained siloxane bridges remain. The estimated ratio of single to geminal silanol groups on the surface is 85/15 [252] and is believed not to change with temperature, at least up to ca. 800 °C. Internal silanols begin to condense at ca. 600–800 °C and in some cases at

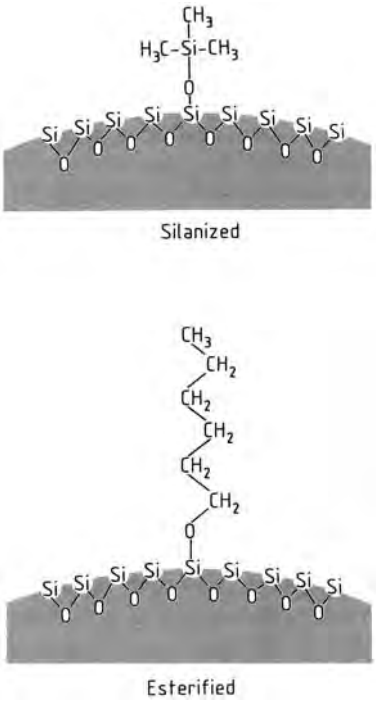

Figure 27. Silylated and esterified silica surface

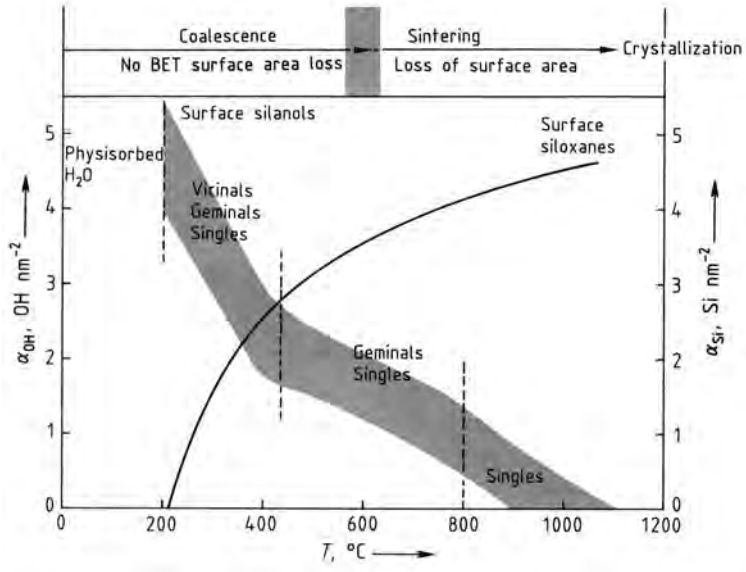

Figure 28. Effect of temperature on silanol groups on the surface of colloidal silica

lower temperatures. Complete evolution of internal silanols occurs at higher temperatures. It appears that at temperatures from ca. 800 °C to ca. 1000–1100 °C, only isolated (single) silanol groups remain on the silica surface.

At a sufficient surface concentration, the OH groups make the silica surface hydrophilic, whereas a predominance of siloxane groups on the silica surface makes the surface hydrophobic.

4.3. Physical and Chemical Properties

Most commercial silica sols consist of dense, discrete, spheroidal particles typically 4–60 nm in diameter and amorphous to X-ray or electron diffraction. Because they are amorphous the silica particles are only slightly soluble in water (100–150 ppm at 25 °C and pH 2–8) and insoluble in alcohol or in inorganic acids except HF. They are soluble in organic bases such as tetramethylammonium hydroxide, forming water-soluble quaternary ammonium silicates, and, as opposed to crystalline silicas, are very soluble in hot sodium hydroxide solution. Specific surface areas vary with particle size, and for the common grades of silica sols are between 50 and 750 m^2/g. Less typical grades have particle diameters between 60 nm and 1.5 μm with specific surface areas much lower than 50 m^2/g, depending on their particle diameter. The specific surface area A in m^2/g of a system made of solid monodisperse amorphous silica spheres with a smooth surface and bulk density 2.2 g/cm^3 is:

$$A = 6000/2.2\,D$$

where D is the diameter of the spheres in nanometers.

Table 12 lists typical properties of representative commercial silica aquasols. The table also shows the dependence of relative density and viscosity on the silica content. Viscosity also depends on particle size and degree of cross-linking of the particles. In 30 % silica aquasols it is generally < 10 mPa · s.

Silica sols obtained by dispersion of pyrogenic silica powders generally differ from those synthesized in solution. The dispersion of pyrogenic silica to a sol of separate, discrete ultimate units is difficult, even using intense mechanical shearing forces, due to the extensive coalescence of the particles. Thus, the disperse product consists mainly of short chain-like aggregates made up of small silica particles (see Section 4.5). Typical properties of commercial sols made in this way are listed in Table 13.

Table 12. Typical properties of commercially available negative and positive silica aquasols[a] [254]

	Particle diameter, nm	Specific surface area, m^2/g	Silica, wt %	pH	Na_2O, wt %	Viscosity at 25 °C, mPa · s	Relative density at 25 °C
Negatively charged surface	4	750	15	10.4	0.80	18	1.10
sodium stabilized	7	360	30	9.9	0.56	6	1.22
	12	230	40	9.7	0.41	20	1.31
	21	130	50	9.0	0.21	35	1.40
	60	50	50	8.5	0.25	10	1.40
	50–80	NA	40	9–10	NA	NA	NA
	70–100	NA	40	9–10	NA	NA	NA
	100	NA	20	8–10	NA	NA	NA
	300	NA	20	8–10	NA	NA	NA
	500	NA	20	8–10	NA	NA	NA
alumina modified surface	12	230	30	8.9	0.24	11	1.21
ammonium stabilized	21	130	40	9.0	0.08	9	1.30
Positively charged surface chloride stabilized alumina surface	13–15	210	30	4.4	NA	NA	NA

[a] NA = not available.

Table 13. Typical properties of silica aquasols made of short chain-like aggregates of colloidal particles[a] [255]

Stabilizer	Ultimate particle size, nm	Solids, wt %	pH	Relative density	Viscosity, mPa · s
Acidic medium	11–14	20	2.0–4.0	NA	5–25
NH_4^+	7	12	7.5–7.8	1.07	<100
	14	17	9.5–10.0	1.10	<250
	14	12	5.0–5.5	1.07	<100
	17	17	9.5–10.0	1.10	<100
	30	20	5.0–5.5	1.12	<100
K^+	17	18	8.6–9.0	1.11	<150
	30	28	7.5–7.8	1.18	<200
	30	30	10.0–10.3	1.19	<150
Na^+	7	14	10.0–10.5	1.08	<100
	8	15	9.5–10.0	1.09	<100
	14	17	9.5–10.0	1.10	<100

[a] NA = not available.

Table 14 lists particle size, silica concentration, and viscosity of commercially available organosols.

Silica sols are said to be stable because they do not settle or aggregate for long periods of time. Aggregation and rate of settling, as well as color, appearance, viscosity, density, growth, and solubility in water are functions of particle size. At optimum pH, electrolyte and SiO_2 concentration, aquasols of particle size 4 to ca. 40 nm are extremely stable to settling, whereas aquasols of particle size larger than ca. 60 nm tend to show some settling in a period of months. Particles larger than 100 nm settle on standing, leaving a clear upper layer after a few weeks or days. When the concentration of the silica aquasol is > 10–15 wt % the particle size can be judged visually by the turbidity. If the particles are smaller than ca. 7 nm in diameter the sol is almost as clear as water; from 10–30 nm there is a characteristic opalescence or translucency when seen in bulk; above 40 or 50 nm the appearance is white and milky [235].

Commercial silica aquasols are stabilized near the optimum pH and are concentrated to the maximum concentration permitted by the particle

Table 14. Properties of commercially available silica organosols[a] [256]

Liquid phase	Particle diameter, μm	SiO_2, wt %	Viscosity at 25 °C, cP	Relative density
Methanol	0.01	30	1–5	NA
2-Propanol	0.01	30	3–20	NA
Water/2-propanol	0.02	30	10	NA
Ethylene glycol mono-*n*-propylether	0.01	20	5–20	NA
Dimethylacetamide	0.01	20	1–10	NA
Ethylene glycol	0.01	20	10–20	1.23
Ethylene glycol	0.18 ± 0.03	20		1.23
DMF	0.02	35	5	NA
Oil	0.02	50	80	NA
Ethylene glycol	0.28 ± 0.03	20		1.23
Ethylene glycol	0.43 ± 0.03	20		1.23
Ethylene glycol	0.50	20	10–20	1.23
Ethylene glycol	0.53 ± 0.03	20		1.23
Ethylene glycol	0.73 ± 0.03	20		1.23
Ethylene glycol	0.80 ± 0.04	20		1.23
Ethylene glycol	0.90 ± 0.05	20		1.23
Ethylene glycol	1.50 ± 0.10	20		1.23

[a] NA = not available.

size [257]: ca. 15 wt % for 4–5 nm, ca. 30 wt % for 8–9 nm, ca. 40 wt % for 14 nm, ca. 50 wt % for 22 nm (Fig. 29).

When silica sols are gelled, dried, or frozen the original degree of dispersion cannot be restored without dissolution of the interparticle bonds that develop. Special dried grades are made of particles with the surface esterified with primary or secondary C_2–C_{18} alkoxy groups. These are organophilic and hydrophobic and can be dispersed in organic solvents or in organic products such as elastomers or plastics. Silica sols surface-modified with organic base cations such as $(CH_3)_4N^+$ can be evaporated to a dry powder that disperses spontaneously in water [258].

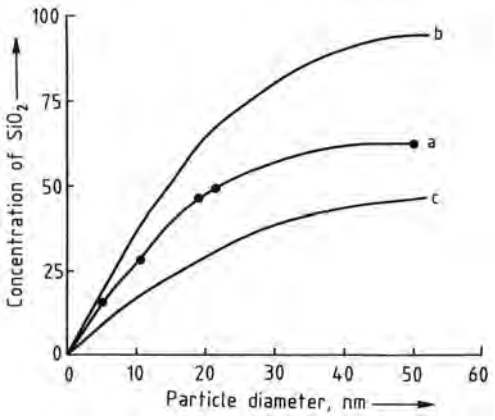

Figure 29. Maximum concentration versus particle size in stable aqueous silica sols at about pH 9.5
a) Concentration in wt %; b) Concentration in grams SiO_2 per 100 mL; c) Volume fraction of SiO_2 (×100) [257]

4.4. Stability

Three types of stability may be distinguished in colloidal systems [259]:

1. Phase stability, analogous to the phase stability of ordinary solutions.
2. Stability to change in *dispersity* [259], that is particle size or particle-size distribution. For example, commercial concentrated silica sols, normally said to be 3 or 4 nm in particle size usually grow within hours or a few days to 5 nm or more on standing at room temperature. Concentrated sols normally labeled 7 nm, if not substantially homodisperse, may grow within months to 8–9 nm. This ripening effect also occurs for larger particle sizes, although at a much slower rate. A concentrated silica sol of 14 nm particle size was found to grow to 17 nm in twenty years at room temperature [260].
3. *Aggregative stability* [259], the central issue in colloidal silicas, and for that matter in colloidal systems in general. In this case *colloidally stable* means that the colloidal particles do not aggregate at a significant rate

[257]. The term aggregate is used to describe the structure formed by the cohesion of colloidal particles [232].

Two mechanisms of sol stabilization are generally believed to exist: electrostatic stabilization and steric stabilization (see → Colloids, Chap. 5.). Electrostatic stabilization is based on an interplay of electrostatic repulsion between electrically charged colloidal particles and van der Waals forces of attraction between particles. The DLVO theory (Derjaguin, Landau, Verwey, and Overbeek) constitutes an attempt to describe quantitatively this interplay (see → Colloids, Section 5.0.0.0.0.3., → Colloids, Section 5.0.0.0.0.7.). Steric stabilization is generally caused by long-chain molecules or macromolecules adhering on the colloidal particle surface (e.g., by grafting or by physical adsorption), thus preventing the particles from aggregating [261].

Colloidal silica particles aggregate by linking together and forming three-dimensional networks as is the case in gelation, coagulation or flocculation, or by coacervation [262]. In coacervation the silica particles are surrounded by an adsorbed layer of material which makes the particles less hydrophilic but does not form bridges between particles [263].

When a sol is gelled it first becomes viscous and then develops rigidity, filling the volume originally occupied by the sol. On the other hand when a sol is coagulated or flocculated, a precipitate is formed that settles out. A simple way to differentiate between a precipitate and a gel is that a precipitate encloses only part of the liquid in which it is formed [262].

Stability of silica aquasols against irreversible gelation decreases with increasing silica concentration, increasing electrolyte concentration of the aqueous medium, decreasing particle size, and increasing temperature. Water-miscible organic liquids have a similar destabilizing effect on silica aquasols as added electrolyte. The variation of stability as a function of pH and salt concentration is shown in Fig. 30 [264].

According to Iler [265] the basic step in gel formation is the collision of two silica particles with sufficiently low charge on the surface that they come into contact so that siloxane bonds are formed, holding the particles irreversibly together. Formation of this linkage requires the catalytic action of hydroxyl ions (or, as interpreted by some, the dehydration of the surface of particles at higher pH). This is evidenced by the fact that the rate of gel formation in the pH range 3–5 increases with pH and is proportional to the hydroxyl concentration.

Above pH 6, scarcity of hydroxyl ions is no longer the limiting factor on the rate of gelling. Instead, the rate of aggregation decreases

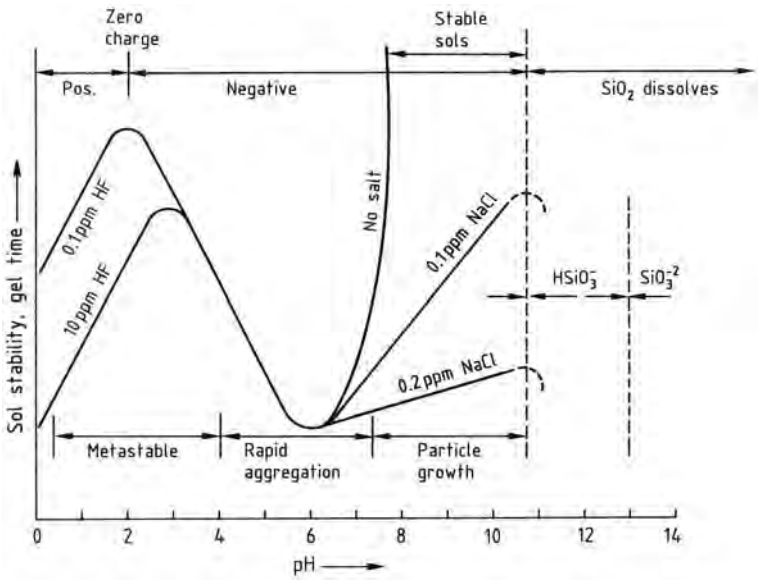

Figure 30. Effect of pH in the colloidal silica–water system [258]

because of fewer collisions between particles owing to the increasing charge on the particles and thus decreases with higher pH. Lines in Figure 30 schematically represent the increase in the catalytic effects of hydroxyl ions with increasing pH, and the decrease in the number of effective collisions between particles with increasing pH and particle charge. The net result of these two effects is a maximum in rate of gelling at around pH 5. In the pH range 8–10, sols are generally stable in the absence of salts.

There is also a region of temporary stability at about pH 1.5. Below pH 1.5, traces of HF catalyze aggregation and gelling [266]. In essentially all silicas, traces of fluoride ions, even less than 1 ppm, are present so that the concentration of HF increases with increasing acidity. The fluoride effect is influenced by the aluminum impurities present, since these inactivate some of the fluoride by forming complex ions such as AlF_6^{3-} and other species [267]. However, the gelling rate increases as the pH falls below 3 even when fluorine is absent.

Once the siloxane bonds have formed between particles, further deposition of silica occurs at the point of contact owing to the negative radius of curvature. This occurs rapidly above pH 5, and is slow at pH 1.5.

Since the curves shown in Fig. 30 are constructed on the basis of irrefutable experimental evidence it is quite obvious that silica sols do not conform to the DLVO theory as originally formulated. For example, the DLVO theory predicts minimum stability at the point of zero charge (pH 2–3), whereas the experimental curve shows metastability. Also, the plot shows minimum stability in the pH range 4–7, whereas the DLVO theory predicts a continuous increase in stability in this pH range. Research is being conducted to study the possibility of modifying or amending the DLVO theory or developing a new theory of stability applicable to silica sols.

In addition to common electrolytes such as NaCl, NH_4Cl, and KF, silica aquasols are destabilized and gelled by positively charged sols. When frozen at ca. 0 °C or lower, silica sols gel irreversibly. Long-chain nitrogen bases are effective flocculating agents for silica aquasols that form planar rather than spheroidal aggregates. Flocculation may also result from the addition of water-miscible organic solvents to alkali-stabilized silica sols.

Commercial silica aquasols are stabilized at pH 8.5–10.5 by alkalies, usually sodium hydroxide. Ammonia or potassium hydroxide is used when the presence of sodium ions is undesirable.

Surface-modified silica aquasols made by coating the silica particles with tetrahedral aluminum (e.g., sodium aluminate) are much more stable towards gelling in the pH range 4–6 where unmodified sols gel most rapidly. Silica sols modified in this manner are also less sensitive to salts [268].

Coating the negative silica surface with oxides of polyvalent metals such as Al, Cr, Ga, Ti, and Zr reverses the charge of the surface to produce positive aquasols stable at acid pH values [269]. An important characteristic of these sols is that they can be dried and repeptized. Only polymeric hydrolyzed species such as $Al_2(OH)_5Cl$ and not the single Al^{3+} ion can cause charge reversal of silica sols [270, 271].

4.5. Production

The classic silica aquasols of particle size 5–100 nm are prepared by nucleation, polymerization, and growth in aqueous systems. The particle-size range can be extended to at least 300 nm by autoclaving. Silica organosols can be obtained by transferring aquasols to an organic solvent or by hydrolysis of a silane precursor in a mixture of alcohol/ammonia and sufficient water [272] followed by transfer to the solvent.

The most important processes to make silica sols are based on neutralization of soluble silicates with acids, ion exchange, hydrolysis of silicon compounds, dispersion of pyrogenic silica, electrodialysis, dissolution of elemental silicon, and peptization of gels [273].

Most commercial silica sols are prepared by ion exchange of dilute solutions of sodium silicate. Several methods have been proposed since the pioneering work of Bird [236], Bechtold and Snyder [237], Alexander [274], Atkins [275], Wolter and Iler [276], Mindick and Reven [277], and Dirnberger [278]. Sodium silicate can be deionized in a batch operation by adding simultaneously a dilute solution of sodium silicate and a cationic ion-exchange resin in the hydrogen form to a vigorously stirred weakly alkaline aqueous reaction medium in the pH range around 9, at 60–100 °C [276] (Fig. 31).

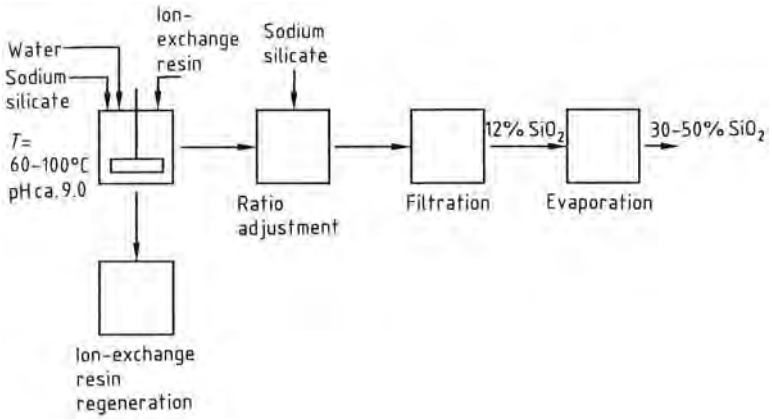

Figure 31. Ion-exchange process for silica aquasols

Under these conditions the system is stabilized against aggregation and the original silica nuclei grow while the sol concentration increases to about 10–15 % silica. Rate of addition, pH, and temperature determine the particle size and quality of the sol.

After separation of the resin for regeneration, more sodium silicate is added to adjust the SiO_2/Na_2O ratio as needed for further stabilization of the sol. The product is filtered and concentrated to the desired level. Sols of small particle size, such as 7 nm, may be used as "heels" to build up the particle size, for example, to 14 or 22 nm.

An alternative method of deionizing sodium silicate is to pass a relatively dilute solution through a bed of ion-exchange resin to produce a sol which is then stabilized with alkali and concentrated. The particles grow during evaporation. The addition of further deionized sol to the evaporating liquid allows silica to build up on previously nucleated particles resulting in larger particle size.

Silica sols can also be made by dispersion of pyrogenic silica in water or in an organic solvent. Commercial pyrogenic silica, also known as fumed silica or aerosil, is made from silicon tetrachloride at high temperatures by a flame hydrolysis–oxidation process (see Chap. 6) [279]. The product is a highly aggregated silica powder. Pyrogenic silicas can be partially disagregated and dispersed to obtain aquasols or organosols of relatively high silica concentration. The silica units in this case consist mainly of short chain-like aggregates composed of silica particles ca. 7–25 nm in diameter.

Monodisperse silica sols of exceptionally large particle size can be prepared by hydrolysis of tetraethoxysilane (TEOS) in a basic solution of water and alcohol [272]. It is claimed that the largest mean particle size that can be produced with TEOS is about 0.8 μm [280]. However, particles up to ca. 2 μm can be made by using tetrapentoxysilane [279], performing the reaction at low temperature [281], or growing the particles by adding more alkoxide after the particles have formed [281]. Wolf [282] has adapted the TEOS method to produce commercial quantities of silica sols.

Viable processes for making commercial silica sols are based on the electrodialysis of sodium silicate solutions to continuously remove sodium ions until a sol is obtained. In the Iler [283] and the Bergna [284] processes there are three compartments separated by two parallel, closely spaced cation-exchange membranes between which the process or "heel" solutions of silica sol in dilute Na_2SO_4 as a conducting electrolyte are rapidly circulated at a specified temperature. Sulfuric acid is circulated in the anode compartment and an alkali in the cathode compartment where sodium hydroxide is generated. Dilute sodium silicate is fed to the third compartment to form SiO_2 by electrolysis. The silica or polysilicic acid that forms is deposited on the silica particles of the "heel" solution, and circulation of the solution is continued until the desired particle size is achieved. Sols of 25 % silica, 15 nm particle size can be prepared directly. Concentrated sols of ca.8 nm particle size with very narrow particlesize distribution can be

obtained by seeding in a first step at a lower temperature and raising the temperature in a second step to accelerate silica deposition [284].

Among the advantages of the electrodialysis process are that alkali, oxygen, and hydrogen can be recovered, and that there is much less salt-containing wastewater to be disposed of. The disadvantages of the process are higher electrical and maintenance costs.

4.6. Analysis and Characterization

Characterization of silica sols is aimed at identifying:

1. Physical and chemical properties of the sol
2. Compatibility and stability properties of the sol
3. Purity of the sol
4. Use-related characteristics

Selection of silica sols for commercial uses is commonly based on the nature of the liquid phase (water or organic solvent), particle size, particle-size distribution, degree of aggregation, pH, silica and counterion (stabilizing agent) concentration, viscosity, relative density, and specific surface area.

However, to fully understand and predict the behavior of silica sols and derived powders, it is necessary to determine other characteristics such as particle and particle surface structure; chemical composition including total carbon, organic carbon, soluble salts of alkali metals, total solids, nonsiliceous ash, and trace metals (especially Al and Fe); and physical properties such as turbidity, percent S (the percent by weight of silica in the dispersed phase of a silica sol [285]), refractive index, light scattering, sedimentation rate by ultracentrifugation, porosity, rate of dissolution of the particles, and coalescence factor of derived powders (the coalescence factor is the percent silica that must be dissolved to restore the light transmission under standard conditions of a silica powder redispersed in water [286]). In addition, most manufacturers of colloidal silicas use special tests for specific uses.

A new concept in the characterization of colloidal silica is the application of the fractal approach to sols and gels. The concept of fractal geometry, developed by MANDELBROT [287] in the early eighties, provides a way of quantitatively describing the average structure of certain random objects. For the application of the fractal concept to colloidal silica, see [241, 250].

Most of the methods utilized to characterize silica sols for commercial uses and for research purposes are listed below:

Chemical analysis
- % total solids
- % and nature of liquid phase
- % SiO_2
- % NH_4
- SiO_2/Na_2O weight ratio
- Sulfates as % Na_2SO_4
- Chlorides as % NaCl
- Carbon including CO_2
- Organic carbon
- Metals including Al and Fe
- Nonsiliceous ash

Physical characteristics
- pH
- Relative density
- Viscosity
- Turbidity
- Refractive index
- Light scattering
- Specific conductivity

Particle characteristics
- Size and size distribution
- Specific surface area (SEARS titration of the sol [260] and BET measurement of the derived dried powder)
- Porosity
- Degree of aggregation
- % S (silica in the dispersed phase)
- Turbidity
- Viscosity
- Surface charge
- Electrokinetic potential (isoelectric point)
- Silanol number

Stability tests
- Gelation tests
- Flocculation tests

The following methods are used to measure the particle size and particle-size distribution of silica sols [288–291]:

Chemical methods
Gas adsorption (e.g., BET) [288]
Titrations (e.g., Sears titration) [289]
Rate of dissolution of particles [290]

Instrumental methods [291, 292]
Transmission electron microscopy (TEM)
Dynamic light scattering: photon correlation spectroscopy (PCS): Malvern Correlator, Coulter N4 Analyzer
Sedimentation field flow fractionation (SF3)
Size-exclusion chromatography (SEC)
Hydrodynamic chromatography
Capillary zone electrophoresis (CZE)

Methods for characterizing the surface of colloidal silica particles are [250, 292]:

Spectroscopy
FTIR (Fourier transform infrared spectroscopy)
DRIFT (diffuse reflectance)
Probe molecule adsorption by DRIFT
^{29}Si CP MAS NMR spectroscopy (^{29}Si cross-polarization magic angle spinning nuclear magnetic resonance spectroscopy)
^{1}H MAS NMR spectroscopy
^{1}H CRAMPS (combined rotation and multiple pulse spectroscopy)
SIMS (secondary ion mass spectrometry)
SNMS (sputtered neutrals mass spectrometry)
EXAFS (extended X-ray absorption fine structure spectroscopy)
XPS (X-ray photo emission spectroscopy) (ESCA)

Thermal and calorimetric methods
Microcalorimetry
TGA (thermogravimetric analysis)
DTA (differential thermogravimetric analysis)
DSC (differential scanning calorimetry)
Thermoporometry

Heterogeneous isotopic exchange
Use of deuterated and tritiated substances combined with mass spectrometry, IR, and ^{1}H NMR

Adsorption and wetting
Adsorption of gases and vapors combined with IR, microcalorimetry
Fractality (fractal dimension)
TPD (temperature programmed desorption) of adsorbed substances (NH_3, pyridine, etc.) coupled with spectrometry and IR
Adsorption of bases (*n*-butylamine) using Hammett or arylmethanol indicators
Wetting with liquids

Microscopy
TEM (transmission electron microscopy)
SEM (scanning electron microscopy)
FESEM (field emission scanning electron microscopy)

Scattering
SAXS, SANS (small angle X-ray and neutron scattering)

Chemical methods
Use of chemically reactive substances: chlorine, metal halides, Grignard compounds, reactive chloro- and alkoxysilanes

4.7. Uses

This section gives a brief description of the major industrial uses of silica sols. The many minor uses are too numerous to be discussed here.

Colloidal silica is widely used as a binder in the modern version of the ancient lost wax process for casting metal [293]. In this process, known as *shell investment casting,* a wax original or a cluster of originals is dipped in a slurry of colloidal silica and refractory powder. Excess slurry is drained from the wax parts and a dry refractory sand is applied to the wet surface. The coating is then allowed to dry. These coating steps are repeated until a ceramic shell of sufficient thickness, usually about 5–10 mm, is built up around the wax.

The wax is then melted out, and the ceramic shell fired to increase its strength and to remove the last traces of wax. Molten metal is poured into the hollow left by the wax. When the metal has cooled, the shell is broken away and the metal, now an exact replica of the original wax shape, is recovered.

This process is widely used to produce jet engine components as well as a large number of other metal parts. The tolerances of the finished casting can be held very close to the final requirements, thus minimizing the need for additional finishing operations.

Refractory fibers can be bonded with colloidal silica to give *insulators* that have excellent high-temperature resistance. The process is similar to papermaking in that the fibers are suspended in water and the mixture passed through a screen which retains the fibers and allows the water to pass through and be recycled. The thickness of the fiber mat can vary from 0.1–10 cm depending on the insulating properties required. The screen is often contoured to give a shaped insulator. Usually, vacuum is used to assist the flow of water through the screen.

Colloidal silica is used two ways in this process. It is often used in small quantities together with starch in the original fiber suspension to help flocculate the fibers and the starch for better drainage and retention on the screen. The starch acts as the binder in the unfired or green state. Additional colloidal silica is often added to the final shape to stiffen and strengthen it and provide additional strength when the part is heated and the starch is burned out.

More recently, colloidal silica has been applied to the *papermaking* process itself. By adding small amounts of high surface area colloidal silica and a high molecular mass starch to the paper pulp, drainage rates and fiber and filler retention are improved. This allows for higher filler loadings, use of more recycled pulp, and in some cases, higher production rates [294–298].

Small amounts of colloidal silica increase the coefficient of friction of surfaces. One of the earliest uses of colloidal silica was to diminish the slipperiness of floor waxes while not affecting their gloss [299, 300]. It is widely used to improve the frictional character of paper and boxboard, which facilitates handling and reduces breakage resulting from falling boxes [301].

Carpets and other surfaces coated with colloidal silica resist soiling because the colloidal silica occupies the sites which would most likely retain visible soil.

The strength and adhesion of latex-based adhesives and paints can be enhanced by the addition of colloidal silica.

Silicon wafers cut from silicon single crystals must be polished to an almost atomically smooth surface before being used as substrates for electronic chips [302, 303]. Colloidal silica is the main component of the final polishing compounds for these materials. They act both as a fine, uniform abrasive and as a scavenger for reaction products of polishing additives that chemically attack the silicon.

Colloidal silicas have been used to bond and improve the attrition resistance of catalyst powders used in streams of reacting gas or liquid. The silica provides sufficient strength and hardness to prevent the catalyst pellets from being broken down and swept away by the stream. Acrylonitrile is made from propylene and ammonia by such a fluidized bed reaction [304, 305]. Ammonia-stabilized colloidal silicas are generally used in these applications because of the poisoning effect of sodium.

Photographic films and papers often incorporate colloidal silicas as grain growth regulators or dye receptors.

Beverages, such as wine, beer, or fruit juices can be clarified using colloidal silica as an aid to the flocculation of the proteins which cause the materials to be hazy.

4.8. Storage, Handling, and Transportation

Colloidal silicas generally undergo irreversible precipitation of the silica if frozen. Therefore, they are generally stored in heated buildings. If outdoor bulk storage is required, tanks should be heated and insulated in climates where freezing might occur. Heated trucks are typically used in cold climates for shipping colloidal silicas.

Colloidal silica is sometimes freeze-stabilized by addition of organic substances such as glycols. The amount added is insufficient to prevent freezing, but does prevent irreversible precipitation.

Storage in plastic, fiberglass-reinforced plastic, stainless steel or lined steel tanks is usually recommended.

Typically, the main hazard associated with colloidal silicas is their alkalinity. However, since the pH of most commercially available materials is < 10.5 they may irritate the skin or eyes, but do not cause irreversible burns. In applications where a respirable mist can be formed, operators should be protected by engineering design or suitable respirators. Since colloidal silica is amorphous, it is less toxic than crystalline silica.

4.9. Economic Aspects

Major manufacturers of colloidal silica and their trade names are as follows:

Bayer	Baykisol	(Germany)
Du Pont	Ludox	(United States)
Eka Nobel	Bindzil, Nyacol	(Sweden)
Hispano Química	Hispacil	(Spain)
Monsanto	Syton	(United Kingdom)
Nalco Chemical	Nalcoag	(United States)
Nippon Shokubai	Seahostar	(Japan)
Nissan	Snowtex	(Japan)

Estimates of the colloidal silica market discussed in this section are based on [238, 239].

The U.S. market for colloidal silica is the largest in the world. The total market for North America is estimated at > 14 000 t (100 % silica basis) and valued at $ 50×10^6 [236]. These figures include ca. 1500 t consumed in Canada. Kline estimates that the total West European market for colloidal silica was 5500 t (100 % silica basis) in 1992, valued at over € 15×10^6 [239]. In Japan colloidal silica production in 1988 was estimated at 4500 t (100 % silica basis) and was expected to grow significantly [238].

The total annual capacity for the manufacture of colloidal silica in North America is estimated at 16 000–21 000 t (100 % silica basis). The total capacity in Europe is estimated at 6000 t.

Nalco is the largest producer for the North American market followed by Du Pont and PQ Corporation. Eka Nobel of Sweden has a relatively small plant in the United States (Pro-Comp Inc.). Alchem, a joint venture of C-I-L Inc. and Nalco in Ontario, is the sole Canadian producer.

In the United States, Monsanto imports colloidal silica from its plant in Wales and small amounts are also imported from Japan. Exports from the United States are believed to be relatively small at about 1800 t/a. Nalco and Du Pont are the main exporters, and Japan, Taiwan, and Canada are the principal destinations. Some colloidal silica is also exported to Europe.

The largest producers of colloidal silica in Western Europe are Bayer in Germany, Eka Nobel in Sweden, and Monsanto in the United Kingdom, followed by Akzo in the Netherlands and Hispano Química in Spain. There are a few smaller producers in Italy and France.

Western Europe imports some colloidal silica from the United States and exports relatively small amounts to the United States, Eastern Europe, the Far East, and the CIS.

In 1987–1988 the North American market for colloidal silica was expected to grow at an average rate of 5 %/a, and the Western European market at 3.5 %/a in volume. The author estimates that the actual growth for both markets has been lower due to the world economic situation.

Colloidal silica prices vary with grade, silica concentration, volume purchased, and country in which it is sold. In the United States the price is about $ 1.80–1.95 per pound for electronic-grade material, and $ 1.15–1. 40 per pound for other grades (100 % silica basis). In Western Europe the prices vary in the range 5.5–8.3 DM/kg (100 % silica basis).

5. Silica Gel

5.1. Introduction

Silica gel [*63231-67-4*] (revised 1990 SiO_2: [*112926-00-8*]) has the nominal chemical formula $SiO_2 \cdot x\ H_2O$ and is a solid, synthetic amorphous form of hydrous silicon dioxide distinguished by its microporosity and hydroxylated surface. The structure of silica gel is an interconnected random array of ultimate polymerized silicate particles, called micelles, which are spheroidal and 2–10 nm in diameter (resulting in high surface areas of ca. 300–1000 m^2/g SiO_2). The properties of silica gel are a result of the silica micelles, their state of aggregation, and the chemistry of the micelle surface.

Control of the surface area, porosity, and surface chemistry of silica gel has led to numerous and diverse uses. Examples include adsorbents for water or other species, abrasives and thickeners in dentifrice, efficient matting agents in coatings, chromatographic media, and catalyst supports. The utility is reflected in an estimated world consumption of > 150 000 t/a.

The development of silica-gel science and technology began with the pioneering work of Graham reported in 1861 [306], although observations of gelation had been reported earlier [307, 308]. Commercial production began at the Silica Gel Corporation (now part of W. R. Grace & Co.-Conn.) with the process invented by Patrick in 1919 [309]. Commercial development and applications expanded worldwide [307], and

the colloid chemistry of silica was explored further [310]. With the application of NMR spectroscopy, small-angle X-ray scattering, and fractal geometry [311], further fundamentals of silica gel chemistry are being elucidated.

5.2. Structure, Properties, and Characterization

Structure. Silica gel is prepared by the neutralization of aqueous alkali metal silicate with acid [307, 309, 310]; for example:

$$Na_2O{\cdot}3.3\,SiO_2 + H_2SO_4 \rightarrow Na_2SO_4 + 3.3\,SiO_2\downarrow + H_2O$$

A complete synthesis of silica gel by this typical commercial route is outlined in Figure 32. Alternatively, stable silica sols may also be gelled [310]. Another method involves the hydrolysis of silicon alkoxides with water, catalyzed by acid or base [311].

The neutralization of sodium silicate initiates a polymerization of silicate tetrahedra in a random, amorphous manner to form small spheroids called micelles. The solution containing the micelles while still liquid is known as a hydrosol.

Gel formation occurs when the interaction of separate micelles through hydrogen bonding and eventual interparticle condensation becomes significant. The rate of gelation depends on many variables such as SiO_2 concentration, pH, temperature, and mixing; this is discussed in detail in [310, 311]. Polymerization and cross-linking continue after the hydrosol has solidified into a hydrogel. The random, amorphous structure is reflected in a lower skeletal density for silica gel of 2.1–2.2 g/cm^3 compared to quartz (2.65 g/cm^3) and the lack of X-ray crystallinity. The micelle, which is the ultimate particle, consists of SiO_2 in its interior and Si—OH on its surface. Solid-state ^{29}Si NMR indicates tetrahedral geometry about the silicon atoms and confirms the presence of bulk SiO_2 and surface Si—OH [312]. The micelle's size determines the specific surface area of the silica gel; a typical micelle size of ca. 2.5 nm in diameter corresponds to ca. 1000 m^2/g.

Once the gel network forms, several processing steps are performed to give the finished gel

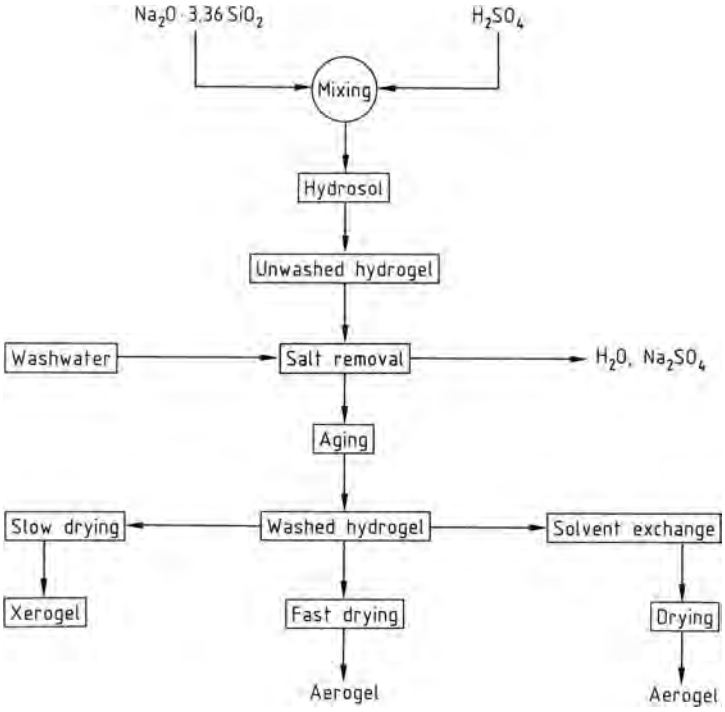

Figure 32. Schematic of silica gel manufacture

[313]. First, washing is normally performed to remove dissolved salts. Because silica gel has a very low ion-exchange capacity for cations or anions at moderate pH, salt removal is a diffusion-controlled dilution process. Next, if desired, the interaction between micelles and micelle growth can be accelerated by aging in aqueous media under conditions where silica is slightly soluble. A process in which silica dissolves from regions of positive curvature and redeposits at regions of negative curvature reinforces the hydrogel network. Thus, a continuous gel structure is formed.

During the drying process, the surface tension of the solvent in the pores can act to shrink the hydrogel volume. In slow drying, as water is evaporated from a silica hydrogel, the structure collapses gradually due to the surface tension of water. Eventually a point is reached where even though water is still evaporating the gel structure no longer shrinks. At this point the gel is called a xerogel. Fast drying can minimize the shrinkage, and removal of water by solvent exchange followed by drying has the same effect. Materials that are dried with negligible loss of pore volume are known as aerogels. Solvent exchange with a water-miscible liquid such as ethanol to remove water from the hydrogel preserves pore volume after drying. Single or multiple solvent exchanges to lower surface tension results in less pore collapse during drying.

Drying of silica gels can also be carried out under conditions where the solvent in the pores is above its critical point and is vented while maintaining temperature and pressure. KISTLER [314] dried gels supercritically after replacing the water of the hydrogel with alcohol. Alternatively the liquid in the pores can be exchanged for liquid CO_2, which has more convenient critical-point properties [315, 316]. Considerable interest has been focused on such techniques due to the high porosity and mechanical properties achievable [311, 315, 317].

The resulting products from a scheme as in Figure 32 are high purity silica gels with controlled porosity. Transmission electron micrographs showing the pore structure of a silica gel are shown in Figure 33. Typical properties are as follows:

Chemical analysis (dry basis)	
SiO_2	99.71 wt%
Al_2O_3	0.10 wt%
TiO_2	0.09 wt%
Fe_2O_3	0.03 wt%
Trace oxides	0.07 t%
Physical analysis	
Total volatiles	5–6.5 wt%
Surface area	750–800 m^2/g
Pore volume	0.43 cm^3/g
Average pore diameter	2.2 nm
Apparent bulk density	0.72 g/cm^3
Skeletal density	2.19 g/cm^3
Specific heat	920 J kg^{-1} K^{-1}
Thermal conductivity	522 J m^{-1} h^{-1} K^{-1}
Refractive index	1.45

Surface Chemistry and Stability. The physical microporosity of silica gel is an

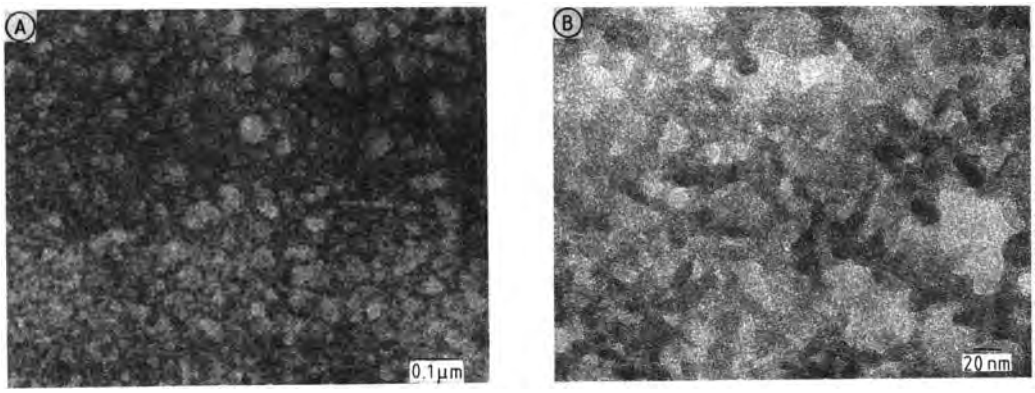

Figure 33. Transmission electron micrographs of a silica gel similar to the fast-dried, high pore volume silica gel in Table 15, showing the micelle structures (ca. 20 nm) and apparent pores also ca. 20 nm in diameter
A) magnified ×235 000; B) magnified ×688 000

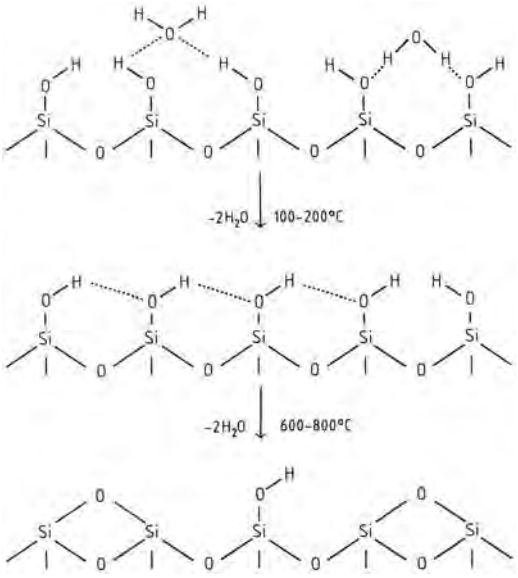

Figure 34. Schematic representation of the dehydration of a silica gel surface

important property, as is the chemistry of its bulk and surface species (Fig. 34). Pure silica gel has a hydroxylated surface covered with silanol groups. These hydroxyl groups are neither very acidic nor basic, with $pK_a \approx 6$ and an isoelectric point at ca. pH 2. The hydroxylated surface is hydrophilic and adsorbs moisture readily. This adsorbed moisture can be desorbed thermally at 100–200 °C leaving behind ≈5.5 OH/nm^2 (or ca. 5 wt % silanol groups on a 300 m^2/g silica). These silanols are more difficult to remove but this can be done thermally by condensation to form siloxanes and water. Temperatures near 600–800 °C are required to dehydroxylate to ca. 1 OH/nm^2. At this silanol concentration the surface is hydrophobic.

Characterization. Numerous methods have been developed to characterize the porosity, structure, and chemistry of silica gels [310] and new methods continue to be applied [311].

With regard to porosity, differently prepared silica gels can be described on the basis of pore diameter d as microporous ($d < 2$ nm), mesoporous ($d \approx 2$–50 nm), or macroporous ($d > 50$ nm) [318]. The most generally useful methods for characterizing these structures with respect to surface area, pore volume, and pore-size distribution are nitrogen adsorption/desorption techniques. The primary method for surface area is the BET procedure [319] (ASTM D 3663–84 or DIN 66 131). Methods have been proposed to improve on the BET technique in small pores, such as the t-plot method [320], and the α_s method [321]. The related N_2 pore volume and pore-size distribution (pore volume as a function of pore diameter) methods are ASTM procedures D 4222–83 and D 4642–87, respectively. The porosity of a silica gel, determined by N_2 porosimetry, is shown in Figure 35. Alternative porosity measurement techniques include mercury porosimetry, water pore volume, and oil absorption.

Elemental analysis of silica gel focuses on trace elements in the range of < 1 wt %. Inductively coupled plasma atomic emission spectroscopy (ICP-ES) is becoming the preferred technique. pH measurement is performed on slurries and reflects the balance of residual trace elements (ASTM D 1208, DIN ISO 787 1X, JIS K 5101/24).

The moisture content of silica gel is important to provide an anhydrous basis for chemical analysis and because the hydration of the surface and pores (Fig. 34) is important to performance in applications. Most standards require two measurements: moisture loss on drying for 2 h at 105 °C (ASTM D 280, DIN ISO 787/II, or JIS K 5101/21) and loss on ignition after this drying by heating for 2 h at 1000 °C (ASTM D 1208, DIN 55 921, or JIS 5101/23). Another method often used in the United States prior to analysis to provide a solids basis is to measure total volatiles

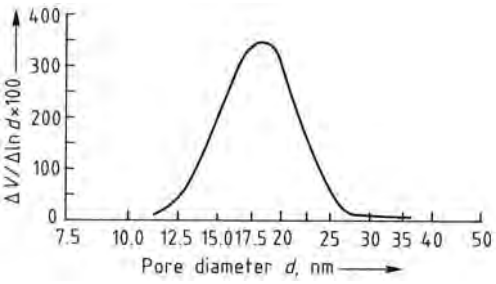

Figure 35. Nitrogen pore-size distribution of a silica gel similar to the fast dried sample of Table 15
V = pore volume

as a weight per cent loss on heating for 1 h at 954 °C.

The surface hydroxyl groups of silica gel can be characterized by thermogravimetric analysis [310], vibrational spectroscopy [311, 322], and nuclear magnetic resonance [311, 312, 323]. The information obtained concerns hydroxyl concentration, hydrogen bond interaction between hydroxyl groups, and distribution of ≡Si—OH and =Si—$(OH)_2$ species on the surface. The adsorptive properties of variously hydroxylated silica materials are an indirect means of characterizing the surface.

Particle-size measurement is also important in silica-gel characterization (DIN 53 206). The method for granular gel is standardized sieve screening (ASTM D 4513). For particle sizes of roughly 1 to 1000 μm, static light scattering (ASTM) and conductivity methods are preferred for particle size analysis. For particle sizes of roughly 10 to 1000 nm, dynamic light scattering [352], electron microscopy, and small-angle X-ray scattering are used.

Table 15. Typical properties of various silica gels

Property	Regular density	Intermediate density	
	Slow dried	Slow dried	Fast dried
Total volatiles[a]	5	6	6
Na_2O dry basis, wt %	<0.1	<0.1	<0.1
SO_4 dry basis, wt %	<0.1	<0.1	<0.1
Al_2O_3 dry basis, wt %	0.05	0.05	0.05
pH[b]	4.0	7.5	4.0
Specific surface area, m^2/g	750	325	390
Pore volume, cm^3/g	0.40	1.1	1.8
Average pore diameter, nm	2.1	13.5	18.5
Water adsorption, wt %			
10 % R.H.	7.5	2.0	
80 % R.H.	35	17.0[c]	

[a] Weight loss after heating in air at 954 °C.
[b] pH of an aqueous slurry of the gel at 5 wt % solids.
[c] >90 wt % water adsorption at 100 % R.H.

5.3. Production

Processes. The original production process of Patrick [309] as practiced by the Silica Gel Corporation starting in 1919 contains the main elements of modern processes using aqueous silicate raw materials. The initial step is the batch neutralization of sodium silicate (1.185 g SiO_2/cm^3) at 35–80 °C with 10 % HCl to form a hydrosol. A hydrogel then forms after 3–5 h at ambient temperature and is sized, washed with water to remove salts, and dried first at 75 –120 °C then 300–400 °C. A typical small pore gel made by this process is described in Table 15.

The Patrick gelation conditions, with relatively minor variation, have been the basis of most silica gel manufacture since. The next major change in silica gel products was the development of gels of higher pore volume and pore diameter by washing and aging hydrogels under basic conditions. Early references [324, 325] refer to this technology but large scale commercial introduction occurred around 1945. Base washing was a common industrial practice before 1950. In one example [326] a 17 % SiO_2 hydrosol gelled in about one hour. The hydrogel was broken up and washed with an aqueous ammonia solution of pH 9 for ca. 45 h then tray dried. Similar conditions are described for intermediate-density gel [313]. Alternative washing schemes are numerous and affect rates and equipment design or cost [353, 354]. In one such method that provides for faster throughput of silica hydrogel through the wash stages [354], the hydrogel particles containing reaction product salts are small (50–200 μm) and washing occurs via a hydrocyclone. In this case, the dried product typically has a surface area of 500 m^2/g and a nitrogen pore volume of 0.25 cm^3/g. A further variation involves fast drying [327] which increases the pore volume and diameter of such gels. Typical properties of acid-washed regular density, ammonia-washed intermediate density, and a flash-dried product are shown in Table 15.

Several methods of forming hydrogel, typically into spherical shapes, have been developed. Some methods employ a rapid gelation after mixing in a nozzle followed by spray setting [328–331], while others form beads in an oil phase immiscible with the hydrosol [332]. In some bead processes, recycled, dried, and powdered gel is mixed with the fresh sol to improve the physical integrity of the dried gels toward disintegration after contact with liquid water

[333]. The direct formation of 5–10 μm gel particles by emulsion polymerization or particle-forming techniques is also possible. A process for the direct formation of 1–5 μm particles with "double structure", i.e., with a core of dense silica and a shell of bulky amorphous silica, has been disclosed [334].

The supercritical preparation of aerogels has undergone a renaissance since earlier commercial production [335] because of renewed interest in the insulation and light-transmittance properties of these materials. The shift in applications toward large panels has created the need for what are described as aerogel monoliths [311]. One such process [315] forms a silica alcogel then exchanges the alcohol for liquid CO_2 before supercritical drying. The resulting monoliths show good light-transmittance properties. The monoliths, typically $500 \times 500 \times 2.5$ cm, can be used to fill the space in the middle of double-pane windows. Another process involves reacting silanol groups on the internal pore surface with a reagent such as trimethylchlorosilane, which then minimizes shrinkage of the gel under drying conditions [355]. Dried gels of very high porosity and low density are thus obtained.

Environmental Protection. In the sodium silicate/H_2SO_4 processes the main environmental concerns are the fate of byproduct process chemicals, normally aqueous Na_2SO_4 and small amounts of aqueous NH_3, and pH control of this stream.

Quality Specifications. Typical quality criteria for silica gel are chemical purity, moisture content, and porosity. These properties depend on manufacturing conditions such as concentrations, gelling and washing times, pH, and drying conditions. Typical properties of silica gels are reported in Table 15. Application-specific properties are often measured for certain end uses (see Section 5.4).

Silica gel has been described by numerous organizations for the purpose of defining the quality necessary for use in food, cosmetic, and pharmaceutical applications. In the United States, monographs for silica gel are included in the Food Chemicals Codex (1981) and The United States Pharmacopeia–The National Formulary (1990). In Japan it is described in the Japanese Pharmacopeia, Standard for Cosmetic Materials, and JIS Z 0701. It is also on the "Positive" list for use in food-grade polyolefins. The EC is compiling permitted silica gel uses into a complete listing for member states. Until that listing is complete member states will maintain individual regulations.

5.4. Uses

Silica gel is used extensively in a wide variety of applications; here, some major uses are described.

Desiccants. The earliest well-identified use for synthetic amorphous silica gel was as an adsorbent for water. The affinity of silica gel for water is affected by its state of activation (or moisture loading) and the degree of saturation of the surrounding fluid by water vapor. A plot of the affinity of silica gel for water vapor as a function of equilibrium relative humidity at ambient temperature is shown in Figure 36. The properties of two silica desiccants have been described in Table 15.

Silica gel is widely used in the narrow pore form to keep enclosed spaces dry, such as in cable

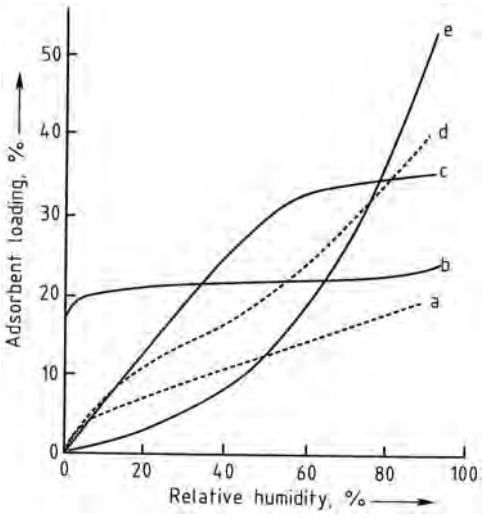

Figure 36. Water adsorption isotherms at room temperature as a function of relative humidity for several materials
a) Granular Al_2O_3; b) Zeolite A (Na^+ form); c) Regular density silica gel; d) Spherical Al_2O_3; e) Intermediate density silica gel

junctions, pharmaceutical containers, and consumer goods. Silica gel is also used for drying natural gas. The wider pore form of silica is used to prevent local condensation in high-moisture environments and to absorb condensed mists of moisture. Another application is to use silica gel to maintain a constant humidity environment around art objects [336].

Desiccants have been described in several countries by standards Mil-D-3716B (United States), DEF STAN 80–22 (United Kingdom), and JIS Z 0701–77. These descriptions include standard properties and methods of analysis.

Adsorbents. Silica gel can adsorb many species other than water, particularly polar substances [337]. In addition to chemical processing, silicas have many uses in food processing. Treatment of beer with hydrogels, hydrous gels, or xerogels to remove haze-forming proteins is one example [325, 338]. Another food use is the adsorptive purification of glyceride oils [339]. This use has been extended beyond food purification of glyceride oils to purification for the preparation of biodiesel fuel. Silica gels also are used extensively in chromatography [340].

Dentifrice. Silica gels have long been components of dentifrice formulations [341] but more recently were employed more for their suitable abrasiveness for cleaning than simply as carriers or thickeners. Xerogels [342] and hydrous gels [343] are used, but must compete with precipitated silicas [344] in this application. The abrasiveness of a dentifrice can be measured [345] and generally correlates with how effectively it cleans the teeth.

Coatings. Fine sized silicas (2–15 μm) are used extensively to control the reflectance of coatings [326, 327, 335]. By interrupting the surface of the coating the gloss of the surface (as measured by ASTM D 523) is reduced but particles too large can harm the appearance of the surface. The fineness of grind (ASTM D 1210–79) can be measured and specified. In clear coatings, the refractive index of the silica is important to maintain clarity. A typical matting agent has a particle size of ca. 10 μm, a pore volume of ca. 1.8 cm^3/g, and a fineness of grind on the Hegman scale of > 4 (ASTM test). A relatively new application for silica gels is in paper coatings for digital imaging, particularly by ink-jet printers [356]. In this application, the silica-rich coating serves to absorb ink-liquids and to control image appearance.

Microelectronics. The application of silica gels as insulators with low dielectric constants in microelectronics is developing. This use takes advantage of the air-containing pore structure to reduce the dielectric constant [357].

Catalysts and Catalyst Carriers. The high surface area of silica gel makes it an attractive solid on which to effect catalysis. Silica itself does not catalyze many reactions of commercial significance. Silica aluminas have acidic catalytic properties best exemplified in catalytic cracking [307, 346]. Silica gel is also used as a support in olefin polymerization [347–349].

Suppliers. A partial list of silica gel suppliers are summarized: DDC Basic Chemicals, DongGuan Vita pac, Engelhard Process Chemicals, Fuji Silysia, Grace Davison, Ineos, Qingdao Makall, Qingdao Haiyang, Philadelphia Quartz, Silicycle, and Uetikon.

5.5. Economic Aspects

Between 30–50 % of silica gel is estimated to be used in desiccant applications. Estimated production of silica gel in 2007 is $> 150\,000$ t/a.

5.6. Legal Aspects

Toxicology and Occupational Health. (see also Chap. 9). Silica gel is listed under TSCA in the United States, the Domestic Substances List (DSL) in Canada, the European Inventory of Existing Commercial Substances (EIECS), the Australian Inventory of Chemical Substances, and the Japanese Core Inventory (MITI) [358].

Silica gel is generally classified as synthetic amorphous silica. Epidemiological studies have indicated low potential for adverse health effects

in humans [350]. Silica gel is not listed on IARC, National Toxicology Program (NTP), or OSHA carcinogen lists.

The IARC evaluation of amorphous silica is that there is inadequate evidence for carcinogenicity to humans or experimental animals. The phrase "inadequate evidence" indicated that the studies cannot be interpreted as showing either the presence or absence of a carcinogenic effect. For synthetic amorphous silica, there is no evidence of carcinogenicity to animals or humans [359].

A study found that amorphous silica particles are regarded as rather innocuous, not causing chronic adverse pulmonary effects [359]. In contrast, exposure to crystalline silica particles can cause both acute and chronic pulmonary inflammatory responses. The objective of this study was to evaluate mechanisms of pulmonary responses to amorphous and crystalline SiO_2 after subchronic inhalation. The study compared the pulmonary response of rats inhaling amorphous silica for three months at concentrations which resulted in a similar acute inflammatory response for both compounds at the end of exposure. The conclusion is that the persistence of crystalline SiO_2 appears to be most important for its long-term effects and that amorphous silica shows significant in vivo solubility. A further conclusion is that acute inflammatory parameters cannot be used as predictors for long-term outcome and that type II cell activation appears to be associated with fibrotic lesions. The study suggests that persistence of high level of cell replication and inflammation may be mechanistically involved in the development of neoplasia.

Cellular changes identified as neoplasms in this study were seen for rats exposed to crystalline silica and were not seen in the rats exposed to amorphous silica. Also, any pathology seen in animals exposed to high doses of amorphous silica was reversible, whereas the pathology for animals exposed to crystalline silica continued to the development of neoplasia [360].

Tests conducted for United States FDA approval for use in foods (see 21 CFR 160.105, 160.815, and 172.480) showed:

LD_{50} (mouse) 8000 mg/kg (limit of test)
LD_{50} (rat) 4500 mg/kg (limit of test)
6-month feeding tests (rat) at levels up to 10 % of diet produced no effects.

A long-term bioassay of chronic toxicity on mice and rats concluded that "proper dietary administration of micronized silica has proven to be generally safe with no long-term toxic effects" [351].

Storage and Transportation. Silica gel should be stored in sealed containers to protect product quality, particularly to avoid moisture adsorption or desorption. Silica gel is not considered a hazardous material by the International Air Transportation Association (IATA Resolution 618, Attachment "A", 1992), the U.S. DOT (49 CFR), or in EEC Council Directive 67/548/EEC.

6. Pyrogenic Silica

The term pyrogenic silica refers to highly dispersed silicas formed from the gas phase at high temperature. Nowadays, the most important production process is flame hydrolysis. The electric-arc process is of little and the plasma process of no economic significance. The designation pyrogenic used in this chapter therefore always refers to silica produced by flame hydrolysis.

6.1. Flame Hydrolysis

The flame hydrolysis process was developed in the late 1930s and patented in 1942 [361]. The original aim was to develop a "white carbon" as a reinforcing filler for rubber. However, for technical and economic reasons precipitated silicas (see Chapter 7) were adopted for this use.

In the meantime pyrogenic silica [*112945-52-5*] has found applications in numerous branches of industry.

Capacities for pyrogenic silicas amounted to ca. 100 000 t worldwide in 1991. Producers are Degussa (Aerosil), Cabot (Cab-o-sil), Wacker (HDK), and Tokuyama Soda (Reolosil).

6.1.1. Production Process

Silicon tetrachloride is the usual raw material for flame hydrolysis. It is continually vaporized,

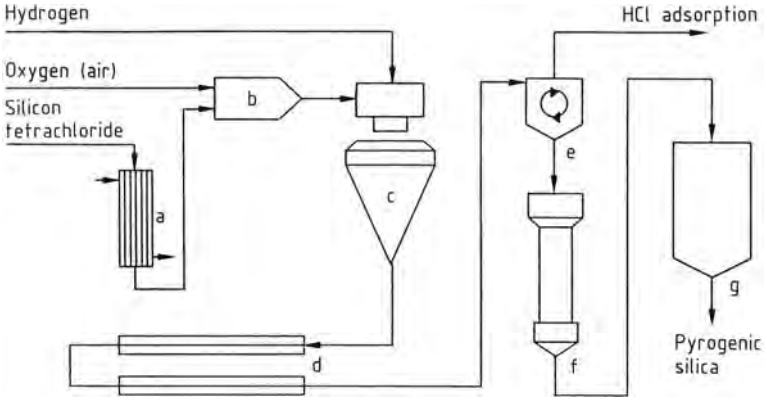

Figure 37. General process scheme of flame hydrolysis
a) Vaporizer; b) Mixing chamber; c) Burner; d) Cooling section; e) Separation; f) Deacidification; g) Hopper

mixed with dry air and then with hydrogen, fed to a burner, and hydrolyzed:

$$2\,H_2+O_2\rightarrow 2\,H_2O$$

$$SiCl_4+2\,H_2O\rightarrow SiO_2+4\,HCl$$

The gases leaving the reaction chamber contain all of the silica in the form of an aerosol.

The silica is separated almost quantitatively from the hydrochloric acid- containing off-gas by cyclones (centrifugal separators) or filters. Treatment with steam and air in a fluidized-bed reactor is then carried out to remove residual hydrochloric acid adsorbed on the large surface of the silica. The hydrogen chloride is washed from the off-gases in adsorption columns to give hydrochloric acid in commercial concentrations. The hydrochloric acid formed can be reused by reacting it with silicon to produce silicon tetrachloride and hydrogen.

The properties of pyrogenic silica can be controlled by varying reaction parameters such as flame composition and flame temperature. Thus, desired specific surface areas in the range 50 to 400 m^2/g can be produced selectively.

The product, with a bulk density < 20 g/L, is pneumatically transported to packing machines, where the tapped density is increased to 50 – 120 g/L by compacting rollers or vacuum packers.

A schematic of the flame hydrolysis process is shown in Figure 37.

It is also possible to use methyltrichlorosilane alone or mixed with silicon tetrachloride as raw material. In this case, however, simultaneous hydrolysis and oxidation is required, which requires modification of the production process.

6.1.2. Morphology

Flame hydrolysis produces extremely fine, mostly spherical particles with diameters of ca. 10 nm. The size of the average primary particles, which can be measured by transmission electron microscopy (TEM), ranges from 7 to 40 nm. The particle-size distribution becomes narrower with decreasing primary particle size (see Fig. 38).

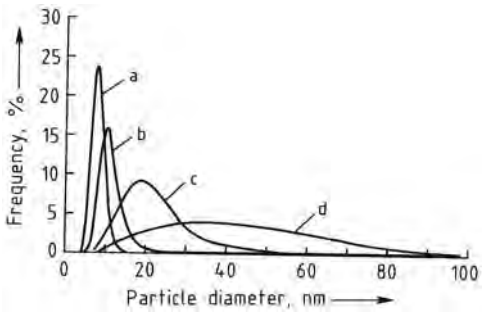

Figure 38. Primary particle-size distribution of pyrogenic silicas with various specific surface areas
a) 300 m^2/g; b) 200 m^2/g; c) 90 m^2/g; d) 50 m^2/g

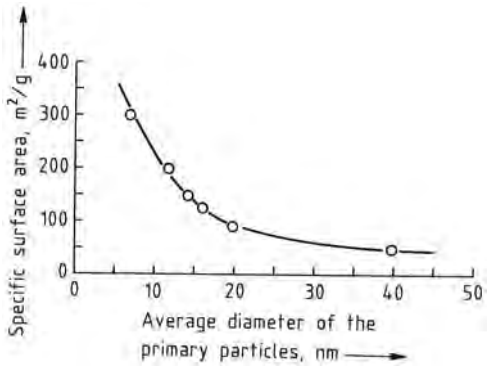

Figure 39. Correlation of the average primary particle size with the specific surface area of different pyrogenic silicas

The small particles give rise to high specific surface areas of ca. 50–400 m^2/g. This consists almost entirely of outer surface, which is not formed by pores, and is readily accessible to diffusion processes. The specific surface areas determined by adsorption (e.g., by the BET method [362]), are in agreement with those determined by TEM within certain limits. Figure 39 shows the BET surface area as a function of the mean particle size measured by TEM.

The primary particles do not occur in isolation, but form aggregates by intergrowth, and agglomerates through cohesion forces. In contrast to precipitated silicas, pyrogenic silicas cannot be produced in the form of defined aggregates or agglomerates. The primary particles can be identified by TEM, but it is not possible to distinguish aggregates from agglomerates [363].

The size of the agglomerates actually present in a liquid or powder mixture depends mainly on the dispersion and mixing intensity during preparation.

Figure 40 shows a TEM photograph of a pyrogenic silica with an average primary particle size of ca. 40 nm and a specific surface area of ca. 50 m^2/g, while Figure 41 shows one with an average primary particle size of ca. 7 nm and a specific surface area of ca. 300 m^2/g.

6.1.3. Solid-State Properties

Pyrogenic silicas are X-ray amorphous. For example, X-ray diffraction photographs with a detection limit of 0.2 % for Aerosil 200, a hydrophilic pyrogenic silica with a specific surface area of ca. 200 m^2/g, show no crystallinity [364]. This fact is of considerable significance for industrial hygiene, since current experiences indicate that the development of silicosis on inhalation of silica dust is associated with the crystallinity.

The refractive index of 1.45 is similar to that of silica glass. The particle size and the surface chemistry have a small but measurable influence on the refractive index. Transparent mixtures can be prepared from pyrogenic silicas and most organic polymers.

Pure pyrogenic silicas are thermally quite stable. Thus, heating for 7 d at 1000 °C results in no change of the morphology and no crystallization. The thermal stability is, however, significantly lower if other substances are present. Traces of alkali or alkaline-earth metal ions in particular act as mineralizers [365].

Since pyrogenic silicas are produced from readily vaporizable starting materials that can be easily purified by distillation, impurity concentrations resulting from the raw materials are very low. Generally, the silicon dioxide content is > 99.8 % after ignition for 2 h at 1000 °C to remove chemically and physically adsorbed water. The content of hydrochloric acid byproduct can be reduced to less than 250 ppm by suitable measures, which is adequate for most applications.

The purity of pyrogenic silicas is specified particularly for their use in pharmacy. The most important monographs concerning this are:

1. European Pharmacopeia 2 (Silica Colloidalis Anhydrica)
2. DAB 10 (Hochdisperses Siliciumdioxid)
3. U.S.P./National Formulary XVII (Colloidal Silicon Dioxide)

Pyrogenic silicas are largely inert chemically. They dissolve in strong alkali solutions with silicate formation and in hydrofluoric acid with the formation of silicon tetrafluoride. The solubility in pure water is similar to that of quartz (ca. 150 mg/L). Figure 42 shows the solubility behavior of a pyrogenic silica with a specific surface area of 200 m^2/g in the alkaline pH range.

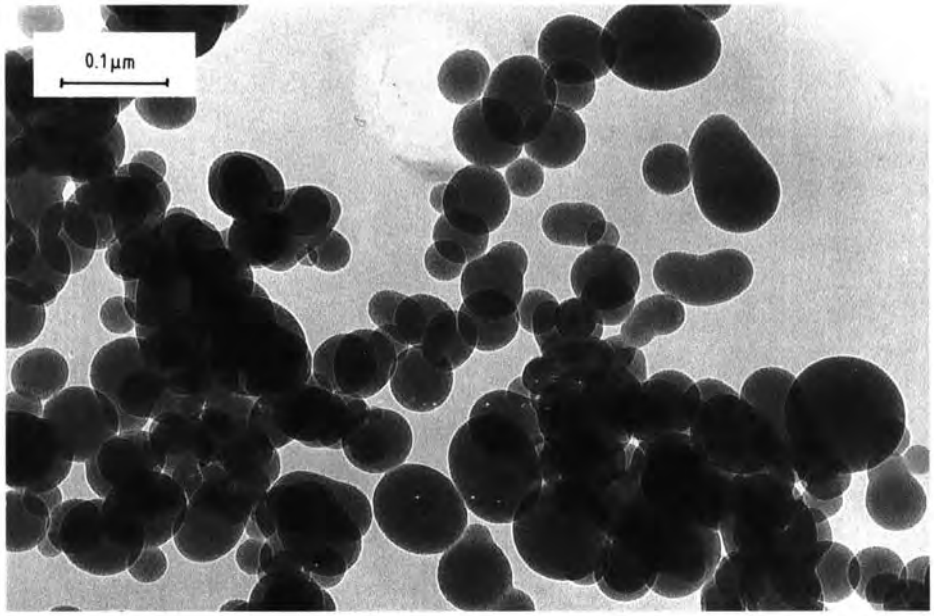

Figure 40. TEM photograph of a pyrogenic silica with an average primary particle size of ca. 40 nm and a specific surface area of ca. 50 m^2/g

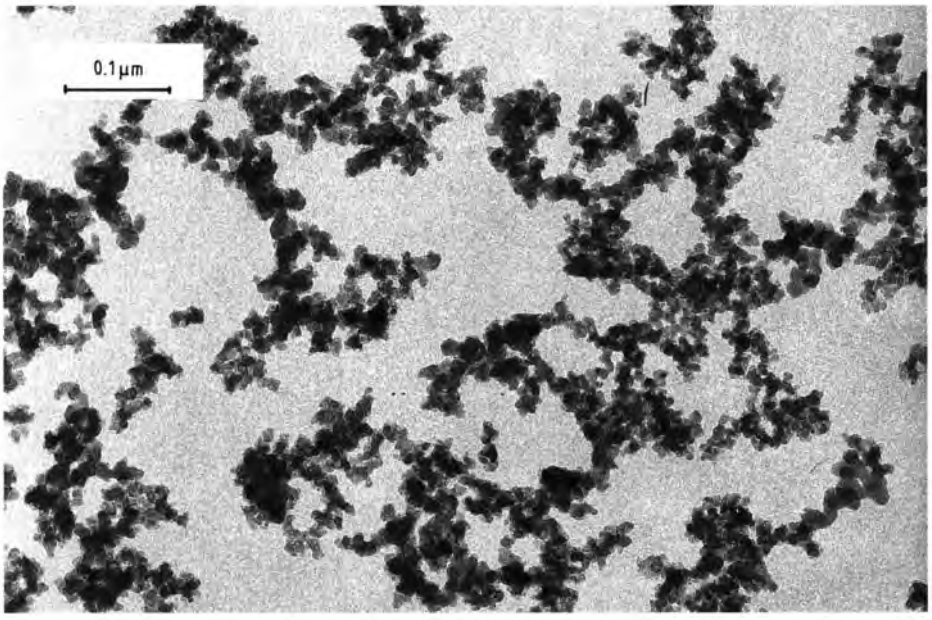

Figure 41. TEM photograph of a pyrogenic silica with an average primary particle size of ca. 7 nm and a specific surface area of ca. 300 m^2/g

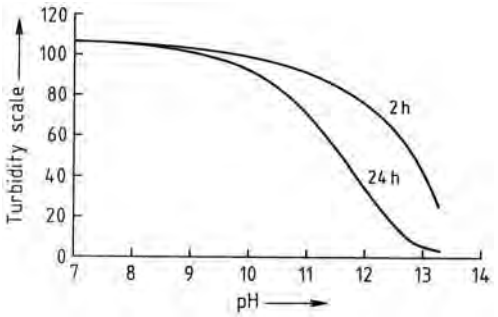

Figure 42. Time dependence of the solubility of a pyrogenic silica in caustic soda

6.1.4. Surface Chemistry

Siloxane and silanol groups occur on the surface of the silica particles. The former are hydrophobic while the latter are hydrophilic and make the pyrogenic silica wettable. The silanol groups can occur isolated, bridged, or geminal (Fig. 43).

The silanol groups can be determined quantitatively by reaction with lithium aluminum hydride and measurement of the amount of hydrogen formed. The densities lie between 2.5 and 3.5 SiOH/nm^2 [366, 367]. The silanol groups are weakly acidic, which causes a zeta potential for the pyrogenic silicas of zero at a pH value of approximately two [368]. Pyrogenic silicas become preferably negatively charged by friction [369].

IR spectroscopy is important for the analysis of the surface chemistry of pyrogenic silicas [367, 370–373], and methods such as solid-state NMR spectroscopy promise further results. The following IR bands are of significance:

– O–D	2760 cm^{-1}
– C—H	2900–3000 cm^{-1}
—SiOH isolated	3750 cm^{-1}
—SiOH bridged	3000–3800 cm^{-1}
—SiOH combination band	4550 cm^{-1}
H_2O adsorbed	5200 cm^{-1}

Immediately after production pyrogenic silicas show mainly isolated silanol groups. In the course of time, adsorbed water reacts with strained siloxane groups and forms bridged silanol groups. This aging can easily be followed by IR spectroscopy (Fig. 44) [367].

The desorption energies of both the chemically and physically bound water can be determined by gravimetric adsorption and temperature-programmed desorption [374]. Thus, the following energies were determined: 50 kJ/mol, for water hydrogen bonded to a silanol group, and 84 kJ/mol for water bonded to two neighboring silanol groups. The elimination of water from neighboring silanol groups and isolated silanol groups requires 122 kJ/mol and 130 kJ/mol, respectively.

The silanol groups undergo acid-specific reactions; examples include:

1. With hydride ions (e.g., $LiAlH_4$) [366]

$$= Si —OH + H^- \rightarrow = Si —O^- + H_2$$

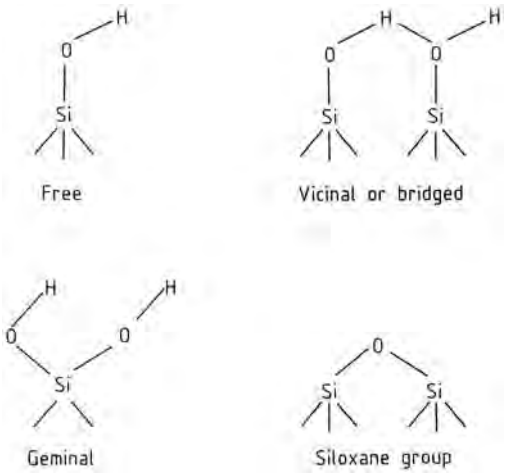

Figure 43. Siloxane and silanol groups on the silica surface

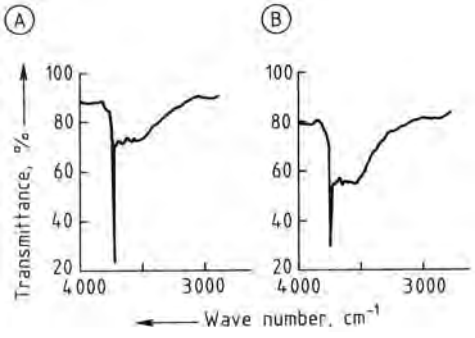

Figure 44. IR spectra of pyrogenic silica (200 m^2/g specific surface area) shortly after production (A) and after storage for one year (B)

2. Deuterium exchange [367]

$$\equiv Si—OH + D_2O \rightarrow \equiv Si—OD + HDO$$

3. Neutralization [375]

$$\equiv Si—OH + NaOH \rightarrow \equiv Si—ONa + H_2O$$

4. Chlorination [376]

$$\equiv Si—OH + SOCl_2 \rightarrow \equiv Si—Cl + SO_2 + HCl$$

5. Esterification with diazomethane [376]

$$\equiv Si—OH + CH_2N_2 \rightarrow \equiv Si—O—CH_3 + N_2$$

Summaries of the surface chemistry of finely divided silicas are given in [377, 378].

6.1.5. Surface Modification with Silicon Compounds

Pyrogenic silicas are hydrophilic; however, a hydrophobic character is more favorable for some applications. This requirement can be met by reaction with dimethyldichlorosilane [379, 380]. The resulting silica thus is no longer wettable by water and was introduced on the market in 1962 under the name Aerosil R 972. Apart from chloroalkylsilanes, mainly hexamethyldisilazane, alkoxyalkylsilanes, and polydimethylsiloxanes are used.

Apart from methyl and longer chain alkyl groups, organofunctional groups can also be anchored on the surface of pyrogenic silicas by using silanes. This form of modification was first used on a large scale for applications in dental materials. A pyrogenic silica with a low specific surface area is treated with γ-methylacryloxypropyltrimethoxysilane to give an active filler that can be chemically bonded to the polymethylmethacrylate matrix and provides the dental material with very good mechanical properties [381–383].

Another use of pyrogenic silicas modified with organofunctional silanes is in toners. Until recently photocopiers generally fixed the latent electrostatic image on a positively charged selenium layer. An electrostatically negatively chargeable toner is required for development, which contains a hydrophobic pyrogenic silica to improve the flow behavior and chargeability. In more modern copier systems the latent image is formed on an organic semiconductor layer, which is negatively charged and requires a positively chargeable toner. However, pyrogenic silicas tend to become negatively charged due to the presence of silanol groups even in hydrophobized products. Hence, a surface modification is necessary to allow positive charging. This can be achieved by using aminofunctional silanes, which undergo hydrolysis-stable anchoring to the silica surface [384–386].

6.1.6. Characterization

Pyrogenic silicas can be characterized well on the basis of chemical and physicochemical data; however, these do not allow a definite assessment of their suitability for a particular use, which requires application testing. The following test methods have proved useful to test the suitability for many uses and also for the quality control of hydrophilic, pyrogenic silicas:

1. BET surface area, m^2/g (DIN 66 131)
2. Drying loss, % (2 h at 105 °C; DIN ISO 787/II)
3. pH value (4 % aqueous suspension; DIN ISO 787/IX)
4. Silicon dioxide content, % (fuming with hydrofluoric acid, relative to the substance heated at 1000 °C for 2 h)

For hydrophobic or surface-modified pyrogenic silicas it is advisable to determine the carbon content instead of the silicon content, since the former provides information on the extent of surface loading.

6.1.7. Uses

Reinforcing Fillers. Pyrogenic silica is used in large quantities as an active filler in silicone rubber (→ Silicones). In RTV silicone sealants, both hydrophilic and hydrophobic pyrogenic silica are used (ca. 10 %) to modify mechanical properties such as Shore hardness, tensile strength, and tear strength. High temperature vulcanizing (HTV) silicone rubber requires ca. 30 % pyrogenic silica to improve the mechanical properties. Hydrophobic pyrogenic silicas with strongly reduced thickening action are used in liquid silicone rubbers. Theories of the

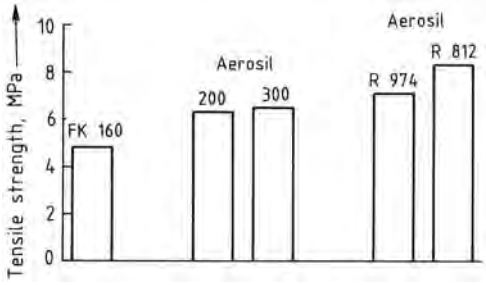

Figure 45. Tensile strength of silicone vulcanizates containing a precipitated silica (FK 160), two hydrophilic (Aerosil 200/300), and two hydrophobic (Aerosil R 974/R 812) pyrogenic silicas

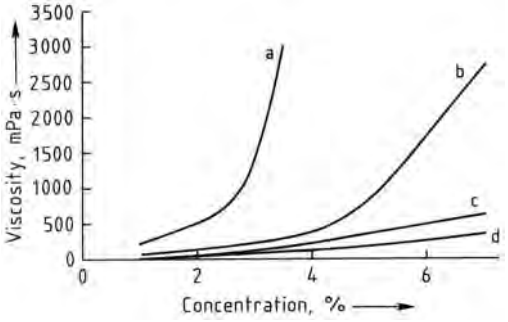

Figure 46. Thickening effect of a pyrogenic silica with 200 m^2/g specific surface area (Aerosil 200) in various solvents
a) Xylene; b) Butylacetate; c) Diacetone alcohol; d) Butanol

reinforcing action of pyrogenic silica in silicone rubber are discussed in [387–389].

The tensile strength of vulcanized silicones with various silica fillers is shown in Figure 45.

Pyrogenic silicas are also used as active fillers in natural and synthetic rubber, particularly if extremely high mechanical properties are required, as in cable sheathing, seals, or conveyor belts.

In fluoroelastomers, both hydrophilic and hydrophobic silicas improve the mechanical properties [390, 391], even under the action of aggressive gases.

Thickening and Thixotropization. An important application for pyrogenic silicas is the adjustment of the rheological properties of liquid systems such as paints, thermosetting resins, and printing inks. The increase in viscosity generally plays a minor role; thixotropization and the development of a yield value are decisive in practice. These effects are generally attributed to the formation of a three-dimensional network of silica agglomerates, which fixes the liquid in "cells" and thus increases the viscosity. The silica particles interact via silanol groups. The spatial network is destroyed by mechanical stress (e.g., stirring or shaking) to an extent which depends on the intensity and duration of energy input, whereby the viscosity decreases. The silica network regenerates when the stress is removed, and the original viscosity returns. This theory has proved suitable for simple, nonpolar liquids, but is not applicable to complex and/or polar systems, in which adsorption and solvation effects determine the rheological activity [392], especially in the case of hydrophobic pyrogenic silicas.

Hydrophilic pyrogenic silicas show the best thickening action in nonpolar liquids (Fig. 46).

Antisettling Agents. Closely linked with the control of the rheological properties of liquid systems is the action of pyrogenic silicas as antisettling agents. The establishment of a flow limit hinders settling of suspended particles, depending on their density, size, and shape. If settling does occur, pyrogenic silica generally prevents caking of the sediment and ensures easy dispersibility.

This effect is mainly utilized in filler- or pigment- containing paints and plastics. Not only suspensions of lighter solids can be stabilized, such as silica-based matting agents, but also heavy anticorrosion pigments such as zinc dust or micaceous iron oxide. Both hydrophilic and hydrophobic pyrogenic silicas can be used as antisettling agents. The most suitable type must be determined for each individual case, whereby additional effects, such as the water repellency of hydrophobic products in corrosion protection systems, must also be taken into consideration [393, 394].

Dispersants. In solid-containing liquid systems, pyrogenic silicas reduce the reagglomeration of the solid particles during the dispersion process, whereby a more favorable state of distribution is achieved. This effect is particularly important in pigment-containing systems, where both the gloss and also the tinting strength, and in the case of carbon black pigments also the jetness, can be improved by adding small quantities of pyrogenic silica [393].

Free Flow Agents. Some powders exhibit poor fluidity or they agglomerate on storage, particularly under the influence of pressure or moisture. The causes of agglomeration include solid bridges, which form by drying or pressure sintering processes, liquid bridges, electrostatic charging, and van der Waals forces [395, 396]. This can make use of the material difficult or even impossible. In many cases this can be remedied by the addition of hydrophilic or hydrophobic silicas. The reasons for this are complex. Thus, the small silica particles can envelop the powder particles and act as "ball bearings", hydrophilic pyrogenic silica can adsorb moisture and "render it harmless", or hydrophobic pyrogenic silica can slow down the absorption of moisture. The significantly smaller silica agglomerates can decrease the van der Waals forces between two powder particles by acting as spacers [396, 397]. Pyrogenic silica is used in fire extinguisher powders, tablet mixtures, toners, powder coatings, and table salt.

Other uses of pyrogenic silica include:

1. Adsorbents
2. Antiblocking agents for plastic films
3. Coatings
4. Catalyst supports
5. Matting agents
6. Grinding agents
7. Polishing agents
8. Raw materials for silica glasses
9. Thermal insulation
10. Additive carriers

6.1.8. Industrial Hygiene and Safety

Pyrogenic silica does not cause silicosis on inhalation (see also Chap. 9). So far no indication for this illness has been found for those employed in production who undergo regular medical tests [398]. However, since it can lead to irritation of the respiratory tract due to the fine particles, a MAK of 4 mg/m^3 total dust in inhaled air was applicable in 1991. This MAK value is not exceeded if suitable precautions are taken, e.g., lowest possible dust development upon handling or extraction of air (ventilation). Otherwise dust masks should be used. According to the findings so far pyrogenic silica is basically harmless by oral intake [399, 400]. Pyrogenic silica can cause a feeling of dryness on the skin, which can be easily remedied by washing and creaming.

Pyrogenic silica is susceptible to electrostatic charging on handling. If it is likely to come into contact with combustible gases or vapors, it is necessary to take the corresponding safety measures, such as careful earthing and utilization of explosion-proof plants.

6.2. Electric-Arc Process

The reduction of quartz sand with coal in an electric-arc furnace gives gaseous silicon monoxide, which is oxidized to finely divided amorphous silica by atmospheric oxygen [401]:

$$SiO_2 + C \rightarrow SiO + CO$$

$$SiO + CO + O_2 \rightarrow SiO_2 + CO_2$$

In a variant of this process the thickening effect of the electric-arc silica is increased by adding steam during oxidation followed by thermal treatment [402].

The matting agent TK 900 [*112926-00-8*] used in paints is a silica produced by Degussa using this process.

6.3. Plasma Process

Finely divided amorphous silicas can be produced in plasma burners. In one case quartz sand is reduced to silicon monoxide with methanol at ca. 2000 °C. Subsequently, reduction with steam is carried out [403]. At present such silicas are not available commercially. A schematic of the plasma process can be found in [404].

7. Precipitated Silicas

7.1. Introduction

Precipitated silicas, like pyrogenic silicas and silica gels, are a synthetic, finely divided, white, amorphous form of silicon dioxide. Precipitated silicas have only been produced commercially since the 1940s. In the meantime, they have become the most important group of silica products on the basis of the amounts produced. Worldwide production capacity in 1999 was ca. 1 100 000 t, compared to ca. 400 000 t in

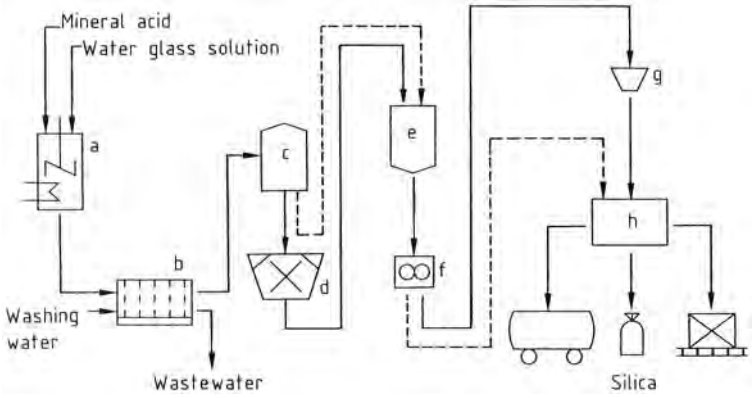

Figure 47. Process scheme for the production of precipitated silicas
a) Precipitation; b) Filtration; c) Drying; d) Grinding; e) Storage; f) Compacting; g) Granulation; h) Packaging

1970. Capacities in Europe, America, and Asia amount to 400 000, 340 000, and 360 000 t, respectively.

The largest producers worldwide are Degussa-Hüls, Rhodia, Akzo, and Crosfield in Europe, as well as PPG and Huber in the United States. The Asian market is additionally supplied by numerous local producers. Among these, the companies with the largest capacities are Nippon Silica and Tokuyama Soda in Japan, and Sam Yung and Kofran in Korea.

7.2. Production

Raw materials for the production of precipitated silicas are aqueous alkali metal silicate solutions (e.g., water glass) and acids, generally sulfuric acid [405–420]. Precipitation with hydrochloric acid [421, 422], organohalosilanes [423, 424], carbon dioxide [425, 426], or a combination of the latter with mineral acids [427] are of minor economic importance.

In the reaction of alkali metal silicate solution with mineral acid, the silica precipitates according to the following equation:

$$Na_2O{\cdot}3.3\,SiO_2 + H_2SO_4 \rightarrow 3.3\,SiO_2 + Na_2SO_4 + H_2O$$

In contrast to silica gels, which are produced under acidic conditions, in this case precipitation is carried out in neutral or alkaline media. The properties of the precipitated silicas can be influenced by the design of the plant equipment and by varying the process parameters.

The production process consists of the following steps: precipitation, filtration, drying, grinding, and, in some cases, compacting and granulation (Fig. 47).

Numerous possibilities exist for carrying out the precipitation [405–427]. So far only batch precipitation processes have attained economic importance, although continuous precipitations have also been reported [420]. Generally, acids and alkali metal silicate solution are fed simultaneously into water in a stirred vessel with the formation of silica seeds. In the course of the precipitation, three-dimensional silica networks are formed, accompanied by an increase in viscosity. The networks are reinforced by further precipitation of oligomeric silica and grow further into discrete particles with a decrease in viscosity. The formation of a coherent system and thus a gel state is avoided by stirring and increasing the temperature.

The properties of the silica can be influenced by varying important precipitation parameters such as pH, temperature, duration, and solid concentration. Additionally, the rate of addition of the acid and the intensity of stirring, which can be supplemented by a shearing action, also influence the properties of the silica.

The separation of the silica from the reaction mixture and the washing out of the salts contained in the precipitate is carried out in filter aggregates such as rotary filters, belt filters, or filter presses (chamber, frame, and membrane filter presses).

The solids content of the washed filter cake is 15–25 % depending on the type of silica and

filter; therefore, drying requires the evaporation of large quantities of water. Depending on the desired properties of the end product, drying is carried out in spray, nozzle spray, plate, belt, or rotary dryers. Special product properties can be achieved by spray drying the filter cake after redispersion in water or acid [410, 413, 428].

To control the desired fineness of the particles, various mills and, if required, classifiers [429] are used. Special degrees of fineness can be achieved by air-jet or mechanical grinding [410, 430]. The silica is separated from the air in cyclones or filters.

Figure 48 shows scanning electron micrographs of a spray-dried, unground silica and a conventionally dried, ground silica.

Processes for the compression and granulation of precipitated silica have been developed [431, 432] to reduce the volume for transport and for certain uses and also to decrease the formation of dust on handling and processing.

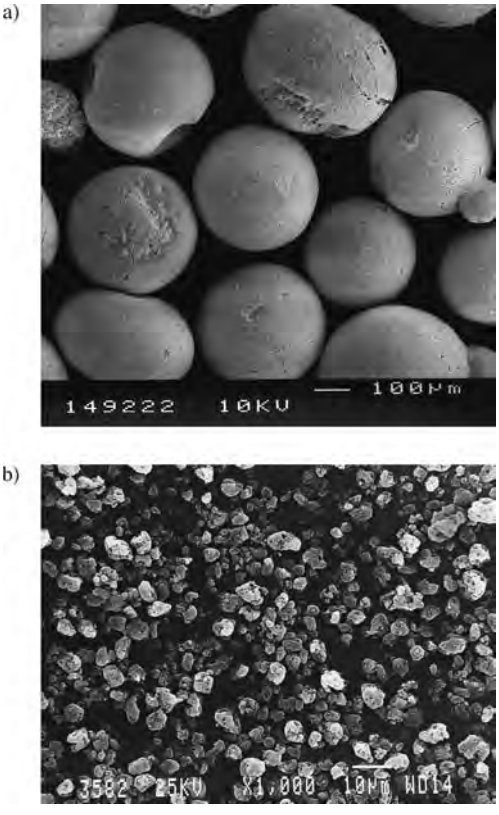

Figure 48. REM photographs of precipitated silicas
Top: spray-dried unground silica; bottom: conventionally dried, ground silica

Bags, big bags, containers, or transport silos are used for packaging and shipping. Information about the different methods of packaging and shipping is given in [433]; dust-free handling of precipitated silicas is described in [434]. In Germany the general dust limit of 4 mg total dust/m^3 air must be adhered to when handling precipitated silicas. Similar regulations apply in other countries.

7.3. Properties

7.3.1. Physicochemical Properties

Precipitated silicas consist mainly of spherical primary particles, generally intergrown in three-dimensional aggregates. These aggregates can pack together to form larger agglomerates. The terms primary particle, agglomerate, and aggregate are defined in DIN 53 206.

Some important physicochemical properties of several precipitated silicas are listed in Table 16.

The specific surface area is generally determined by the BET method (DIN 66 131; ISO 5794–1, Annex D), which measures both the outer surface and the surface of accessible pores. The specific surface area is of importance especially in reinforcement and adsorption applications. Precipitated silicas can be produced with specific surface areas of 25–800 m^2/g.

The mean particle size is important in the use of precipitated silicas as matting or antiblocking agents for paint systems and plastic films. The particle size can be determined by various methods either on the powder or after incorporation in a medium (e.g., water, paint, silicone rubber) [435].

The tamped density (ISO 787–11) is a measure of the weight of the powder and thus gives indications of the spatial requirement for transportation and a general guide for handling. The tamped densities of precipitated silicas lie in the range of 50–500 kg/m^3.

The loss on drying (ISO 787–2) includes the majority of the water physically bound to the silica and for precipitated silicas generally lies between 2.5 and 7 % (on leaving the supplier).

The loss on ignition (ISO 3262–11) includes the additionally chemically bound water (a siloxane group is formed from two neighboring silanol groups with the loss of a water molecule).

Table 16. Physicochemical data and chemical composition of several precipitated silicas [CAS registry nos.: [*112926-00-8*] except for Sipernat D17 [*60842-32-2*]; appearance: flutty white powder except for Utrasil 7000 GR (granulate); behaviour towards water: hydrophilic except for Sipernat D17 (hydrophobic)]

	Ultrasil 7000 GR	Sident 9	Sipernat 22	Sipernat 50 S	Sipernat 570	Acematt OK 412[n]	Sipernat D 17[o]
BET surface area (N_2)[a], m^2/g	170	45	190	450	750	130	100
Mean particle size, μm	3000[l]	10.5[j]	100[l]	7.5[j]	6.7[j]	3[m]	7[j]
Tamped density[b], g/L	280	430	280	90	150	120	150
Loss on drying[c], %	5	3	6	6	6	5	4
Loss on ignition[d,g], %	4	3	5	5	5	11.5	7
pH value, 5 % in water[e]	6.5	6.9	6.5	6	6	6	8.0[p]
DBP absorption[f,g], g/100g	210[g]	120	260	325	250	265	225
SiO_2 content[h], %	98	99	98	98.5	99	99	98
Na content as Na_2O[h], %	1	0.5	1	0.6	0.5	0.3	1
Fe content as Fe_2O_3[h], %	0.03	0.03	0.03	0.03	0.02	0.03	0.03
Sulfate content as SO_3[q], %	0.8	0.3	0.8	0.7	0.3	0.3	0.8
Sieve residue 45 μm[i], %		0.1	0.5	0.1	0.01	<0.01	0.1

[a] ISO 5794–1, Annex D.
[b] ISO 787–11.
[c] ISO 787–2.
[d] ISO 3262–11.
[e] ISO 787–9.
[f] ASTM D 2414.
[g] Based on dried substance.
[h] Based on ignited substance.
[i] ISO 787–18.
[j] Coulter Multisizer, 100 μm capillary.
[k] Coulter Multisizer, 140 μm capillary.
[l] Alpine sieving, ISO 8130–1.
[m] Determined from SEM photos.
[n] Matting agent.
[o] Contains ca. 2 % chemically bound carbon.
[p] 5 % in water : methanol (1 : 1).
[q] Based on original substance.

Ignition losses for precipitated silicas generally lie between 3 and 7 %.

Generally the pH value (ISO 787–9) of precipitated silicas is ca. 7.

The dibutyl phthalate (DBP) absorption (ASTM D2414) is a measurement of the absorptive capacity and for precipitated silicas lies in the range of 175–320 g/100 g. The absorptive capacity is important for the conversion of liquids and pastes into powders.

The determination of the sieving residue (ISO 787–18) provides an indication of the amount of difficultly dispersible fractions in a precipitated silica.

7.3.2. Surface Chemistry and Surface Modification

Precipitated silicas have two different functional groups on their surfaces: silanol (Si—OH) groups and siloxane (Si—O—Si) groups.

These two groups substantially influence the surface properties and hence the application properties of precipitated silicas. The surface has 5–6 silanol groups per nm^2, which results in the hydrophilic character of precipitated silicas. Whereas the siloxane groups are generally chemically inert, the reactivity of the silanol groups allows chemical surface modification [436] of precipitated silicas. Thus, the reaction with organosilanes [437–439] or silicone fluids [440, 441] leads to hydrophobic precipitated silicas.

Hydrophobization is carried out industrially both by wet processes (e.g., addition of organochlorosilane to the precipitate suspension; see Fig. 49) and dry processes (e.g., the reaction of precipitated silicas with silicone fluids).

In coating processes, in contrast, no chemical reaction takes place; the coating agents are adsorbed on the silica surface. Wax coating with wax emulsions has become industrially important [410, 442, 443].

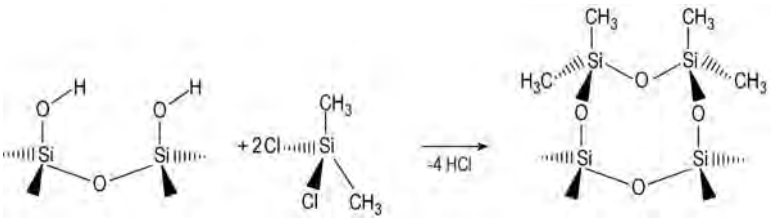

Figure 49. Schematic of the reaction of the surface silanol groups of a precipitated silica with dimethyldichlorosilane

Surface modification is advantageous for certain applications (e.g., free flow agents, defoamers, and matting agents; see Section 7.4).

7.3.3. Chemical Composition and Analysis

The chemical composition of precipitated silicas (see Table 16) is generally less important than the physicochemical data with regard to the application properties. Furthermore, commercially available precipitated silicas differ only slightly in their composition.

The SiO_2 content is determined gravimetrically by fuming off with hydrofluoric acid (ISO 3262–17); the analysis of the metal- containing impurities is performed by atomic absorption spectrometry (AAS). The sulfate content is determined by complexometric titration (DIN 38 405/5), colorimetric titration (DIN 2462/8), or potentiometric titration.

The carbon content of modified silicas is determined by converting the carbon-containing component into CO_2 (ISO DIS 3262–19: 1994).

A survey of the chemical analysis of precipitated silicas is given in [444].

7.4. Uses

Precipitated silicas can be tailor-made to meet the requirements of various uses. Only the most important of the numerous applications (Fig. 50) are mentioned here.

The oldest and most important use of precipitated silicas is the reinforcement of elastomer products such as shoe soles, technical rubber articles, cable sheating, and tire compounds [445, 446].

The addition of 20–100 parts by weight of precipitated silica to 100 parts by weight of natural or synthetic *rubber* improves the tensile strength, hardness, tear strength, and abrasion resistance of the vulcanized material [447]. Furthermore, special precipitated silicas enable the production of transparent vulcanized materials. The reinforcing effect of precipitated silicas is superior to that of natural or mineral fillers and, in contrast to carbon blacks, they allow the production of white and colored rubber articles.

In *cables*, they are used mainly in sheathing compounds for cables that are not fixed and must be differentiated from the background by a colored exterior (e.g., mining or excavator-hauling cables). The high resistance of the cable sheath to friction and tearing protects the inside of the cable from abrasion and damage.

Since the early 1990s precipitated silica has been used as a high-performance reinforcing filler in rubber compounds for *tires*. To take full benefit of silica in terms of tire performance, it is essential to use highly dispersible silica grades such as Ultrasil 7000 GR (Degussa-Hüls) or

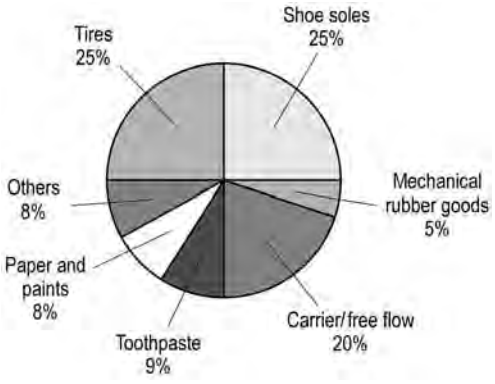

Figure 50. Worldwide consumption and use of precipitated silica in 1999

Zeosil 1165 MP (Rhodia) with a silane coupling agent. The use of highly dispersible silica in tread compounds leads to significant improvements in rolling resistance and wet traction of tires. Due to the possibility of achieving the best compromise of the three main tire-performance criteria ("magic triangle") — rolling resistance, wet traction, and tread wear — silica is now widely used in Europe, and demand in North America and Asia is growing significantly. The use of silica in the bodies of car and truck tires is becoming increasingly interesting owing to the need to further reduce rolling resistance to cut fuel consumption and CO_2 emissions [448–450].

Precipitated silicas are also used as reinforcing agents in *silicone rubber* [451, 452], where they replace the more expensive pyrogenic silicas in certain formulations.

In *thermoplastics*, precipitated silicas are used to improve specific properties. They act as antiblocking agents and are used to prevent plate-out effects in films and film production. They are also used to improve the mechanical properties of PVC flooring.

A further major application is the use as *carrier silicas* for liquids and semiliquids and as free flow agents for powder formulations, particularly of hygroscopic and caking substances. Of particular importance is high adsorptivity and good flowability of the silica. Such precipitated silicas absorb liquids or solutions to give powder concentrates that contain up to 70 % of the liquid [453]. In this way liquid materials are converted into a dry, free-flowing form, which can be mixed in any ratio with other dry substances. This is of particular importance in the animal-feed industry for the mixing of feed additives [454]. Materials converted into powder form include: choline chloride, ethoxyquin, molasses, and vitamin E acetate [455]. Fats can be converted into free-flowing powders for use as milk-substitute feeds [453, 455], mainly for the fattening of calves (Fig. 51). The same effects are utilized in the food industry, where products such as coffee whiteners (nondairy creamers) and mixed spices are produced and kept intact with the aid of the specific properties of synthetic silicas [462, 463]. Precipitated silicas are used as carriers for crop protection agents and insecticides [456, 464, 465].

Precipitated silicas are being used increasingly in *toothpastes* as cleaning agents, since they clean effectively with a minimum of scratching [457]. Additionally, they control the rheological properties of toothpastes and also enable the production of transparent gels [458].

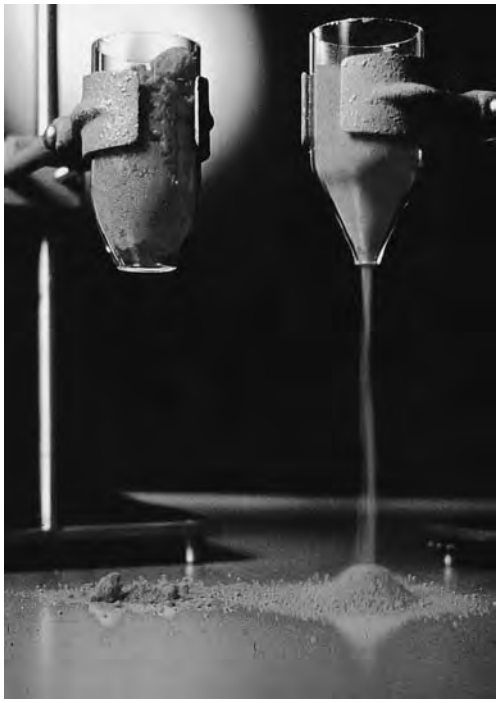

Figure 51. Milk substitutes
Left: without addition; right: after addition of 1.5 % Sipernat 22 S

The surfaces of objects are matted for reasons of fashion but also to increase safety by avoiding dazzle. Special silica *matting agents* have been developed for matting of paints and varnishes [410, 429, 443]. The matting effect is the result of roughening of the surface on the microscopic scale, whereby the light is diffused and no longer directionally reflected (Fig. 52).

In the *paper industry* precipitated silicas are used as advanced fillers in, for example, newsprint to improve adsorptivity for printing ink. Strike through is reduced, and the coefficient of friction is adjusted. Silicas are used in special coated papers for ink-jet and direct thermal printing to enhance ink absorption [466].

Hydrophobic precipitated silicas are used increasingly in mineral-oil and silicone-oil *antifoam agents* to increase the antifoaming effect. They are used as foam regulators in laundry detergents [459] and in the production of paints and paper.

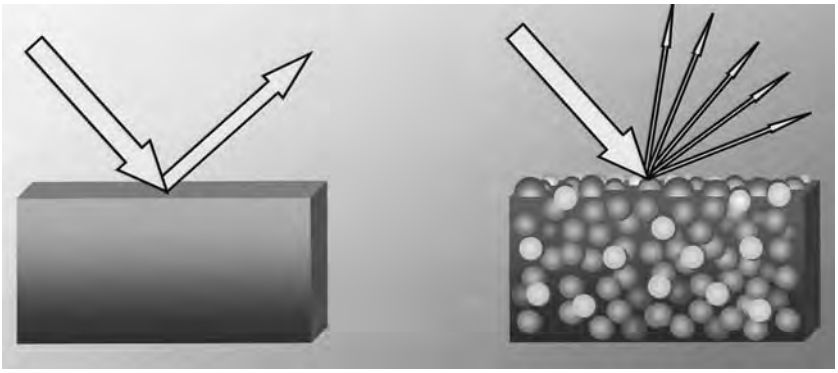

Figure 52. Reflection of light from shiny (left) and matted surfaces (right)

Further uses for precipitated silicas include the purification and stabilization of beer [460], and the analysis of blood [461].

Trade Names. Trade names for precipitated silicas include Sipernat, Ultrasil, Sident, Acematt (Degussa-Hüls); Hi-Sil, Flo-Gard, Lo-Vel (PPG); Tixosil, Zeosil (Rhodia); Zeodent, Hübersil (Hüber); Ketjensil, Perkasil (AKZO); Nipsil (Nippon Silica); and Neosyl (Crosfield).

7.5. Industrial Hygiene and Safety

Precipitated amorphous silica is nontoxic in rats after oral intake [462–464]. Neither eye irritation nor skin irritation is observed [465, 466]. Dryness of the skin after skin contact can be alleviated by washing and creaming. Inhalation of precipitated amorphous silica does not result in silicosis [467]. In addition, several epidemiological studies show no indication of silicosis in exposed employees [468–471].

When working with precipitated amorphous silica, the MAK value (4 mg/m^3 total dust) must be observed [472]. When appropriate precautions such as lowest possible dust development during handling and ventilation are taken, this value is not exceeded. Otherwise, dust masks should be worn.

8. Porosils

8.1. Introduction

Porosils are crystalline porous silicas of the general composition $SiO_2 \cdot M$, where M is an organic or inorganic guest molecule residing within the pores of the silica host framework. R. M. Barrer coined the name porosils to differentiate between porous aluminosilicate zeolites and a new class of compounds of distinct composition [473]. Due to their porous crystal structure porosils have properties similar to the zeolites; however, differences in chemical composition are responsible for their specific properties in catalysis, sorption, and molecular sieving.

Work in the field was initiated in 1978 by Flanigan et al. [474] who reported on the synthesis and crystal structure of the siliceous analogue of the commercially most important zeolite ZSM-5.

The guest species M can be expelled by thermal treatment to give the pure silica form of the porosil. Therefore, porosils are considered to be the porous polymorphs of the structure family SiO_2. Up to now, 34 porosil structure types have been made, either by template-directed synthesis or post-synthesis treatment of aluminosilicate zeolites (Table 17) [475, 476]. In the synthesis of porosils the guest species M act as templates for the pores, defining their size and geometry [477]. During the post-synthesis treatment framework aluminum is substituted by silicon, and M is atmospheric gases or sorbate molecules [478].

Porosils are subdivided into zeosils and clathrasils according to the pore structure of the silica framework. Zeosils have channel-type pores with pore openings larger than 0.4 nm (Fig. 53). The channels may intersect to give a two- or three-dimensional pore system (see Table 17). Clathrasils have cage-type voids with pore

Table 17. Porosil structure types [475, 476]

Porosil	Framework density (Si atoms per 1000 Å^3)	IUPAC code	Pore system[b]
Zeosils			
Silica-faujasite[a]	12.7	FAU	3 D 12 MR
Silica-ECM	12.7	ECM	3 D 12 MR
Silica-A[a]	12.9	LTA	3 D 8 MR
ITQ-7	15.0	ISV	3 D 12 MR
Silica-beta	15.1	BEA	3 D 12 MR
Silica-levyne	15.2	LEV	2 D 8 MR
Silica-offretite[a]	15.5	OFF	1 D 12 MR
ITQ-3	15.7	ITE	2 D 8 MR
ITQ-1	15.9	MWW	2 D 10 MR
Silica-mazzite[a]	16.1	MAZ	1 D 12 MR
CIT-5	16.8	CFI	1 D 14 MR
UTD-1F	17.1	DON	1 D 14 MR
ITQ-4	17.2	IFR	1 D 12 MR
Silica-mordenite	17.2	MOR	1 D 12 MR
Silica-SSZ-24	17.5	AFI	1 D 12 MR
Decadodecasil 3R	17.6	DDR	2 D 8 MR
Decadodecasil 3H	17.6		2 D 8 MR
Silica-ZSM-5	17.9	MFI	3 D 10 MR
Silica-ZSM-11	17.9	MEL	3 D 10 MR
Silica-ferrierite	19.3	FER	1 D 10 MR
Silica-ZSM-12	19.4	MTW	1 D 12 MR
Silica-theta-1	19.7	TON	1 D 10 MR
Silica-ZSM-23	19.7	MTT	1 D 10 MR
VPI-8	20.2	VET	1 D 12 MR
Silica-ZSM-48	19.9		1 D 10 MR
MCM-35	20.7	MTF	1 D 8 MR
Clathrasils			
Silica-A[a]	12.9	LTA	0 D 8 MR
Silica-levyne	15.2	LEV	0 D 8 MR
ITQ-3	15.7	ITE	0 D 8 MR
Silica-sodalite	17.4	SOD	0 D 6 MR
Decadodecasil 3R	17.6	DDR	0 D 8 MR
Decadodecasil 3H	17.6		0 D 8 MR
Octadecasil	17.6	AST	0 D 6 MR
Sigma-2	17.8	SGT	0 D 6 MR
Dodecasil 1H	18.4	DOH	0 D 6 MR
Dodecasil 3C	18.6	MTN	0 D 6 MR
Silica-RUB-10	18.7	RUT	0 D 6 MR
Melanophlogite	19.0	MEP	0 D 6 MR
Nonasil	19.3	NON	0 D 6 MR
MCM-35	20.7	MTF	0 D 8 MR

[a] Dealuminated zeolites.
[b] Pore dimensionality and pore size (n-membered ring of SiO_4 units).

openings much smaller than the free diameter of the cage and less then 0.45 nm (Fig. 53).

With the exception of melanophlogite, a rare mineral formed by low-temperature, low-pressure metamorphosis in, e.g., serpentine veins [479], all porosil structure types are synthetic materials. The ever increasing number of new porosil structure types reflects the efforts in the systematic investigation of the mechanism of formation of zeolites, for which porosils represent a simplified system. Besides porosils, water (clathrate hydrates), $AlPO_4$ (AlPO's), $GaPO_4$, and other III–V oxides (e.g., arsenates) also form neutral inorganic porous framework structures when synthesized in the presence of structure-directing guest molecules [475].

8.2. Physical and Chemical Properties

The physical and chemical properties of porosils are closely related to their crystal structure and composition. Porosils are colorless materials of hardness close to that of quartz. Since they are framework silicas, they exhibit no pronounced cleavage. Refractive indices vary systematically with the density of the silica framework (Fig. 54) [480]. This confirms that the nature of the Si—O bond accounts for most of the physical properties and is closely related to the natural polymorphs of the SiO_2 structure family. The porosils are thermodynamically metastable and transform reconstructively to cristobalite at high temperature (e.g., melanophlogite: $T > 950$ °C [481]). Below 200 °C structural phase transitions to lower symmetry space groups have been reported for melanophlogite [482], dodecasil 3 C [483], decadodecasil 3 R [484], silica-ZSM-5 [485], and silica ZSM-11 [486].

For dodecasil 3 C, three consecutive phase transitions have been reported, with transformation from cubic to tetragonal, orthorhombic, and finally monoclinic symmetry [487]. This reflects the flexibility of the silica framework. Several phase transitions are ferroic (e.g., ferroelastic) indicating interesting physical properties for the material.

A number of porosils in the high-symmetry form exhibit negative volume expansion coefficients β. For example, silica-ZSM-5 contracts in the temperature range 393–975 K with $\beta = -15.1 \times 10^{-6}\ K^{-1}$ [488].

Since the composition of the host framework is SiO_2, porosils are electroneutral. The pores, therefore, contain only electroneutral guest species (i.e., ion pairs, molecules, and/or atoms). In contrast to aluminosilicate zeolites, porosils are hydrophobic [474, 489], preferentially sorbing aprotic organic molecules. The weak Lewis acidity of the electroneutral SiO_2 framework of the porosils reduces considerably their potential as materials for heterogeneous acid catalysis, for

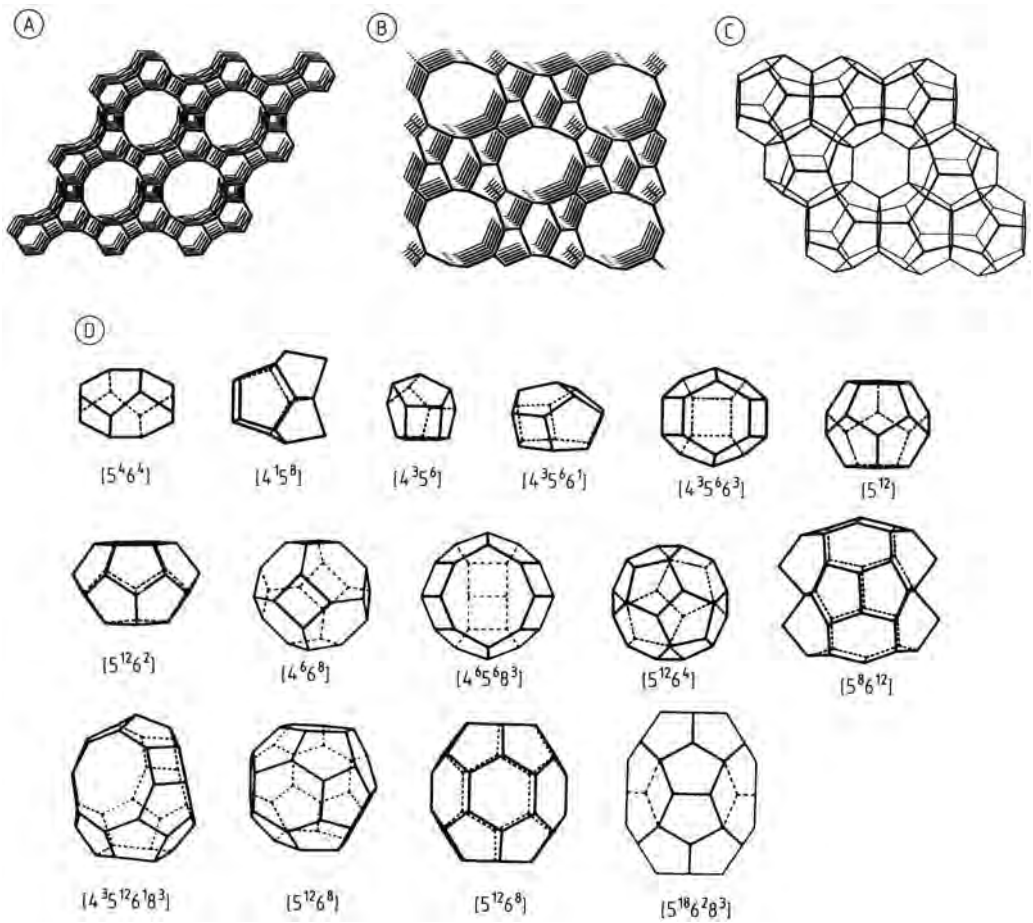

Figure 53. Skeletal projections of porosil framework structures
Si atoms are located in the nodes of the framework O atoms, which are close to the midpoint between 2 Si atoms, but are omitted for clarity
A) Projection of the AFI structure along the channel axis. The channel pore opening is confined by 12 Si atoms (12 MR); B) Projection of the FER, TON, MTT, MEL, and MFI structures along the straight channel axis. The channel pore opening is confined by 10 Si atoms (10 MR); C) Projection of the dodecasil layer. Pentagonal dodecahedra are arranged in layers which are the basic structural feature of DOH, MTN, DDR, and decadodecasil 3 H; D) Compilation of types of cage as found in clathrasil structure types ($[5^{12}]$ represents pentagonal dodecahedron, i.e., 12 five-membered rings)

which the isostructural aluminosilicate zeolites are widely used [490]. The pore geometry of the porosil structure types varies from zero-dimensional pores (i.e., cavities) to three-dimensional pore systems (i.e., intersecting channels) (see Table 17). The pore openings are confined by $[SiO_4]$ units arranged in a ring (Fig. 53) (e.g., ten-membered ring, 10 MR: 10 SiO_4 units per ring). In general the sorption properties of the materials are related to the largest pore opening of the structure, which provides for the release of guest molecules and the access of sorbates to the internal surface. In clathrasils the maximum pore opening (6–8 MR) is too small for the exchange of the occluded species. The template-free material can be obtained only by calcination at > 600 °C. For 6 MR as maximum pore opening only very small atoms or molecules such as H_2 or He could be sorbed onto the silica framework (Table 18). Zeosils with pore openings of 8–12 MR are calcined at lower temperatures and could be used for the selective sorption of, e.g., *n*-alkanes (8 MR materials) or *p*-substituted aromatic compounds (10 MR materials) (Table 18). Because of the uniform character of the pore opening and the possibility of tailoring the size

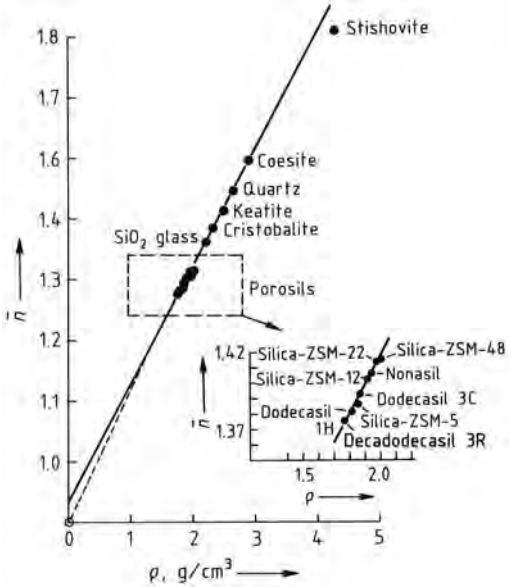

Figure 54. Density of the silica framework of porosils and dense silicas versus refractive indices

of the pores, porosil-containing membranes, such as those already available for zeolites, could be useful for separation processes [491, 492].

8.2.1. Zeosils

Physical and chemical properties specific to zeosils are related to their crystal structure. The channel-like pores allow access to the internal surface of the material for sorbates that meet the geometrical requirement of the pore window.

The free diameter of the individual materials, however, varies considerably due to the flexibility of the silica framework. Idealized values for the pore openings are given in Table 18. Because of the hydrophobic properties of the silica framework and the geometry of the internal pore system, zeosils are of particular interest for various applications. In the presence of water zeosils sorb selectively hydrophobic organic molecules in the vapor and liquid phase [493]. Sorption of monomers into the silica framework followed by polymerization leads to one-, two- or three-dimensional polymeric filaments inside the zeosil framework, as already demonstrated for zeolites [494]. The deposition of semiconducting materials [495] and metal atom clusters [496] inside, e.g., the zeosil cavity of silica-A or silica-faujasite creates new materials with interesting properties due to the limited size of crystallites built within the pores. The sorption of polar organic molecules such as *p*-nitroaniline also leads to changes in symmetry and polarization of the host–guest composites, leading, e.g., to nonlinear optical properties [497]. For a review on new applications of zeosils, see [498].

Table 18. Idealized pore diameters and potential sorbates for various pore openings

Pore opening	Planar ring diameter, nm	Potential sorbates (diameter in nm)
6 MR	0.27	He (ca. 0.23) H_2 (ca. 0.23)
8 MR	0.44	alkane (ca. 0.43)
10 MR	0.60	aliphatic and aromatic six-membered rings (ca. 0.6)
12 MR	0.77	substituted ring systems

8.2.2. Clathrasils

The clathrasil structure types have cagelike pores. Species inside the cavities are too large to pass through the 4 MR, 5 MR, 6 MR, or 8 MR windows without their decomposition. In general, clathrasils in the as-synthesized form have no exchange capacity or sorption properties. After calcination at high temperature (> 600 °C) the decomposition of the guest species may lead to a guest-free porosil with very narrow pores that is suitable for sieving and sorption processes (cf. Table 18). The properties of clathrasils are, therefore, linked to properties introduced by the guest molecules clathrated in the formation process. Because of the high thermal and chemical stability of the silica host framework, clathrasils have been proposed as containers for radioactive gases (e.g., krypton) [499]. The synthesis of the clathrasil dodecasil 3 C with a number of nonglobular guest molecules leads to a distortion of the cubic symmetry of the silica framework. At room temperature the materials have acentric symmetry and, therefore, nonlinear optical properties [500]. The temperature of the phase transition to the acentric space group depends on the nature and the concentration of the guest molecule in the silica framework and is in the range between slightly below room temperature and ca. 200 °C.

8.3. Manufacture of Porosils

With the exception of melanophlogite, all porosil structure types are synthetic materials made directly from an active form of SiO_2 or by dealumination of high-silica zeolites.

8.3.1. Synthesis of Porosils

Structure-directing templates play a key role in the synthesis of porous silicas [501, 502]. Since the templates are occluded within the pores during synthesis, it is their size and shape which determine the size and shape of the pores of the silica framework. Organic amines have proved to be the most efficient templates. Up to now ca. 100 different molecules have successfully been used for the synthesis of porosils [501, 503, 504]. Globular species such as xenon, quinuclidine, and 1-aminoadamantane preferentially stabilize the cage-like voids characteristic of clathrasils. Chain-like amines such as the α,ω-diamines of propane, butane, pentane, etc., stabilize channel-like voids. The size of the pore depends on the size of the template. Whereas pyrrolidine leads to preferential formation of dodecasil 3 C by occupying a 16-hedral cage, 1-aminoadamantane is occluded within a 20-hedral cage in dodecasil 1 H (Fig. 55). Zeosil structure types with 10 MR channels are formed in the presence of aliphatic chain-like templates (α, ω-diamino-*n*-alkanes); 12 MR channels are formed with molecules containing sequences of *p*-substituted heterocycles (e.g., 4,4′-trimethylenedipiperidine).

8.3.2. Dealumination of Aluminosilicate Zeolites

Porosils marked with an asterisk in Table 17 have been obtained exclusively by post-synthesis treatment of aluminosilicate zeolites. Aluminum is selectively extracted from the silicate framework and replaced by silicon [505]. The dealumination procedure includes successive chemical and hydrothermal treatment of the material in order to extract and remove the framework aluminum atom. A typical procedure is the calcination of the synthesis product at 300–500 °C to expel the organic template, exchange of the cations with ammonium, and steaming at ca. 600 °C to remove the aluminum.

8.3.3. Formation of Melanophlogite

So far melanophlogite is the only known natural porosil. In synthesis experiments the conditions of formation have been simulated and are of low temperature (ca. 100–200 °C) and low (authogenic) pressure. The material has been described as a trace occurrence from five localities in very different geological settings. However, the nature of the porosil structure types and the wide range of structural features suggest that further

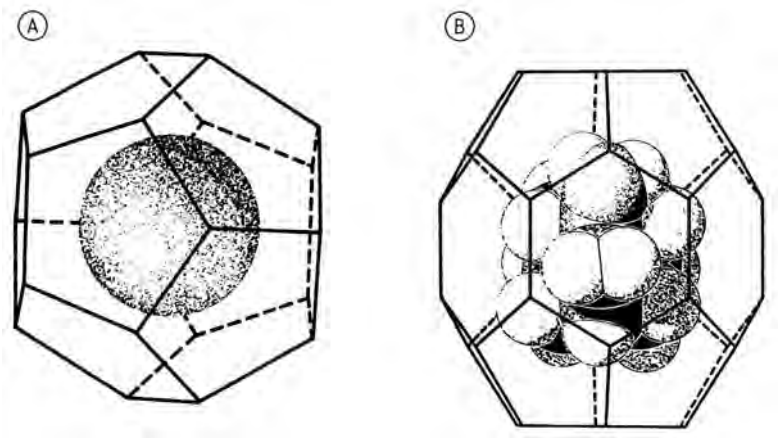

Figure 55. A) Van der Waals model of Xe as guest atom within the pentagonal dodecahedral cage; B) Van der Waals model of 1-aminoadamantane as guest molecule within the icosahedral cage

natural variants may exist, especially in hydrothermally active areas (e.g., geysers).

9. Toxicology

The effect of the dust that arises when working with silica is of primary importance from a toxicological point of view, especially in the case of long-term exposure of several hours per day. This applies to naturally occurring and synthetic as well as to crystalline and amorphous. As far as industrial medicine is concerned, local contact with the skin and mucous membranes is important. In the case of inhalation of the dust, the effect on the respiratory tract is significant.

The effect of silica-containing dust on the respiratory tract depends on:

1. The physical and chemical properties (e.g., the particle size and the specific surface area)
2. The concentration administered
3. The daily and total duration of exposure

9.1. Experiences with Humans

After long-term exposure at work, the effects of crystalline or amorphous SiO_2 dust on the respiratory tract of humans are well known and have been widely reported (for reviews, see [506–509]).

Crystalline Silica Dust. The classification into common, accelerated, and acute forms of silicosis [506] is based on the time interval between the beginning of exposure to silica and the first appearance of silicotic changes that are detectable in a X-ray picture. A rapid manifestation and an accelerated course of the disease are caused primarily by long-term inhalation of higher concentrations of SiO_2 dust.

The common form of silicosis (simple silicosis) occurs roentgenologically after about twenty or more years of exposure. The content of crystalline SiO_2 in the dust that causes silicosis in workers is often less than 30 % [506].

The accelerated form of silicosis (5–15 years) develops after a shorter exposure to higher concentrations of SiO_2 dust. Progressive massive fibrosis is often observed on the X-ray picture [506].

The acute form, also known as silicoproteinosis, develops in 1–3 years. The clinical symptoms include rapidly deteriorating function of the lungs, which is always fatal.

The progression of silicosis even after the termination of exposure is especially characteristic, and there is still no effective treatment.

For this reason, it is essential that the legal regulations for working with crystalline SiO_2 are obeyed [510–512].

Amorphous Silica Dust.

Amorphous Synthetic Silica. From experimental long-term inhalation tests on rats, it is known that high concentrations of some synthetic amorphous silicas can cause nodular (fibrotic) changes in the lungs of the animals during the exposure phase [513]. However, the regression of the nodules (fibrosis) in the lungs after the termination of the exposure phase is characteristic of the biological action of these amorphous silica dusts. In a treatment-free, follow-up observation phase of several months, a clear time-dependent regression of the changes in the lungs of the experimental animals could be detected after three, eight, and up to twelve months (see below) [513, 514]. In the case of the neighboring lymph nodes, the regression of the morphological changes observed within the inhalation phase was established histologically [513, 514].

In-depth investigations carried out by company doctors over periods of up to 12 years [515] and from 1 to 32 years [516] have confirmed that until now long-term contact with amorphous synthetic silicas has not resulted in a single case of silicosis.

Established MAK [511] and TLV regulations [512] must be complied with when working with amorphous synthetic silicas. If these fixed limiting values are exceeded — especially for a longer period of time — an overtaxing of the respiratory passages and a corresponding biological defense reaction in the bronchial tubes and, especially, in the lung tissue must be expected.

Vitums et al. observed that fibrosis of the lungs was caused by exposure to flue dust containing silica with a wide particle-size distribution, such that as produced in the manufacture of ferrosilicon or quartz glass [517].

Amorphous Natural Silicas. A distinction is made between exposure to amorphous synthetic silica dust and exposure to natural amorphous silica dust (diatomite). The latter can contain

small amounts of crystalline SiO_2 and, according to some studies, can cause silicosis in humans on long-term exposure [507].

Carcinogenicity of Silica Dusts in Humans. In many cases, industrial workers exposed to crystalline silica dust exhibit a higher incidence of lung cancer. However, exposure to silica dust is often complicated by other hazards such as polycyclic aromatic hydrocarbons, asbestos, and smoking, which makes a causal analysis extremely difficult. According to GOLDSMITH et al. [518], at least two studies show a strong association between silicosis and lung cancer: the analysis of the Swedish pneumoconiosis register by WESTERHOLM [519] and a similar study by FINKELSTEIN [520] in Ontario, Canada. However, the same authors [518] also stated that a completely convincing causal relationship cannot be concluded. A possible association between silicosis and lung cancer is also discussed in [521], based on data from a clinical cancer monitoring register. A relationship between tumors of the upper intestinal tract and the ingestion of quartz particles in food in North China has been suggested [522]. A correlation was made between the incidence of cancer of the esophagus and the consumption of plant products that contain silica fragments and fibers for a region in North China, in northeast Iran, and in Transkei.

9.2. Animal Experiments

Long-Term Inhalation of Silica Dust. In specifically designed, practice-oriented long-term inhalation studies, various types of crystalline and amorphous silica dust have been thoroughly tested on rodents. Rats [513, 514, 523, 524] were mainly used, but rabbits [514, 525, 526] and guinea pigs [514] were also employed.

The elimination rate in rats has been determined in an inhalation experiment with highly disperse *amorphous silica*. In the case of Aerosil 200, for example, after the termination of inhalation, 65–75 % of the dust was eliminated in one month, 80–90 % in two months, and 95 % in three to five months. It is possible that the rate of solubilization of these hydrophilic silicas also plays a role [513].

It was found in retention studies on rats [513] that in the case of longer term inhalation (28 times four hours in 36 days) of highly disperse *amorphous silica* dust, the continuous elimination during the exposure phase is very high. This means that the formation of large SiO_2 deposits in the lungs is improbable [513]. In contrast, in long-term inhalation experiments with *quartz* dust the tendency towards formation of deposits was higher [513].

After the termination of a long-term inhalation study on rats with Aerosil 200 (12 months, 4 per day; concentration: 45 mg/m^3), some of the animals were subjected to treatment-free observation for another 3 to 8 months and then killed [513]. Subsequently, a histological investigation and chemical analysis of SiO_2 in the lungs and lymph nodes were performed. In the follow-up observation period, it was found that the nodules in the lungs were reduced to small residual foci. The lymph nodes, which were still enlarged after three months, had greatly regressed after eight months. Similar observations have also been made in previous inhalation experiments with Aerosil.

In a long-term inhalation experiment on rats with *quartz* [524] (12 months, 5 per day, 5 per week; concentration:10 mg/m^3; standard quartz No. 12, Dörentrup quartz), some of the animals were subjected to treatment-free observation for another 4 weeks to 6 months after the termination of exposure and then killed. In this follow-up observation period, it was possible to detect silicotic reactions in the lungs and reticulohistiocytic cells typical of quartz in the lymph nodes. There was an increase in the silicotic nodules in the lungs after six months and fibrosis of the mediastinal lymph nodes had clearly increased.

Examination of lungs and accompanying lymph nodes of the individual groups of animals at various time intervals showed that in the case of *quartz*, a long residence time in the lungs must always be expected, but that deposits of finely divided *amorphous silica* are relatively quickly and extensively eliminated [513, 524]. This is true of amorphous silicas with a specific surface area of > 100 m^2/g [513].

Injection of Silica Dust. The tissue reaction typical of a particular silica dust can be determined in animal experiments by means of a single intratracheal or intraperitoneal injection.

The intratracheal injection of a high dose of *quartz* resulted in a massive local accumulation of dust [524]. The tissue reaction caused by an injection of this type is similar to the picture of

acute silicosis. Fast reactions of this kind in the lung tissue — comparable with the exposure of workers to high concentrations of quartz [515] — can also be produced in animal experiments with very high inhalation concentrations (400 mg/m^3) [524].

The general effect of a particular dust (acute toxicity) and the local harmful (cytotoxic) effects are deduced from the tissue reaction observed in rats after intraperitoneal SiO_2 injections. Cytotoxicity can occur in the form of nodular fibrosis (dust nodules) or surface fibrosis that leads to extensive coalescence of the abdominal organs [513].

The reaction of lung tissue on longer term inhalation of SiO_2 dust cannot be directly inferred from the results of the intratracheal and intraperitoneal injections. Thus, the physiologically important reactions of the organism in the course of SiO_2 retention and SiO_2 elimination can be determined only in long-term inhalation tests with a sufficiently long, treatment-free, follow-up observation period.

The morphological changes in the lungs after long-term inhalation of *natural crystalline* SiO_2 progress after the termination of exposure, whereas with *synthetic amorphous silica* dust the morphological changes regress after the termination of exposure (reversibility).

Carcinogenicity of Silica Dusts in Animal Tests. Lymphomas have been found in rats after intrapleural, i.p., i.v., and direct application in the thymus gland of various silica modifications [527, 528]. The tumor incidence differed for various species of rat, and no tumors were observed in mice and hamsters. A synergistic effect has been reported for silica dust and benzo [*a*]pyrene [529], as has been found for other dusts (e.g., coal, TiO_2). This is presumably the result of chemicophysical surface effects, which may also be involved in tumor promotion. Tests have shown that Min-U-Sil causes tumors in rats in the intratracheal test [530]. Tissue scarring has been discussed as the cause. Min-U-Silis strongly fibrogenic and extremely finely divided.

References

1 R. Siever in Ref. [4]

2 H. Füchtbauer (ed.): *Sedimente und Sedimentgesteine*, 4th ed., Schweizerbarth, Stuttgart 1988.

3 *Ind. Miner. (London)* **236** (1987) 22–39.

4 K. C. Condie in K. H. Wedepohl (ed.): *Handbook of Geochemistry*, vol. II-2, Springer, Berlin 1970, Section 14.

5 O. W. Flörke *et al.*, *Neues Jahrb. Mineral. Abh.* **163** (1991) 19–42.

6 V. Swamy, S. K. Saxena, B. Sundman, J. Zhang, *J. Geophys. Res.* **99** (1994) 11787–11794.

7 R. D. Aines, G. R. Rossman, *J. Geophys. Res.* **89** (1984) 4059–4071.

8 A. Nicolas, J. P. Poirier: *Crystalline Plasticity and Solid State Flow in Metamorphic Rocks*, "Chap. 5.9". Wiley, London 1976.

9 O. W. Flörke, A. Nukui, *Neues Jahrb. Mineral. Abh.* **158** (1988) 175–182.

10 C. Frondel: "Silica Minerals", *The System of Mineralogy*, 7th ed., vol. III, Wiley, New York 1962.

11 M. J. Mombourquette, J. A. Weil, *Can. J. Phys.* **63** (1985) 1282–1293.

12 H. Schneider, O. W. Flörke, *Neues Jahrb. Mineral. Abh.* **145** (1982) 280–290.

13 H. Schneider, *Neues Jahrb. Mineral. Monatsh.* 1986, 433–444.

14 M. J. Buerger, *Amer. Mineral.* **39** (1954) 600–614.

15 L. Pauling, *Amer. Mineral.* **65** (1980) 321–323.

16 R. J. Hill, G. V. Gibbs, *Acta Crystallogr.* B 35 (1979) 25–30.

17 M. O'Keefe, B. G. Hyde, *Acta Crystallogr.* B 34 (1978) 27–32.

18 W. H. Baur, *Acta Crystallogr.* B 36 (1980) 2198–2202.

19 F. Liebau: *Structural Chemistry of Silicates*, Springer-Verlag, Berlin–Heidelberg 1985.

20 W. A. Harrison: *Electronic Structure and the Properties of Solids*, Freeman, San Francisco 1980, pp. 257–288.

21 R. D. Shannon, *Acta Crystallogr.* **A32** (1976) 751–767.

22 J. R. G. Da Silva, D. G. Pinatti, C. E. Anderson, M. L. Rudee, *Philos. Mag.* **31** (1975) 731–737.

23 B. Martin, O. W. Flörke, E. Kainka, R. Wirth, *Phys. Chem. Minerals* **23** (1996) 409–417.

24 M. T. Dove, *Amer. Mineral.* **82** (1997) 213–244.

25 G. V. Gibbs, C. T. Previtt, K. J. Baldwin, *Z. Kristallogr.* **145** (1977) 108–123.

26 L. Levien, C. T. Prewitt, *Amer. Mineral.* **66** (1981) 324–333.

27 S. Haussühl: *Kristallphysik*, "Chap. 11.4", Verlag Chemie, Weinheim, Germany 1983.

28 R. E. Newnham: *Structure-Property Relations*, Springer, Berlin 1975.

29 G. Dolino in R. Blinc, A. P. Levanyuk (eds): *Incommensurate Phases in Dielectrics*, vol. 2, Elsevier, Amsterdam 1986, 205–232.

30 W. A. Deer, R. A. Howie, W. S. Wise, J. Zusmann: "Framework Silicates: Silica Minerals, Feldspathoids and the Zeolites" in *Rockforming Minerals* Vol. 4B, 2nd ed., The Geological Society Publishing House, Bath, UK, 2004, pp. 15ff.

31 K. Kosten, H. Arnold, *Z. Kristallogr.* **152** (1980) 119–133.

32 O. Muller, R. Roy: *The Major Ternary Structural Families*, Springer-Verlag, Berlin 1974.
33 C. Chateau, J. Haines, J.-M. Léger, A. LeSauze, R. Marchand, *Amer. Mineral.* **84** (1999) 207–210.
34 D. C. Palmer: "Stuffed Derivatives of the Silica Polymorphs," *Rev. Miner.* **29** (1994) 83–118.
35 R. W. G. Wyckoff, *Am. J. Sci.* **209** (1925) 448–459.
36 D. J. Peacor, *Z. Kristallogr.* **138** (1973) 274–298.
37 A. F. Wright, A. J. Leadbetter, *Philos. Mag.* **31** (1975) 1391–1401.
38 R. L. Withers *et al.*, *Phase Transitions* **16/17** (1989) 41–45.
39 W. W. Schmahl, I. P. Swainson, M. T. Dove, A. Graeme-Barber, *Z. Kristallogr.* **201** (1992) 125–145.
40 D. M. Hatch, S. Ghose, *Phys. Chem. Minerals* **17** (1991) 554–562.
41 O. W. Flörke, H. Schneider, *Ber. Dtsch. Keram. Ges.* **63** (1986) 368–372.
42 H. Schneider, O. W. Flörke, R. Stoeck, *Z. Kristallogr.* **209** (1994) 113–117.
43 O. W. Flörke, K. Langer, *Contrib. Mineral. Petrol.* **36** (1992) 221–230.
44 O. W. Flörke, *Glastechn. Ber.* **32** (1959) 1–9.
45 H. Graetsch, O. W. Flörke, *Z. Kristallogr.* **195** (1991) 31–48.
46 K. Kihara, *Z. Kristallogr.* **152** (1980) 95–101.
47 A. K. A. Pryde, M. T. Dove, *Phys. Chem. Minerals* **26** (1998) 171–179.
48 W. A. Dollase, *Acta Crystallogr.* **23** (1967) 617–623.
49 A. Nukui, H. Nakazawa, M. Akao, *Amer. Mineral.* **63** (1978) 1252–1259.
50 H. A. Graetsch, M. Brunelli, Z. Kristallogr. **220** (2005) 606–613.
51 K. Kihara, *Z. Kristallogr.* **146** (1977) 185–203.
52 H. Graetsch, *Phys. Chem. Minerals* **28** (2001) 313–321.
53 K. Kato, A. Nukui, *Acta Crystallogr.* **B32** (1976) 2486–2491.
54 W. H. Baur, *Acta Crystallogr.* **B33** (1977) 2615–2619.
55 J. H. Konnert, D. E. Appleman, *Acta Crystallogr.* **B34** (1978) 391–403.
56 W. Hoffmann, M. Kockmeyer, J. Löns, C. Vach, *Fortschr. Mineral.* **61** (1983) 96–98.
57 J. Löns, W. Hoffman, *Z. Kristallogr.* **178** (1987) 141–143.
58 H. Graetsch, I. Topalović-Dierdorf, *Eur. J. Mineral.* **8** (1996) 103–113.
59 H. A. Graetsch, Z. Kristallogr. **218** (2003) 531–535.
60 H. Graetsch, *Amer. Mineral.* **83** (1998) 872–880.
61 A. Nukui, O. W. Flörke, *Amer. Mineral.* **72** (1987) 167–176.
62 W. Hoffmann, *Naturwiss.* **54** (1967) 114.
63 W. A. Dollase, W. H. Baur, *Amer. Mineral.* **61** (1976) 971–978.
64 C. B. Sclar, A. P. Young, L. C. Carrison, C. M. Schwartz, *J. Geophys. Res.* **67** (1962) 4049–4054.
65 M. A. Spackmann, R. J. Hill, G. V. Gibbs, *Phys. Chem. Miner.* **14** (1987) 139–150.
66 R. J. Hemley, C. T. Prewitt, K. J. Kingma: "High-Pressure Behavior of Silica," *Rev. Miner.* **29** (1994) 41–74.
67 G. Miehe, H. Graetsch, *Eur. J. Mineral.* **4** (1992) 693–706.
68 O. W. Flörke, J. B. Jones, H. U. Schmincke, *Z. Kristallogr.* **143** (1976) 156–165.
69 O. W. Flörke, U. Flörke, U. Giese, *Neues Jahrb. Mineral. Abh.* **149** (1984) 325–336.
70 P. J. Heaney, J. E. Post, *Science* **255** (1992) 441–443.
71 M. Grasselini Troysi, P. Orlandi, *Atti. Soc. Tosc. Sci. Nat. Mem.* **A79** (1972) 245–250.
72 H. Gies, H. Gerke, F. Liebau, *Neues Jahrb. Mineral. Monatsh.* (1982) 119–124.
73 H. Gies, *Z. Kristallogr.* **164** (1983) 247–257.
74 G. Miehe, H. Graetsch, O. W. Flörke, *Phys. Chem. Minerals* **10** (1984) 197–199.
75 H. Graetsch, O. W. Flörke, G. Miehe, *Phys. Chem. Minerals* **12** (1985) 300–305.
76 J. B. Jones, E. R. Segnit, *J. Geol. Soc. Australia* **18** (1971) 57–68.
77 O. W. Flörke, *Fortschr. Mineral.* **44** (1967) 181–230.
78 O. W. Flörke, *Neues Jahrb. Mineral. Monatsh.* (1955) 217–223.
79 H. Graetsch: "Structural Characteristics of Opaline and Microcrystalline Silica Minerals," *Rev. Miner.* **29** (1994) 209–232.
80 K. Langer, O. W. Flörke, *Fortschr. Mineral.* **52** (1974) 17–51.
81 H. Graetsch, H. Gies, I. Topalović, *Phys. Chem. Minerals* **21** (1994) 166–175.
82 J. Shropshire, P. P. Keat, P. A. Vaughan, *Z. Kristallogr.* **112** (1959) 400–413.
83 F. Liebau, *Amer. Mineral.* **63** (1978) 918–923.
84 B. Martin, K. Röller, *Neues Jahrb. Mineral. Monatsh.* (1990) 462–466.
85 M. G. Fereira da Silva, J. M. F. Navarro, *J. Non-Cryst. Solids* **109** (1989) 191–197.
86 Al. Weiss, Ar. Weiss, *Z. Anorg. Allg. Chem.* **276** (1954) 95–112.
87 O. W. Flörke, J. B. Jones, U. Köster, E. Robarick, *Acta Crystallogr.* A 46 (1990) Suppl. C-247.
88 R. L. Mozzi, B. E. Warren, *J. Appl. Cryst.* **2** (1969) 164–173.
89 H. Graetsch, A. Mosset, H. Gies, *J. Non-Cryst. Solids* **119** (1990) 173–180.
90 R. J. Hemley, H. K. Mao, P. M. Bell, B. O. Mysen, *Phys. Rev. Lett.* **57** (1986) 747–750.
91 H. Graetsch, K. Ibel, *Phys. Chem. Minerals* **24** (1997) 102–108.
92 J. V. Sanders, *Acta Crystallogr.* **A24** (1968) 427–434.
93 D. C. Hurd in S. R. Aston: *Silicon Geochemistry and Biogeochemistry*, Academic Press, New York 1983, pp. 179–186.
94 O. W. Flörke, J. B. Jones, E. R. Segnit, *Neues Jahrb. Mineral. Monatsh.* (1973) 82–89.
95 H. Graetsch, I. Topalović-Dierdorf, *Chem. Erde* **56** (1996) 387–391.

96 G. Lehmann, H. U. Bambauer, *Angew. Chemie* **85** (1973) 281–289.
97 V. S. Balitsky, *J. Crystal Growth* **41** (1977) 100–102.
98 O. W. Flörke, K. Röller, F. Siebers, *Gemmologie* **49** (2000) 85–104
99 G. R. Rossmann: "Colored Varieties of the Silica Minerals," *Rev. Miner.* **29** (1994) 433–467.
100 J. S. Goreva, Chi Ma, G. R. Rossman, *Am. Mineral.* **86** (2001) 466–472.
101 R. Pankrath, O. W. Flörke, *Eur. J. Mineral.* **6** (1994) 435–457.
102 O. W. Flörke, *Mitt. Österr. Miner. Ges.* **140** (1995) 9–34.
103 A. C. McLaren, D. R. Pitkethly, *Phys. Chem. Minerals* **8** (1982) 128–135.
104 F. J. Pettijohn: *Sedimentary Rocks*, 3rd ed., Harper & Row, New York 1975, pp. 195 ff, 300 ff, 392 ff.
105 H. Williams, F. J. Turner, C. M. Gilbert: *Petrography*, 2nd ed., Freeman, San Francisco 1982.
106 P. Harben, *Ind. Miner. (London)* **184** (1983) 28–29, 32.
107 O. W. Flörke, B. Köhler-Herbertz, K. Langer, I. Tönges, *Contrib. Mineral. Petrol.* **80** (1982) 324–333.
108 A. Peschel: *Natursteine*, 2nd ed., Dtsch. Verlag Grundstoffind., Leipzig 1983, pp. 77–80, 243–251, 274–275.
109 S. J. Lefond (ed.): *Industrial Minerals and Rocks, (Nonmetallics other than Fuels)*, 4th ed., Amer. Inst. Mining Metallurg. Petrol. Eng. (AIME), New York 1975.
110 M. Kuzvart: *Industrial Minerals and Rocks*, Elsevier, Amsterdam 1984.
111 M. Smith, *Ind. Miner. (London)* **203** (1984) 19–25.
112 K.-T. Wilke: *Kristallzüchtung*, H. Deutsch, Thun 1988, pp. 1027–1058.
113 E. D. Kolb, K. Nassau, R. A. Laudise, E. E. Simpson, K. M. Kroupa, *J. Crystal Growth* **36** (1976) 93–100.
114 C. G. Kennedy, W. L. Knight, W. T. Holser, *Amer. J. Sci.* **256** (1958) 590–595.
115 W. T. Holser, C. G. Kennedy, *Amer. J. Sci.* **257** (1959) 71–77.
116 G. C. Kennedy, *Econ. Geol.* **45** (1950) 629–653.
117 R. A. Laudise, E. D. Kolb, *Endeavour* **28** (1969) 114–117.
118 N. B. Hannay (ed.): "Change of State", *Treatise on Solid State Chemistry*, vol. 5, Plenum Press, New York 1975.
119 113a G. Johnson, J. Foise, *Encyclopedia of Applied Physics* **15** (1996) 365–375.
120 V. A. Kuznetsov, A. N. Lobachev, *Sov. Phys. Crystallogr.* **17** (1973) 775–803.
121 A. Armington, J. F. Balascio, *38th Ann. Frequency Control Symp.* (1984) 3–8.
122 J. A. Weil, *Phys. Chem. Minerals* **10** (1984) 149–165.
123 M. S. Paterson, *Bull. Mineral.* **105** (1982) 20–29.
124 P. Cordier, J. C. Doukhan, *Amer. Mineral.* **76** (1991) 361–366.
125 J. Flicstein, M. Schieber, *J. Cryst. Growth* **24/25** (1974) 603–609.
126 A. C. McLaren, C. F. Osborne, L. A. Saunders, *Phys. Stat. Solidi* **4** (1971) 235–247.
127 A. C. McLaren, R. F. Cook, S. T. Hyde, R. C. Tobin, *Phys. Chem. Minerals* **9** (1983) 79–94.
128 P. P. Phakey, *Phys. Stat. Solidi* **34** (1969) 105–119.
129 A. C. McLaren, P. P. Phakey, *Phys. Stat. Solidi* **31** (1969) 723–737.
130 D. M. Dodd, D. B. Frazer, *J. Phys. Chem. Solids* **26** (1965) 673–686.
131 W. G. Cady: *Piezoelectricity*, Dover Publ., New York 1964.
132 P. Profos (ed.): *Handbuch der industriellen Meßtechnik*, 4th ed., Vulkan-Verlag, Essen 1987.
133 J. C. Brice, *Rev. Modern Phys.* **57** (1985) 105–146.
134 S. Fujishima, *IEEE Trans. Ultrasonics Frequency Control* **47** (2000) 1–7.
135 prEN 12475, part 11: Classification of dense shaped refractory products. Alumina–silica products, Oct. 1996.
136 DIN 1089, part 1: Refractories for use in coke ovens. Silica bricks, requirements and testing, Feb. 1995.
137 ASTM C 416–97: Standard classification of silica refractory brick.
138 O. W. Flörke, *Ber. Dtsch. Keram. Ges.* **34** (1957) 343–353.
139 O. W. Flörke, *Refractories J.* **11** (1958) 493–516.
140 F. Brunk, D. Schmidt, IREFCON' 96 Proc. Vol. I, Indian Refractory Association, Calcutta 1996, 226–230.
141 H. Schneider, K. Wohlleben, A. Majdic, *Mineral. Mag.* **43** (1980) 879–883.
142 H. Schneider, A. Majdic, *Neues Jahrb. Mineral. Monatsh.* (1984) 559–883.
143 V. Lach, *Sprechsaal* **123** (1990) 811–813.
144 S. J. Stevens, R. J. Hand, J. H. Sharp, *J. Mater. Sci.* **32** (1997) 2929–2935.
145 A. Majdic, H. Schneider, K. Wohlleben, *cfi/DKG* **63** (1986) 176–189.
146 I. Patzak, *Tonind. Ztg.* **96** (1972) 291–297.
147 H. Schneider, O. W. Flörke, A. Majdic, *Proc. Brit. Ceram. Soc.* **28** (1979) 267–279.
148 D. Taylor, *Trans. Brit. Ceram. Soc.* **83** (1984) 129–134.
149 F. Brunk in G. Routschka (ed.): *Refractory Materials*, Vulkan-Verlag, Essen 1997, p. 43.
150 Y. Naruse, Y. Hoshino, T. Tanaka, *Taikabutsu Overseas* **2** (1982) 110–120.
151 H. J. Koschlig: *UNITECR Proc.,* vol. 1, Amer. Ceram. Soc., Columbus, Ohio 1989, pp. 244–283.
152 F. Brunk, W. Weßling: *XXXVI. Int. Col. on Refractories*, Verlag Stahleisen, Düsseldorf 1993, pp. 20–26.
153 J. D. Panda, G. Goswami, *Iron & Steel Review* **39** (1996) 26–28.
154 A. Kumar in S. N. Gosh, S. L. Sarker, S. Harsch (eds.): *Progress in Cement and Concrete*, vol. 4, Abi Books, New Dehli 1993, pp. 342–367.
155 G. H. Beall: "Industrial Applications of Silica," *Rev. Miner.* **29** (1994) 469–506.
156 K. H. Khayat, P.-C. Aitcin in S. N. Gosh, S. L. Sarker, S. Harsch (eds.): *Progress in Cement and Concrete*, vol. 4, Abi Books, New Dehli 1993, pp. 226–265.
157 F. Press, R. Siever: *Earth*, 4th ed., Freeman, San Francisco 1986.

158 B. J. Skinner, S. C. Parker: *Physical Geology*, Wiley-Interscience, New York 1987.
159 L. Jung: *High Purity Natural Quartz,* part I: "High Purity Natural Quartz for Industrial Uses"; Part II: "High Purity Natural Quartz Markets for Suppliers and Users," Quartz Technology Inc., Liberty Corner, New Jersey 1992.
160 R. Weiss: *Formgrundstoffe*, Giesserei-Verlag, Düsseldorf 1984.
161 J. Griffith, *Ind. Miner. (London)* **235** (1987) 25–43.
162 H. Füchtbauer (ed.): *Sedimente und Sedimentgesteine*, 4th ed., Schweizerbarth, Stuttgart 1988.
163 H. J. Blankenburg, J. Götze, H. Schulz: *Quartzrohstoffe*, 2nd ed., Dtsch. Verl. Grundstoffind., Leipzig 1994.
164 W. Koensler: *Sand und Kies*, F. Enke, Stuttgart 1989.
165 W. Lorenz, W. Gwosdz: "Bewertungskriterien Industrieminerale, Steine, Erden", *Quartzrohstoffe,* Geol. Jahrb., part 3, Series H, H. 6, Bundesanst. Geowiss. u. Rohstoffe, Hannover 1999.
166 O. Stier, H. Ortleb: *Gefahrstoffe — Reinhaltung Luft* **59** (1999) 27–31.
167 M. Saller, *Ind. Minerals (London)* **202** (1999) 6, 25–33.
168 Hoffmann Mineral (ed.): *Neuburger Kieselerde*, Neuburg/Donau 1999.
169 O. W. Flörke, B. Köhler-Herbertz, K. Langer, I. Tönges, *Contrib. Mineral. Petrol.* **80** (1982) 324–333.
170 C. Frondel: "Silica Minerals", *The System of Mineralogy*, 7th ed., vol. **3**, J. Wiley & Sons, New York 1962.
171 H. Graetsch, O. W. Flörke, G. Miehe, *Phys. Chem. Minerals* **14** (1987) 249–257.
172 C. Barker, W. D. Underwood, *Analyst* **117** (1992) 1407–1410.
173 R. J. Bodner, *Pure Appl. Chem.* **67** (1995) 873–880.
174 J. Mullis in M. Frey (ed.): *Low Temperature Metamorphism*, Blackie, Glasgow 1987, pp. 162–199.
175 J. T. Nash, T. Theodore, *Econ. Geol.* **66** (1971) 385–399.
176 B. Perney, P. Eberhard, K. Ramseyer, J. Mullis, R. Pankrath, *Amer. Mineral.* **77** (1992) 534–544.
177 Sawyer Research Products, US 3 837 826, 1974 (B. Sawyer).
178 *Ullmann*, 4th ed., **21**, 444–450.
179 R. Weiss, *Erzmetall* **27** (1974) 169–177; **31** (1978) 450–457.
180 D. H. Solomon, D. G. Hawthorne: *Chemistry of Pigments and Fillers*, John Wiley & Sons, New York 1983.
181 *Oberflächenbehandelte Füllstoffe,* Data Sheets, Quartzwerke, Frechen, March 8, 1999.
182 R. Oberste-Pattberg, ARDEX GmbH, Witten, *personal communication.*
183 S. N. Groudev, V. J. Groudeva, *Ind. Minerals (London)* **222** (1986) 81–84.
184 P. Harpen, *Ind. Minerals (London)* **184** (1983) 28–29, 32.
185 H. Scholze (ed.): "Keramische Werkstoffe", *Keramik*, 6th ed., **part 2**, Springer-Verlag, Berlin 1983.
186 B. M. Coope, *Ind. Minerals (London)* **298** (1989) 43–55.
187 A. Peschel: *Natursteine*, 2nd ed., Dtsch. Verlag Grundstoffindustrie, Leipzig 1983.
188 H. Gundlach: *Dampfgehärtete Baustoffe*, Bauverlag, Wiesbaden 1973.
189 W. Eden: *Handbuch zur Herstellung von Kalksandstein*, 2nd ed., Bundesverband Kalksandsteinindustrie, Hannover 1998.
190 W. Eden, E. Eberhard: *Forschg. Ber. Nr. 84,* Forschungsvereinigung Kalk-Sand, Hannover 1996.
191 D. Schlumberger: *Cementing Technology*, Nova Communications, London 1984, p. 218.
192 D. Skudelny, R. Weiss: *GAK — Gummi Asbest Kunststoffe* **36** (1983) 3–11.
193 U. Fuhrmann, D. Skudelny in M. Beyer *et al.* (eds.): *Epoxidharze i. d. Elektrotechnik*, Expert-Verlag, Grafenau 1983.
194 J. Griffith, *Ind. Minerals (London)* **241** (1987) 23–45.
195 F. A. Hofmann, H. D. Merzbach: *Silanbehandelte Füllstoffe und Verwendung in der Farbenindustrie*, Quartzwerke Frechen, 1990.
196 W. Grass, D. H. Merzbach, D. Skudelny, *Farbe + Lack* **92** (1986) 1030–1033.
197 D. Skudelny, *Kunststoffe* **77** (1987) 1153–1156.
198 F. A. Hofmann, D. Skudelny: *Surface treated mineral fillers — growing markets for speciality products*, Quartzwerke Frechen, 1990.
199 H. Insley, V. D. Fréchette: *Microscopy of Ceramics and Cements*, Academic Press, New York 1955.
200 R. Weiss, *Glastech. Ber.* **49** (1976) 12–15.
201 J. Lange: *Rohstoffe der Glasindustrie*, Dtsch. Verlag Grundstoffind., Leipzig 1993.
202 A. G. Pincus, D. H. Davies (eds.): "Major Ingredients", *Raw Materials in the Glass Industry*, part 1, Ashlee Publ., New York 1983.
203 H. Petzold, H. Pöhlmann: *Email und Emailtechnik*, Springer-Verlag, Berlin 1987.
204 *Ind. Minerals (London)* **197** (1984) 19–37, 39–45.
205 E. Roedder in H. L. Barnes (ed.): *Geochemistry of Hydrothermal Ore Deposits*, 2nd ed., John Wiley & Sons, New York 1979.
206 C. Müller (ed.): *Databook für Keramik-Glas-Baustoff-Produktion*, 2nd ed., Sprechsaal-Verlag, Coburg 1975.
207 R. Weiss, *Ber. Dtsch. Keram. Ges.* **55** (1978) 82–91.
208 UNIMIN Corp., New Canaan, Connecticut, USA, *data sheet,* 1998.
209 N. SeveringhausJr. in S. J. Lefond (ed.): *Ind. Miner. Rocks* 1975, 235–249.
210 Roskill Inform. Serv. Ltd.: *The Economics of Diatomite*, 5th ed., London 1988, p. 73.
211 L. Pettifer, *Ind. Miner. (London)* **175** (1982) 47–69.
212 L. Benda, H. Brandes, *Geol. Jahrb. Reihe A* **21** (1974) 3–85.
213 L. Benda, *Schriftenr. GDMB* **38** (1981) 134–140.
214 W. B. Clark, *Calif. Geol.* **31** (1978) 3–9.
215 L. Benda, B. Mattiat, *Geol. Jahrb. Reihe D* **22** (1977) 3–107.
216 F. L. KadeyJr. in S. J. Lefond (ed.): *Ind. Miner. Rocks* 1975, 605–635.
217 *Ind. Miner. (London)* 1987 May, 22–39.
218 *Ullmann*, 4th ed., **21**, 452–456.

219 Mitteleuropäische Brautechnische Analysenkommission (MEBAK): Methodensammlung, Freising 1982, III, pp. 651–659.
220 Supplier: VEL Geldenaaksebaan 464, B-3030 Leuven (Heverlee), Belgium.
221 S. Ward: "Liquid Filtration Theory," in M. J. Matteson, C. Orr (eds.): *Filtration, Principles and Practices,* New York, Basel 1987.
222 J. Kiefer: "Kieselgurfiltration," *Brauwelt* **40** (1990) 1730–1749.
223 E. Krüger, N. Wagner, B. Lindemann: "Einflußgrößen bei der Bierfiltration," *Brauwelt* **50** (1989) 2434–2444.
224 International Agency for Research on Cancer (IARC): "Silica and Some Silicates", *Carcinogenic Risk of Chemicals to Humans*, no. 42, Lyon 1987.
225 International Diatomite Producers Association (IDPA): *Silica Facts Questions and Answers; Health and Safety Aspects of Diatomaceous Earth; The Nature and Safe Handling of Diatomaceous Earth*, San Francisco 1989.
226 *Br. J. Ind. Med.* **46** (1989) 289–291.
227 O. Walton: "Filter Media," *The Brewer* **64** (1978) 261–265.
228 F. Kainer, *Kieselgur*, 2nd ed., Enke, Stuttgart 1951, pp. 39–43.
229 L. Benda, S. Paschen: "Kieselguhr (Diatomit) — ein vielseitig genutzter Rohstoff," *Geol. Jahrb.* **A142** (1993) 383–398.
230 R. O. Y. Breese: "Diatomite", in D. D. Carr (ed.): *Industrial Minerals and Rocks*, 6th ed., AIME, Littleton, CO 1994, pp. 397–442.
231 W. Lorenz, W. Gwosdz: "Bewertungskriterien für Industriemineralien, Steine und Erden, Teil 3: Quartzrohstoffe," *Geol. Jahrb.* (1999) H6, 3–119.
232 D. H. Everett: "Definition Terminology and Symbols in Colloid and Surface Chemistry", *Symbols and Terminology for Physiocochemical Quantities and Units*, **Appendix II, part 1**, International Union of Pure and Applied Chemistry, Butterworths, London 1971.
233 R. K. Iler: *The Chemistry of Silica*, J. Wiley & Sons, New York 1979, p. 174.
234 T. Graham, *Justus Liebigs Ann. Chem.* **121** (1862) 36.
235 R. Griessbach, *Chem. Ztg.* **57** (1933) 253.
236 P. G. Bird, US 2 244 325, 1945.
237 M. F. Bechtold, O. E. Snyder, US 2 574 902, 1951.
238 "Silicates and Silicas Report", *Chemical Economics Handbook*, SRI International, Menlo Park 1990.
239 *Opportunities in Specialty Silicas*, Kline & Co., Fairfield, N. J., 1992.
240 E. S. Gould: *Inorganic Reactions & Structures*, Henry Holt & Company, New York 1957.
241 G. J. Fine, *J. Chem. Ed.* **68** (1991) 765.
242 W. D. Kingery, H. K. Bowen, D. R. Uhlmann: *Introduction to Ceramics*, 2nd ed., J. Wiley & Sons, New York 1976.
243 V. Hofman, K. Endell, D. Wilm, *Angew. Chem.* **30** (1934) 539–558.
244 V. Khavryutchenko et al.: "Abstracts of Papers," in R. K. Iler (ed.): *Memorial Symposium on the Colloid Chemistry of Silica,* Washington, D.C., 1990, Paper no. 100.
245 A. P. Legrand *et al.*, *Adv. Colloid Interface Sci.* **33** (1990) 91–330.
246 R. S. McDonald, *J. Phys. Chem.* **62** (1958) 1168.
247 M. L. Hair: *Infrared Spectroscopy in Surface Chemistry*, Marcel Dekker, New York 1967, p. 82.
248 J. B. Peri, A. L. Hensley Jr., *J. Phys. Chem.* **72** (1968) no. 8, 2926–2933.
249 G. E. Maciel, D. W. Sindorf, *J. Am. Chem. Soc.* **102** (1980) 7606–7607.
250 K. D. Unger: "Porous Silica," *J. Chromatogr. Libr.* **16** (1979) .
251 M. L. Hair in A. T. Bell, M. L. Hair (eds.): "Vibrational Spectroscopies for Adsorbed Species," *ACS Symp. Ser.* **137** (1980) .
252 L. T. Zhuravlev: "Abstracts of Papers," in R. K. Iler (ed.) *Memorial Symposium on the Colloid Chemistry of Silica,* Washington, D.C., 1990, Paper no. 93.
253 R. K. Iller: *The Chemistry of Silica*, J. Wiley & Sons, New York 1979, p. 410.
254 Du Pont Company, Nalco Inc., and Nissan Chemicals, based on product information sheets (not specifications).
255 Cabot Corp., and Nissan Inc. and Nissan Chemicals, based on product information sheets (not specifications).
256 Nalco Inc., Nissan Chemicals, and Nippon Seahostar, based on product information sheets (not specifications).
257 R. K. Iller: *The Chemistry of Silica*, J. Wiley & Sons, New York 1979, p. 325.
258 R. K. Iler: *The Chemistry of Silica*, J. Wiley & Sons, New York 1979.
259 B. V. Derjaguin: *Theory of Stability of Colloids and Thin Films*, Consultants Bureau, New York 1989.
260 G. W. Sears, R. K. Iler, private communication.
261 D. H. Napper: *Polymer Stabilization of Colloidal Dispersions*, Academic Press, London 1983.
262 R. K. Iler: *The Chemistry of Silica*, J. Wiley & Sons, New York 1979, p. 364.
263 R. K. Iler: *The Chemistry of Silica*, J. Wiley & Sons, New York 1979, p. 396.
264 R. K. Iler: *The Chemistry of Silica*, J. Wiley & Sons, New York 1979, p. 367.
265 R. K. Iler: *The Chemistry of Silica*, J. Wiley & Sons, New York 1979, p. 366.
266 R. K. Iler, *J. Phys. Chem.* **56** (1952) 680.
267 E. Matijevic *et al.*, *J. Phys. Chem.* **73** (1969) 564.
268 R. K. Iler: *The Chemistry of Silica*, J. Wiley & Sons, New York 1979, p. 409.
269 G. B. Alexander, A. H. Bolt, US 3 007 878, 1961.
270 J. T. Overbeek, private communiction, 1955, unpublished.
271 E. Matijevic, *J. Colloid Sci.* **19** (1964) 333.
272 W. Stober, A. Fink, *J. Colloid Interface Sci.* **26** (1968) 62.
273 R. K. Iler: *The Chemistry of Silica*, J. Wiley & Sons, New York 1979, p. 331.
274 A. B. Alexander, A. H. Bolt, US 3 007 878.
275 R. C. Atkins, US 3 012 973, 1961.

276 R. K. Iler, F. J. Wolter, US 2 631 136, 1953.
277 M. Mindick, L. E. Reven, US 3 468 813, 1969.
278 L. A. Dirnberger, US 2 703 314, 1955.
279 J. Kloepfner, DT 762 723, 830 786, 1942.
280 C. J. Brinker, G. W. Scherer: *Sol-Gel Science*, Academic Press, San Diego 1990.
281 C. G. Tan *et al.*, *J. Colloid Interface Sci.* **118** (1987) 290–293.
282 J. Wolf, private communication.
283 R. K. Iler, US 3 668 088, 1972.
284 H. E. Bergna, US 4 410 405, 1983.
285 G. B. Alexander, US 2 750 345, 1956.
286 H. E. Bergna, F. A. Simko Jr., US 3 301 635, 1967.
287 H. H. Mandelbrot in D. Avnir (ed.): *A Fractional Approach to Heterogeneous Chemistry*, J. Wiley & Sons, New York 1989.
288 S. Brumauer, P. H. Emmett, E. Teller, *J. Am. Chem. Soc.* **60** (1938) 309.
289 G. W. Sears, *Anal. Chem.* **28** (1956) 1981.
290 R. K. Iler: *The Chemistry of Silica*, J. Wiley & Sons, New York 1979, p. 354.
291 T. Allen, R. Davies in R. K. Iler (ed.): "Abstracts of Papers", *Memorial Symposium on the Colloid Chemistry of Silica*, , Washington, D.C. 1990, Paper no. 37.
292 J. Kirkland in H. E. Bergna (ed.): "Colloid Chemistry of Silica," *Adv. Chem. Ser.* **234** 1994.
293 P. F. Collins, US 2 380 945, 1945.
294 P. G. Batelson, CA 1 154 564, 1983.
295 K. Anderson *et al.*, *Nord. Pulp Pap. Res. J.* (1986).
296 K. A. Johnson, US 4 643 801, 1987.
297 S. C. Sofia et al., US 4 795 531, 1989.
298 J. D. Rushmere, US 4 798 653, 1989.
299 R. K. Iler, US 2 597 871, 1947.
300 R. K. Iler, US 2 726 961, 1955.
301 I. V. Wilson, US 2 643 048, 1953.
302 R. J. Walsh, A. H. Herzog, US 3 170 273, 1965.
303 G. W. Sears, US 3 922 393, 1975.
304 J. L. Callahan, US 2 974 110, 1961.
305 J. L. Callahan et al., US 3 322 847, 1967.
306 T. Graham, *Philos. Trans. R. Soc. London* **252** (1861) 204.
307 J. G. Vail: "Soluble Silicates", *ACS Monograph Series*, vol. **2**, Reinhold, New York 1952, p. 549.
308 *Ullmann*, 4th ed., **21**, pp. 458–462.
309 W. A. Patrick, US 1 297 724, 1918.
310 R. K. Iler: *The Chemistry of Silica*, J. Wiley & Sons, New York 1979.
311 C. J. Brinker, G. W. Scherer: *Solg-Gel Science*, Academic Press, San Diego 1990.
312 Wijnen *et al.*, *J. Colloid Interface Sci.* **145** (1991) 17.
313 M. E. Winyall in B. E. Leach (ed.): *Applied Industrial Catalysis*, vol. **3.** Academic Press, Orlando 1984, p. 43.
314 S. S. Kistler, *J. Phys. Chem.* **36** (1932) 52.
315 P. H. Tervari, A. J. Hunt, US 4 610 863, 1986.
316 BASF, US 4 667 417, 1987 (F. Graser, A. Stange).
317 L. C. Klein (ed.): *Sol-Gel Technology for Thin Films, Fibers, Preforms, Electronics, and Specialty Shapes*, Nayes, Park Ridge, New Jersey, 1988.
318 M. B. Kenny, K. S. W. Sing in H. Bergna (ed.): "The Colloid Chemistry of Silica," *Adv. Chem. Ser.* **234** (1994).
319 S. Brunauer, P. H. Emmett, E. Teller, *J. Am. Chem. Soc.* **60** (1938) 309.
320 R. W. Cranston, F. A. Inkley, *Adv. Catal.* **9** (1957) 143.
321 K. Sing in G. Parfitt, K. Sing (eds.): *Characterization of Powder Surfaces*, Academic Press, New York 1976, p. 34.
322 R. L. White, A. Nair, *Appl. Spectrosc.* **44** (1990) 69.
323 P. Wijnen, T. Beelen, R. van Santen in H. Bergna (ed.): "The Colloid Chemistry of Silica," *Adv. Chem. Ser.* **234**, 1994.
324 V. K. Markov, N. A. Nagornaya, *J. Applied Chem. (USSR)* **10** (1937) 853.
325 E. Heimann, US 2 316 241, 1938.
326 Davison Chemical, US 2 625 492, 1949 (L. O. Young).
327 W. R. Grace & Co., US 2 856 268, 1954 (L. O. Young).
328 Houdry, US 2 232 727 (A. G. Peterkin, H. A. Shabaker).
329 Mizusawa Ind. Chem., DE 1 442 778, 1963 (T. Kuwata, Y. Sugahara, T. Nakazawa).
330 Asahi Chem. Ind., JP 48 013 834, 1966 (K. Takizawa, Y. Ohba).
331 BASF, DE 2 103 243, 1979 (G. Merz, H. Gehrig, W. Chorbacher).
332 Socony-Vacuum Oil Comp., US 2 385 217, 1945 (M. M. Marisic).
333 Kali-Chemie, DE 1 567 617, 1970 (J. Dultz).
334 Mizusawa, EP 884 277, 1998 (T. Masanori, W. Yuuji).
335 J. F. White, I. V. Wilson, *Ind. Eng. Chem.* **33** (1941) 1169.
336 Fuji-Davison, Art-Sorb-Technical Information (in English), 4.11.27 Meieki, Nagoya-shi, Japan 450.
337 R. S. McDonald, *J. Am. Chem. Soc.* **79** (1975) 850.
338 Crosfield, US 3 617 301, 1968 (D. Barby, J. P. Quinn).
339 W. R. Grace & Co., US 4 629 588, 1984 (W. A. Welsh, Y. O. Parent).
340 A. Bertod, *J. Chromtogr.* **549** (1991) 1.
341 J. Freng, GB 203 248, 1922.
342 Lever Bros., US 3 538 230, 1966 (M. Pader, W. Wiesner).
343 W. R. Grace & Co., US 4 303 641, 1978 (R. B. DeWolf, R. Glemza).
344 J. M. Huber, US 4 340 583, 1977 (S. K. Wason).
345 M. Pader: *Oral Hygiene Products and Practice*, Marcel Dekker, New York 1988.
346 J. S. Magee, J. J. Blazek in J. A. Rabo (ed.): "Zeolite Chemistry and Catalysis", *ACS Monogr.* no. 171, 1976, 615.
347 Phillips Petroleum, US 3 378 540, 1964 (D. R. Witt).
348 F. Karol *et al.*, *J. Polym. Sci., Polym. Chem. Ed.* **10** (1972) 2621.
349 Exxon Chemical, US 4 701 432, 1986 (H. C. Welborn).
350 D. D. Dunnom (ed.): *Health Effects of Synthetic Silica Particulates*, no. 732, ASTM Special Technical Publication, Philadelphia 1981.

351 Y. Takizawa *et al.*, *Acta Med. Biol. (Niigata)* **36** (1988) 27.
352 T. Provder: *Particle Size Distribution: Assessment and Characterization,* ACS Symposium Series 332, American Chemical Society, 1987.
353 W. R. Grace & Co., US 3 800 031, 1974 (H. S. Sale, A. Delgrado, C. F. Doyle).
354 Unilever Patent Holdings B. V., US 5 215 733, 1993 (J. K. Potter).
355 University of New Mexico, US 5 565 142, 1996 (R. Deshpande, D. M. Smith, C. J. Brinker).
356 D. M. Chapman, *Proceedings of the 1997 TAPPI Coating Conferenz* (1997) 73–93.
357 Texas Instruments Inc., US 5 847 443, 1998 (C. C. Cho *et al.*).
358 "National Chemical Inventories" (TM) CD-ROM, Copyright 1999, *American Chemical Society.*
359 International Association for Research on Cancer (IARC): *Silica, Some Silicates, Coat Dust and Para-aramid Fibrils*, vol. 68, 1997, pp.
360 C. J. Johnston *et al.*, *Toxicol. Sci.* **56** (2000) 405–413.
361 Degussa, DE 762 723, 1942 (H. Klöpfer).
362 S. Brunauer, P. H. Emmett, E. Teller, *J. Am. Chem. Soc.* **60** (1938) 309.
363 H. Ferch, K. Seibold, *Farbe Lack* **90** (1984) 88.
364 Degussa, *Schriftenreihe Pigmente*, Paper no. 11, Frankfurt 1992.
365 M. Schmücker, "Untersuchungen an nichtkristallinen technischen Kieselsäuren unter besonderer Berücksichtigung des thermischen Transformationsverhaltens," Diplomarbeit, Ruhr-Universität, Bochum 1988.
366 H. Wistuba, "Die Silanolgruppen der Siliciumdioxidoberfläche und ihre chemischen Reaktionen," Dissertation, Universität Heidelberg 1967.
367 J. Mathias, G. Wannemacher, *J. Colloid Interface Sci.* **125** (1988) 61.
368 D. Kerner, W. Leiner, *Colloid Polym. Sci.* **253** (1975) 960.
369 H. Ferch, *Seifen Öle Fette Wachse* **101** (1975) 17, 51.
370 B. A. Morrow, A. J. McFarlan, *J. Non Cryst. Solids* **120** (1990) 61.
371 B. A. Morrow, A. J. McFarlan, *Langmuir* **7** (1991) 1695.
372 K. Yoshinaga *et al.*, *Chem. Lett.* 1991, 1129.
373 C. P. Tripp, M. L. Hair, *Langmuir* **7** (1991) 923.
374 G. Hellwig, *Farbe Lack* **81** (1975) no. 8, 705.
375 A. Meffert, A. Langenfeld, *Fresenius Z. Anal. Chem.* **249** (1979) 231.
376 H.-P. Boehm, M. Schneider, *Z. Anorg. Allg. Chem.* **301** (1959) 326.
377 H.-P. Boehm, *Kolloid Z. Z. Polym.* **227** (1968) 17.
378 H.-P. Boehm, *Angew. Chem.* **78** (1966) no. 12, 617.
379 Degussa, DE 1 163 784, 1962 (H. Brünner, J. Diether, D. Schutte).
380 Degussa, DE 3 211 431, 1982 (H. Klebe *et al.*).
381 Ivoclar, DE 3 632 215, 1986 (V. M. Rheinberger, T. Büchl).
382 Blendax, WO 8 503 220, 1985 (W. Kuhlmann).
383 Kulzer, DE 2 405 578, 1974 (A. Groß, R. Schaefer).
384 Canon, EP 369 443, 1989 (Y. Sato, T. Kukimoto).
385 Nippon Aerosil Corp., JP 58 185 405, 1983 (N. Furuya, T. Morii).
386 Canon, EP 216 295, 1986 (K. Tanaka *et al.*).
387 V. M. Litvinov *et al.*, *Acta Polym.* **39** (1988) no. 5, 244.
388 G. Berrod, A. Vidal, E. Papirer, J. B. Donnet, *J. Appl. Polym. Sci.* **23** (1979) 2679; **26** (1981) 833, 1015.
389 P. Vondracek, M. Schätz, *J. Appl. Polym. Sci.* **21** (1977) 3211.
390 L. A. Peters, J. C. Vicic, D. E. Cain, *GAK Gummi Asbest Kunstst.* **44** (1991) no. 2, 69.
391 H. Ferch, A. Reisert, R. Bode, *Kautsch. Gummi Kunstst.* **39** (1986) 1084.
392 Degussa, *Schriftenreihe Pigmente*, Paper no. 23, Frankfurt 1986.
393 Degussa, *Schriftenreihe Pigmente*, Paper no. 68, Frankfurt 1985.
394 Degussa, *Schriftenreihe Pigmente*, Paper no. 18, Frankfurt 1989.
395 K. Borho *et al.*, *Chem. Ing. Tech.* **63** (1991) no. 8, 792.
396 H. Rumpf, *Chem. Ing. Tech.* **46** (1974) no. 1, 1.
397 R. Tawashi, *Pharm. Ind.* **25** (1963) 64.
398 H. Ferch, H. Gerofke, H. Itzel, H. Klebe, *Arbeitsmedizin Sozialmedizin Präventivmedizin* **22** (1987) 6; **22** (1987) 23.
399 F. Leuschner, unpublished results.
400 J. J. Sarre, unpublished results.
401 Degussa, DE 1 180 723, 1963 (H. Biegler, W. Neugebauer, H. Kempers).
402 Degussa, DE 1 933 291, 1969 (A. Illigen, W. Neugebauer).
403 Lonza, DE 2 337 495, 1972 (C. Schnell, M. Wissler, K. Hengartner).
404 E. R. Schnell, S. M. L. Hamblyn, K. Hengartner, M. Wissler, *Powder Technol.* **20** (1978) 15.
405 Degussa, DE-AS 1 467 019, 1963 (A. Becker, P. Nauroth).
406 Degussa, DE-AS 1 168 874, 1962 (G. Roderburg, P. Nauroth).
407 Degussa, DE-AS 1 299 617, 1965 (H. Reinhardt, K. Achenbach, P. Nauroth).
408 Degussa, EP 0 078 909, 1982 (P. Nauroth, H. Esch, G. Türk).
409 Degussa, DE 1 767 332, 1968 (G. Türk, J. Welsch).
410 Degussa, EP 0 341 383, 1989 (D. Kerner, A. Wagner, F. Schmidt, D. Bauer).
411 Degussa, DE-OS 3 114 493, 1981 (P. Nauroth, R. Kuhlmann, G. Türk, A. Becker).
412 Akzo, DE-AS 2 020 887, 1970 (G. Steenken, E. Seeberger).
413 Rhône-Poulenc, EP 0 018 866, 1980 (J-L. Ray, M. Condurier).
414 Rhône-Poulenc, EP 0 170 578, 1985 (Y. Chevallier).
415 Rhône-Poulenc, EP 0 396 450, 1990 (Y. Chevallier).
416 Degussa, DE-OS 3 639 845, 1986 (H. Reinhardt, A. Becker, R. Kuhlmann, P. Nauroth).
417 Tokuyama Soda, JP-Kokai 59 141 416, 1983.

418 Crosfield, US 4 127 641, 1977 (D. Aldcroft, D. Barby, A. L. Lovell, J. P. Quinn).
419 Huber, US 4 260 454, 1978 (S. K. Wason, R. K. Mays).
420 Sifrance, DE-AS 2 224 061, 1972 (J.-B. Donnet, B. Baudru, M. Condurier, G. Vrisakis).
421 Degussa, DE 966 985, 1950 (K. Andrich).
422 Nippon Silica, JP 03 75 215, 1989 (Y. Mikamoto, K. Sakata).
423 Degussa, DE 1 229 504, 1962 (G. Kallrath).
424 Bayer, DE-OS 3 525 802, 1985 (L. Puppe, O. Schlak, J. Ackermann, T. Naumann).
425 Degussa, DE-AS 1 192 162, 1962 (L. Hüter, G. Steenken).
426 PPG, DE-AS 1 131 196, 1955 (F. S. Thornhill, E. M. Allen).
427 PPG, DE 1 283 207, 1961 (C. B. Lagerstrom).
428 Degussa, DE-AS 2 505 191, 1975 (B. Brandt, P. Nauroth, A. Peters, H. Reinhardt).
429 Degussa, DE-OS 1 467 437, 1965 (G. Bretschneider, K. Pfeiffer, R. Schwarz, K. Laun).
430 Degussa, DE-AS 1 293 138, 1965 (H. Reinhardt, P. Nauroth).
431 Degussa, US 4 179 431, 1979 (E. Kilian, A. Kreher, P. Nauroth, G. Türk).
432 Degussa, DE-AS 1 567 440, 1965 (H. Biegler, K. Trebinger).
433 Degussa, *Schriftenreihe Pigmente*, Paper no. 70, 2nd ed., Frankfurt/Main 1984.
434 Degussa, *Schriftenreihe Pigmente*, Paper no. 28/1, 5th ed., Frankfurt/Main 1998.
435 Degussa, *Schriftenreihe Pigmente*, Paper no. 32, 4th ed., Frankfurt/Main 1989.
436 H. Ferch, *Chem. Ing. Tech.* **48** (1976) no. 11, 922.
437 Degussa, DE 1 172 245, 1963 (G. Kallrath).
438 Degussa, DE 2 513 608, 1975 (H. Reinhardt, K. Trebinger, G. Kallrath).
439 Degussa, DE 2 729 244, 1977 (P. Nauroth *et al.*).
440 Degussa, DE 1 074 559, 1959.
441 Degussa, DE 2 628 975, 1976 (P. Nauroth *et al.*).
442 Degussa, DE 1 667 465, 1967 (P. Nauroth, R. Kuhlmann).
443 Degussa, DE 1 592 865, 1967 (O. Kuehnert, G. Türk, E. Eisenmenger).
444 Degussa, *Schriftenreihe Pigmente*, Paper no. 16/1, 4th ed., Frankfurt/Main 1992.
445 H. J. Bachmann, J. W. Sellers, M. P. Wagner, R. F. Wolf, *Rubber Chem. Technol.* **32** (1959) 1286.
446 G. Kraus: *Reinforcement of Elastomers*, Interscience, New York 1965.
447 S. Wolff, *Kautsch. Gummi Kunstst.* **41** (1988) no. 7, 674.
448 S. Wolff, *Kautsch. Gummi Kunstst.* **34** (1981) no. 4, 280.
449 S. Wolff, *Kautsch. Gummi Kunstst.* **36** (1983) no. 11, 969.
450 Degussa, DE-OS 3 305 373, 1983 (S. Wolff, P. Golombeck).
451 R. Bode, A. Reisert, *Kautsch. Gummi Kunstst.* **32** (1979) no. 2, 89.
452 P. Vondracek, M. Schätz, *Kautsch. Gummi Kunstst.* **33** (1980) no. 9, 699.
453 K. H. Müller, *Mühle Mischfuttertech.* **114** (1977) 28.
454 K. H. Müller, *Kraftfutter* **53** (1970) 436.
455 Degussa, *Schriftenreihe Pigmente*, Paper no. 31/1, 3rd ed., Frankfurt/Main 1999.
456 Degussa, *Schriftenreihe Pigmente*, Paper no. 1, 5th ed., Frankfurt/Main 1989.
457 O. Pfrengle, *Fette Seifen Anstrichm.* **63** (1961) no. 5, 445.
458 Degussa, Technical Information, Paper no. TI 1159, Frankfurt/Main, 1994.
459 W. Leonhardt, *Speciality Chemicals* 1989, 441.
460 Degussa, DE 1 517 900, 1965 (H. Reinhardt, P. Nauroth, K. Achenbach).
461 General Electric, US 4 018 564, 1975 (J. H. Wright).
462 Degussa, unpublished report, 77–0016-DKT, 1977.
463 Degussa, unpublished report, 79–0004-DKT, 1979.
464 Degussa, unpublished report, 81–0016-DGT, 1981.
465 Degussa, unpublished report, 91–0131-DGT, 1991.
466 Degussa, unpublished report, 91–0132-DGT, 1991.
467 Degussa, unpublished report, 87–0004-DGT, 1987.
468 E. R. Plunkett, B. J. DeWitt, *Arch. Environ. Health* **5** (1962) 469–472.
469 Degussa, unpublished report, 75–0018-DKT, 1975.
470 Degussa, unpublished report, 81–0108-DKT, 1981.
471 D. Choudat, C. Frisch, G. Barrat, A. El Kholti, F. Couso, *Br. J. Med.* **47** (1990) 763–766.
472 Deutsche Forschungsgemeinschaft (ed.): *MAK und BAT-Werte-Liste*, WILEY-VCH, Weinheim, Germany 1999. pp. 157–165.
473 R. M. Barrer: "Porous Crystals: A Perspective" in Y. Murakani, A. Jijima, J. W. Ward (eds.): *New Developments in Zeolites Science and Technology,* Kodansha, Tokyo, and Elsevier, Amsterdam, Tokyo 1986, pp. 3–11.
474 E. M. Flannigen *et al.*, *Nature* **271** (1978) 512–516.
475 W. M. Meier, D. H. Olson, C. Baerlocher: *Atlas of Zeolite Structure Types*, Butterworth, London 1987.
476 http://www.iza-online.org/
477 H. Gies, B. Marler, *Zeolites* **12** (1992) 42–49.
478 R. Szostak: "Modified Zeolites" in H. van Bekkum, E. M. Flannigan, J. C. Jansen (eds.): *Introduction to Zeolite Science and Practice,* Elsevier, Amsterdam 1991, pp. 153–199.
479 H. Gies *et al.*, *Neues Jahrb. Mineral. Monatsh.* **3** (1982) 119–124.
480 B. Marler, *Phys. Chem. Miner.* **16** (1988) 286–290.
481 J. F. CooperJr., G. E. Dunning, *Am. Mineral.* **57** (1972) 1494–1499.
482 C. A. Fyfe, H. Gies, *J. Inclusion Phenom.* **8** (1990) 235–239.
483 H. Gies, *Z. Kristallogr.* **167** (1984) 13–82.
484 C. A. Fyfe *et al.*, *Zeolites* **10** (1990) 278–282.
485 C. A. Fyfe *et al.*, *J. Am. Chem. Soc.* **110** (1988) 3373–3380.
486 C. A. Fyfe *et al.*, *J. Am Chem. Soc.* **111** (1989) 2470–2474.

487 J. A. Ripmeester *et al.*, *J. Chem. Soc., Chem. Commun.* 1988, 608–611.

488 S. H. Park *et al.*: "The Thermal Expansion of the Zeolites MFI, AFI, DOH, DDR, and MTN in their Calcined and As Synthesized Forms" in H. Chon, S.-K. Ihm, Y. S. Uh (eds.): *Progress in Zeolite and Microporous Materials, Studies in Surface Science and Catalysis* vol. **5**, Elsevier, Amsterdam 1997, pp. 1989–1994.

489 a) N. Y. Chen, *J. Phys. Chem.* **80** (1976) 60–64. b) D. H. Olson *et al.*, *J. Catal.* **61** (1980) 390–396.

490 R. M. Lago et al.: "The Nature of the Catalytic Sites in HZSM-5-Activity Enhancement" in Y. Murakami, A. Jijima, J. W. Ward (eds.): *New Developments in Zeolite Science and Technology,* Elsevier, Amsterdam 1986, pp. 677–684.

491 T. Bein et al.: "Molecular Sieve Films from Zeolite-Silica Microcomposites" in P. A. Jacobs, R. A. van Santen (eds.): *Zeolites: Facts, Figures, Future,* Elsevier, Amsterdam 1989, pp. 887–896.

492 J. C. Jansen et al.: "Zeolite Coatings — Potential Use in Catalysis and Separation" in M. M. J. Treacy, B. K. Marcus, M. E. Bisher, J. B. Higgins (eds.): *Proceedings of the 12th International Zeolite Conference*, MRS, Warrendale 1999, pp. 603–611.

493 Y. S. Lin, Y. H. Ma: "A Comparative Study of Adsorption and Diffusion of Vapor Alcohols and Alcohols from Aqueous Solutions in Silicalite" in P. A. Jacobs, R. A. van Santen (eds.): *Zeolites: Facts, Figures, Future,* Elsevier, Amsterdam 1989, pp. 877–886.

494 P. Enzel, T. Bein, *J. Phys. Chem.* **93** (1989) 6270–6272. S. D. Cox, G. D. Stucky, *J. Phys. Chem.* **95** (1991) 710–720.

495 N. Herron, Y. Wang, *J. Phys. Chem.* **91** (1987) 2757. S. Miyazaki, H. Yoneuyama, *Denki Kagaku* **58** (1990) 37–40.

496 S. T. Homeyer, W. M. H. Sachtler: "Design of Metal Clusters in NaY Zeolite" in P. A. Jacobs, R. A. van Santen (eds.): Zeolites: Facts, Figures, Future, Elsevier, Amsterdam 1989, pp. 975–984. K. Möller *et al.*, *J. Phys. Chem.* **93** (1989) 6116 –6120.

497 S. D. Cox *et al.*, *Chem. Mater.* **2** (1990) 609 –619.

498 G. Ozin *et al.*, *Angew. Chem.* **101** (1989) 373 –390.

499 H. Gies *et al.*, *Angew. Chem.* **94** (1982) 214–215.

500 H. K. Chae et al.: "Clathrasils: New Materials for Nonlinear Optics" in G. Stucky (ed.): "New Materials for Nonlinear Optics," *Am. Chem. Soc. Symp. Ser.* 1991.

501 H. Gies: "Clathrasils and Zeosils: Inclusion Compounds with Silica Host Framework" in J. L. Atwood, J. E. D. Davies, D. D. McNicol (eds.): *Inclusion Compounds,* vol. 5, Inorganic and Physical Aspects of Inclusion, Oxford Unversity Press, Oxford 1991, pp. 1–36.

502 H. Gies *et al.*: "Synthesis of Porosils: Crystalline Nanoporous Silicas with Cage- and Channel-Like Void Structure" in H. G. Karge, J. Weitkamp (eds.): *Molecular Sieves 1. Science and Technology. Synthesis*, Springer, Berlin 1998, pp. 35–65.

503 K. R. Franklin, B. M. Lowe, *Zeolites* **8** (1988) 491–516.

504 E. W. Valyocsic, L. D. Rollman, *Zeolites* **5** (1985) 123–125.

505 G. T. Kerr, *J. Phys. Chem.* **71** (1967) 4165. C. A. Fyfe *et al.*, *J. Chem. Soc., Chem. Commun.* 1984, 1093–1094.

506 "Silica Flour: Silicosis", *NIOSH, Current Intelligence Bulletin* no. 36, 1981. DHHS (NIOSH) Publication no. 81–137, 1981.

507 Information Profiles on Potential Occupational Hazards, vol. II, Chemical Classes: Amorphous Silicas, NTIS, no. PB 81–147 886, 1979.

508 *Patty*: 3rd ed., 2 B, p. 3012.

509 D. D. Dunnom (ed.): "Health Effects of Synthetic Silica Particulates", *ASTM Spec. Tech. Publ.* **732**, (1981) no. 04–732000–17.

510 E. Quellmalz: "Silikogener Staub", *Das neue Chemikaliengesetz; Arbeitsstoffverordnung*, Anhang II, 12/ 2.8, WEKA-Verlag, Kissing 1982.

511 Deutsche Forschungsgemeinschaft (ed.): *MAKund BAT-Wert-Liste*, VCH, Weinheim, Germany 1992, pp. 96–102.

512 *Documentation of the Threshold Limit Values,* 4th ed. 1980, Suppl. Docum. 1981, Silica (amorphous), p. 362, Silica (fused), p. 363, Silica (quartz), p. 364. *Am. Conf. Gov. Ind. Hyg.,* Cincinnati, Ohio, 1981.

513 W. Klosterkötter, *Arch. Hyg. Bakteriol.* **149** (1965) 577–598.

514 W. H. Schepers *et al.*: *AMA Arch. Ind. Health* **16** (1957) 125–146.

515 H. Volk, *Arch. Environ. Health.* **1** (1960) 125–128.

516 H. Gerofke: *Beobachtungen an Beschäftigten des Aerosil-Betriebes*. Rheinfelden 1981, unpublished.

517 V. C. Vitums *et al.*: *Arch. Environ. Health* **32** (1977) no. 2, 62–68.

518 F. D. Goldsmith, T. L. Guidotti, D. R. Johnston: *Am. J. Ind. Med.* **3** (1982) 423.

519 P. Westerholm: *Scand. J. Work Environm. Health (Suppl).* **2/6** (1980) 1.

520 M. Finkelstein, R. Kusiak, G. Suranyi: *J. Occup. Med.* **24** (1982) 663.

521 H. Gulbergsson, K. Kurppa, H. Koskinen, M. Vasama: "Association between Silicosis and Lung Cancer: A Register Approach", *VI. International Pneumoconiosis Conference,* Bochum, Sept. 20–23, 1983.

522 C. G. O'Neill *et al.*: *Lancet* **202** (1982) 1202.

523 W. Klosterkötter, H. J. Einbrodt: *Arch. Hyg. Bakteriol.* **149** (1965) 367–384.

524 W. Klosterkötter: *Retention, Penetration und Elimination von Quarz bei einem Langzeit-Inhalationsversuch (Konzentration 10 mg/m^3)* vol. 9, Verlag Glückauf, Essen 1973, p. 177.

525 H. Gärtner: *Arch. Hyg. Bakt.* **136** (1952) 451–467.

526 K. W. Jötten: *Gutachtliche Untersuchung und Beurteilung der Wirkung von Aerosilstaub auf das Lungengewebe von Versuchstieren*, Deutsche Gold- und Silber-Scheideanstalt, Frankfurt am Main 1952.

527 M. M. E. Wagner: *J. Natl. Cancer Inst.* **57** (1976) 509.

528 M. M. E. Wagner, J. C. Wagner, R. Davies, D. M. Griffiths.: *Br. J. Cancer* **41** (1980) 908.

529 F. Stenbäck, J. Rowland.: *Oncology* **36** (1979) 63.
530 L. M. Holland, M. Gonzales, J. S. Wilson, M. I. Tillery: "Pulmonary Effects of Shale Dusts in Experimental Animals," *Environmental Health Conference,* Park City, April 6–9, 1982.

Further Reading

H. E. Bergna, W. O. Roberts (eds.): *Colloidal Silica*, vol. 131, Taylor & Francis, Boca Raton 2006.

R. Hidalgo-Álvarez (ed.): *Structure and Functional Properties of Colloidal Systems*, vol. 146, CRC Press, Boca Raton 2010.

A. P. Legrand (ed.): *The Surface Properties of Silicas*, Wiley, Chichester 1999.

M. Pagliaro: *Silica-based Materials for Advanced Chemical Applications*, RSC, Cambridge 2009.

E. Papirer: *Adsorption on Silica Surfaces*, Dekker, New York, NY 2000.

S. Uhrlandt: *Silica, Kirk Othmer Encyclopedia of Chemical Technology*, 5th edition, vol. 22, p. 365–379, John Wiley & Sons, Hoboken, NJ, 2006, online: DOI: 10.1002/0471238961.0914201816012020.a01.pub2 (June 2006).